Stony Brook University

Process Design for Reliable High Velocity Thermal Spray Coatings: An Integrated Approach through Process Maps and Advanced *in situ* Characterization

A Dissertation Presented

by

Alfredo Valarezo

to

The Graduate School
in Partial Fulfillment of the
Requirements
for the Degree of

Doctor of Philosophy

in

Materials Science and Engineering

Stony Brook University

May 2008

Stony Brook University
The Graduate School

Alfredo Valarezo
We, the dissertation committee for the above candidate for the
Doctor of Philosophy degree, hereby recommend
Acceptance of this dissertation

Prof. Sanjay Sampath – Dissertation Advisor
Professor, Materials Science and Engineering Department

Prof. Herbert Herman
Distinguished Professor Emeritus
Materials Science and Engineering Department

Prof. Andrew Gouldstone
Adjunct Professor, Materials Science and Engineering Department

Prof. Toshio Nakamura
Professor, Mechanical Engineering Department

Dr. Richard Karl Schmid
Chief Technology Offficer, CTO – Sulzer Metco Switzerland

This dissertation is accepted by the Graduate School

Lawrence Martin
Dean of the Graduate School

Abstract of the Dissertation

Process Design for Reliable High Velocity Thermal Spray Coatings: An Integrated Approach through Process Maps and Advanced *in situ* Characterization

by

Alfredo Valarezo
Doctor of Philosophy

in

Materials Science and Engineering
Stony Brook University
2008

The ambitious goal to design repeatable and reproducible coatings with enhanced performance is the driving motivation to implement science based strategies to control thermal spray (TS) processes. With the goal to design the process and resultant coating, sensors have been implemented during the coating deposition to monitor particle state, coating formation, and final properties. However, only if fundamental principles are applied to understand the process-microstructure-property relations, will production of designed *prime reliant* coatings be possible.

The methodology *of Process Maps* has been advanced towards this purpose by developing systematically controlled parametric states that interrelate process variables with particle state, stress evolution and properties. In the present study, *Process Maps* have been utilized to investigate the process window in which a high velocity thermal spray (HVTS) system can produce coatings of desired properties. A Diamond Jet torch spraying Ni-20Cr was chosen to systematically explore the particle energy space (thermal and kinetic energy) and produce coatings with different properties. A relatively small range in property values was found for the system in question. Further investigation was carried out to obtain significantly different particle states in a broader range of flame energy levels by depositing coatings with various types of HVTS systems (high velocity

-HV- gas fuel guns, HV liquid fuel guns, and HV plasma gun). A common analysis of melting state (by melting index) and kinetic energy among the different processes explained the significantly larger processing range resulting in higher versatility in properties, microstructures and stress formation mechanisms.

The monitoring of stress development during thermal spraying revealed important differences in coating formation and properties. This principle was investigated further in several materials and process systems. The associated mechanisms of stress relief or stress build-up can be used to evaluate the deposit-substrate system including adhesion/cohesion strength, micro-cracking, peening, etc. An in-depth analysis of stress evolution was carried out to study peening effect (impact induced work hardening) in coatings sprayed with particles at supersonic velocities. Analysis of residual stress profiles when peening effect dominates is also discussed using parallel results from neutron diffraction.

The applied principles to study flame energies, heat and momentum transfer to the particles in-flight, stress evolution and microstructure have shed light to understand deposit formation dynamics and ensuing evolution of the coating properties. Eventually, the attained understanding can lead to design the TS process that would deposit coatings of desired microstructure and properties; with the ultimate goal of maximizing performance of the coating-substrate system.

Dedication

This dissertation is dedicated with all my love to my wife and son.

My wife, Lorena, who has been with me lovely and unconditionally all along this project. I thank her for what and what not she had to forgive and do to be with me during these years of research and for listening and encouraging me in the long days and nights of study. I love you so much.

To my smiling prince, Alfredito Ismael, who is the reason of my life. I thank you for keeping me up everyday with your charming soul and filling my heart with so much love. I love you.

I also dedicate this work to my family: my dad, my mother (and her tears of love), my sister, my brother, my sisters/brother -in law, and my nephew and nieces, who have felt our absence and have been always supportive along these years. We have missed you so much. With love and heartfelt appreciation, I also dedicate this work to you.

Table of Contents

List of Figures

List of Tables

Acknowledgement

Many people has contributed and encouraged me along the years of this research. I thank all of them, and I hope I have gathered a little bit of the best of all.

First, I want to express my sincere thanks and appreciation to my advisor and mentor Prof. Sanjay Sampath for having opened me the gates to this wonderful science-technology-industry experience in Thermal Spray. I thank his advice that has promoted my understanding and has lightened my research spirit. I have become a new person thirsty of knowledge and excited for creation. Thank you.

I also want to thank Prof. Andrew Gouldstone for "stretching my brain" and helping me breaking my paradigms. His bright mind brought to me many insights and knowledge that gladly made me less ignorant. I appreciate his guidance during my coursework and research studies.

I have had the pleasure of working with and learning from a number of students and post doctoral researchers. Many people have contributed with their comments and effort. All their support and help is gratefully acknowledged. They are:

Dr. Anirudha Vaidya, Dr. Li Li, Dr. Atin Sharma, Dr. Weiguang Chi, Dr. Vasudevan Srinivasan, Dr. Brian Choi, Dr. Yang Tan, Lorena Bejarano, Shan-Shan Liang, Meng Qu, Wei Zhang, Jae-Hun Kim, José Colmenares, Eduardo Mari, Gopal Dwivedi, Jonathan Gutleber, Joshua Margolis, Glenn Bancke, Rob Greenlaw.

I gratefully acknowledge the support and interaction of: NIST Center for Neutron Diffraction, Dr. Thomas Gnaeupel-Herold and Dr. Vladimir Luzin, VTT Technical Research Centre of Finland, Tommi Varis; Sulzer Metco, Ron Molz; Praxair ST, Dr. Li Li; Stellite Coatings, David Lee; CAT, Dr. Ondrej Racek.

Finally, I express my heartfelt gratitude to my wife and son for their love, encouragement and sacrifice.

Funding support is acknowledged: 1) Materials Research Science and Engineering Center (MRSEC) program of the National Science Foundation to the Center for Thermal Spray Research (CTSR) under award DMR 0080021; 2) Consortium for Thermal Spray Technology at CTSR; and GOALI-FRG program of the National Science Foundation under award number CMMI- 0605704.

Chapter 1
INTRODUCTION TO HIGH VELOCITY THERMAL SPRAY PROCESSING

Thermal spray coatings preamble

Coatings produced by thermal spray (TS) are used in many applications, including but not limited to, thermal protection, electrical insulation/conduction, friction-wear and corrosion-oxidation resistance, and many others, as illustrated in Figure 1-1.

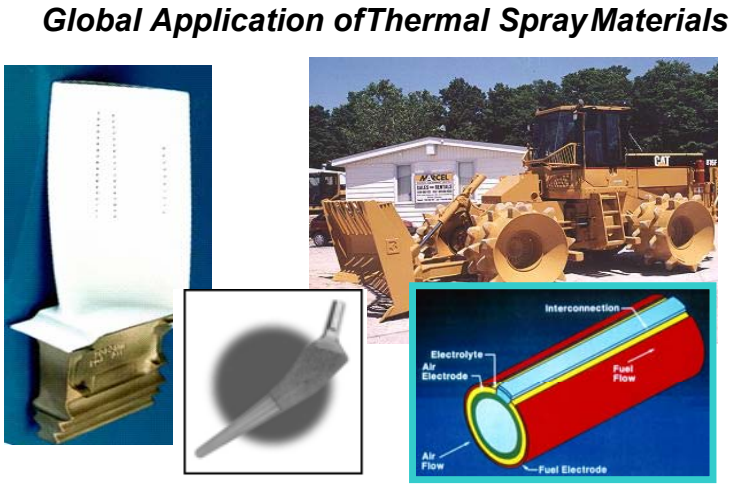

Figure 1-1. Applications of TS coatings span a wide range of engineering systems, from thermal/mechanical protection to orthopedic implants to fuel cell technology

Over the years, industry has increased the operational conditions in equipment, such as gas turbines, automotive systems, earth moving machinery. Although superalloys and high performance steels have been developed for such applications, they are not able to meet the multifunctional requirements of mechanical properties, corrosion, wear or thermal shock resistance at the same time. This is where the TS processes find their market niche, offering a wide variety of coatings, ranging from ceramics for high temperature applications, metallic alloys for corrosion resistance and cermets for wear applications. Recent innovations have allowed the expansion of TS applicability well

beyond 'traditional' overcoatings into the creation of functional surfaces, systems with complex chemistries, and patterned mesoscale devices.

The substantial progress in knowledge, research, and equipment development in the TS industry has raised the application level of coatings to nearly prime reliant coatings in engineering components. The traditional implementation of TS coatings to provide life extension to surfaces and/or repair worn components is changing to a more robust design-based demand of coatings in production. As a result, reliability and reproducibility have become major issues. To address these issues as well as the ability to integrate coatings into design, a science based development strategy is necessary.

1.1 Thermal Spray Processing: Stages of the process

The actual formation of the coatings particle-by-particle involves different stages with multiple interactions between materials (parent powder materials, oxides, substrates) and gases. Concurrent efforts are being developed to advance the understanding of such interactions and to narrow the variability that hardware operation and supplies (powder, gases) may have on the reliability and repeatability in production. To study the complexities of the thermal spray process, we have divided the process in several stages: feedstock, particle-flame interactions (upstream and downstream), coating build-up, and post deposition phenomena.

1.1.1 Feedstock

The quality of any TS coating depends on the initial feedstock material. The resulting splat dimensions depend on the particle size (usually a relatively broad distribution) and morphology. Excessively small particles tend to oxidize or decompose (see Figure 1-2 for an illustrated example) owing to their high surface area to volume ratio. On the other hand, excessively large particles may not absorb sufficient heat during flight, not melt, and end up rebounding. This emphasizes the importance of feeding an appropriate assortment of particle sizes. Processes such as cold spray (CS) are very sensitive to particle size, because particles are subjected to high strain-rates and hence strain-rate hardening which affects the critical velocity (velocity at which deposition is achieved) of particles of different sizes [1].

Grain size may not be as important for TS, because particles melt and re-solidify during the process. However, for CS, powders of small grain size (usually as a result of the production process) shows an intrinsically higher strength because of the finer microstructure, which makes more difficult the consolidation of particles during the spraying. In cermets, since carbides do not melt, they are prone to fracture during impact or even rebound from the matrix. Carbide size has been optimized to smaller sizes as to avoid fracture but not too small as to avoid decarburization in-flight.

An appropriate flowability of the powder is always desired as to assure continuous feeding and to reduce stop-times due to clogging in the hardware. Manufacturer's control of particle morphology, moisture and binders usually assures the quality of powders in production.

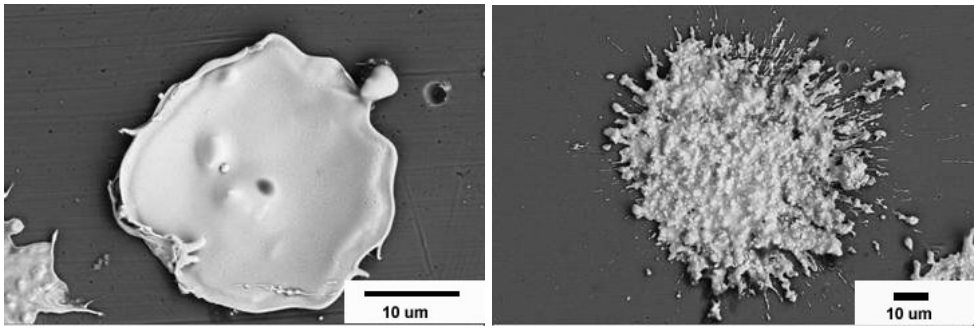

Figure 1-2. Example-illustration of the importance of particle size control during spraying. On the left, small WC-12Co splat fully decomposed in-flight. On the right, larger particle spreading into a splat. Retention of carbide is highlighted in the latter.

1.1.2 Particle-flame Interaction: Upstream and Downstream

When considering effects of operational parameters in the plume, it is anticipated that changes of the variables (e.g., gas flows, gas flow ratios, current, nozzle dimensions) will change the characteristics of the flame, such as: enthalpy, heat density (e.g., temperature distribution and dimensional changes in the flame: length, diameter) and gas-flow dynamics. All of them affect the heat transfer to the particles, the dragging force, and possible trajectories.

Particles are injected axially or radially into the plume. Limited interactions of the carrier gas are expected with the flame. Due to the fact that inert gases (which are commonly used as carrier gases: e.g., argon, nitrogen) and their enthalpies at the feeding conditions are far lower than those of the plume, this interaction is negligible. After the injection, particles absorb significantly the enthalpy of the plume and are melted rapidly. High feed rate levels 'quench' the plume, and there exists the possibility of saturating the capacity of the flame to melt particles. An efficient transference of energy from the plume to the particles is the driving source of melting and kinetic energy that makes possible build up of the coating. Therefore, the control of this flame-particle interaction will enable an optimum particle state control.

Besides flame and particle interactions, the spray environment plays an important role. In-flight oxidation, and chemical reactions (due to the presence of oxygen mainly, e.g., decarburization, point defects) in the flame and especially in the surroundings, make the coating microstructures particular. Vacuum chambers and shrouded flames are sometimes used to reduce this concern.

Upstream the flame chemistry dictates the extent of reactions occurring in the particles, whereas *downstream* the surroundings dominate (see Figure 1-3 for definitions). In air plasma spray (APS), particle melting usually occurs in a few microseconds after the particle is immersed in the flame. Therefore, the molten state of the exterior of the particles makes it more prone to oxidation along the trajectory. On the other hand, in high velocity oxy fuel (HVOF) spraying the melting state is usually described as semi-molten or more appropriately as partially molten (if the regions of the

particle are molten) and/or thermally softened (when the particles are hot and close to melt). This occurs due to the low power flame of HVOF (relative to APS). Although the residence time of particles in the flames (APS and HVOF) are relatively similar (as will be described in Chapter IV), the lower melting state in HVOF can potentially reduce the oxidation.

To minimize oxygen reactions, the control of the flame chemistry by setting oxygen-rich or fuel rich conditions is considered, *upstream;* whereas the reduction of the reactions of hot particles with the air entrained is the key, *downstream.* This is illustrated in Figure 1-3.

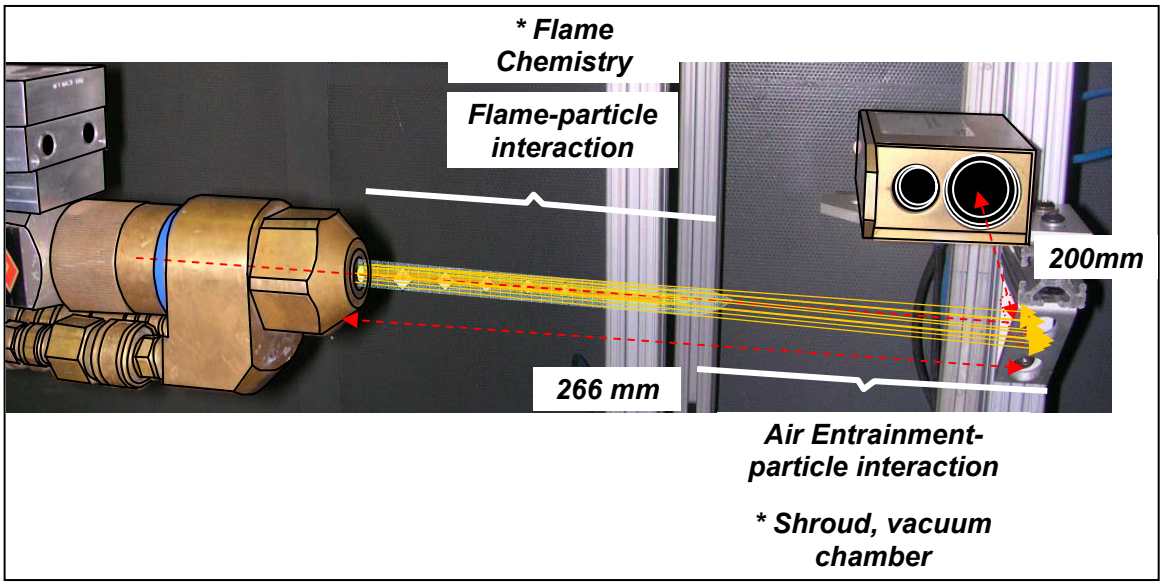

Figure 1-3. Illustration of the stages of the particle flame-interaction. Particles are injected axially. Upstream of the trajectory of the particles the flame chemistry is important whereas downstream the surroundings play the role of oxidant. Shrouds or vacuum chambers have been used to limit the effects of the air entrainment downstream. Picture shows DJ-gun from Sulzer Metco and Accuraspray particle-diagnostics system from Tecnar.

In Chapter III, the benefit of reducing flame chemistries (fuel-rich) will be discussed. A reducing flame in an HVOF-DJ system (DJ-Diamond Jet, from Sulzer Metco) turned out to define a longer flame which not only gives more time to the particle to heat up but also reduces the oxidation of the particle by the surrounding as the flame consumes the oxygen of the atmosphere.

In-flight phase transformations (e.g. oxidation, decarburization) are commonly considered something to avoid. However, in some cases the oxide content brings a positive increment in hardness to the coating. Furthermore, it has been cited in the literature that in-flight oxidation when the enthalpy of formation of the oxide is exothermic (i.e., NiCr forming Cr_2O_3 [2], Mo forming MoO_3 [3], NiCrAlY forming Al_2O_3 [4]) inputs heat that enhances melting of the particle.

For efficient heat transfer from the plume to particles, control of particle trajectory is crucial. In APS by monitoring particle temperature at different carrier gas flows, the

injection of particles is optimized to attain a higher number of molten particles and at a higher melting state (superheated liquid material). This practice not only improves the repeatability of coatings and increases the deposition efficiency but also presumably provides enhanced intersplat bonding with less unmolten particles in the microstructure [5].

In HVOF, the trajectory of particles may not be as important as in APS provided that the particles get accelerated in the constrained section of the barrel/nozzle which propels them "straight" outside axially with the nozzle. This is beneficial to narrow particle state variability within the plume because most of the particles will travel through the hottest sections of the plume with very small angles of deviation. By capturing a splat map (snapshot of the plume) no significant differences have been observed between splats in the center versus the ones in the surroundings, for axial injection HVOF as illustrated in Figure 1-4. Since the particles are heated up along a flame of 150 to 250 mm length, the distribution of temperature and heat *along* the flame are more important than the actual trajectory.

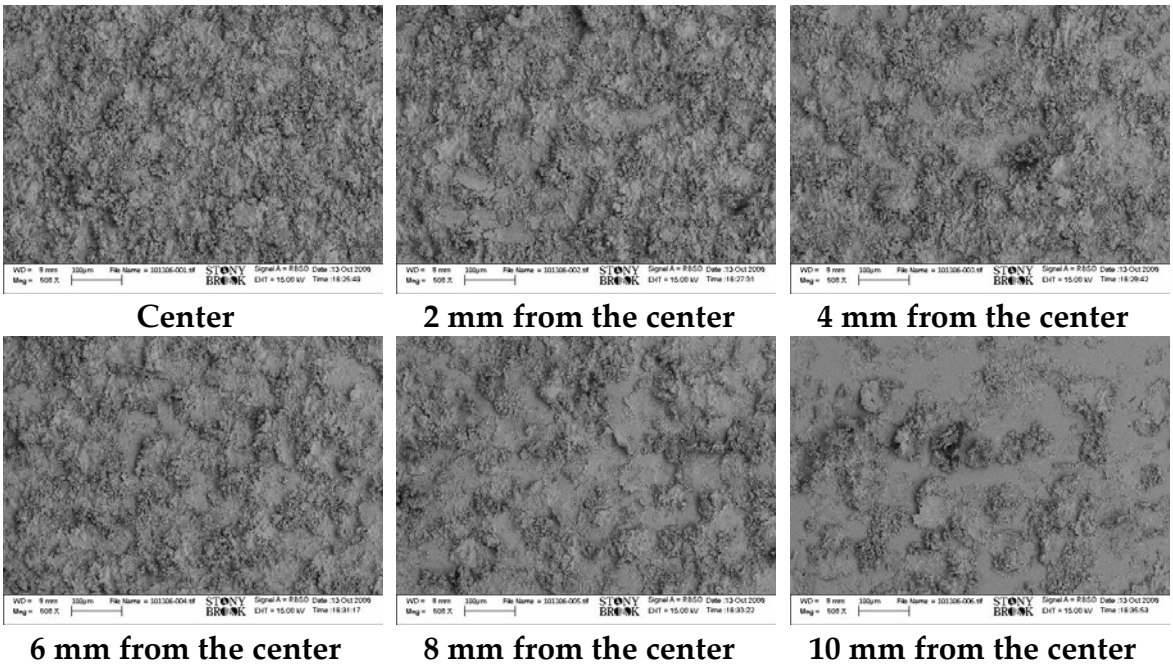

Figure 1-4. Splat Map of NiCr –HVOF spray stream: No appreciable differences in particle state can be observed between splats in the center of the plume comparing to the edges.

1.1.3 Coating Build-up

This stage of the process is characterized by the formation of individual lamella by consecutive/concurrent flattening, bond formation and solidification of particles conforming into splats. Splat formation is dependent on the particle state as well as on

substrate condition ('substrate' describes the underlying layer during spraying). Some considerations of both are described as follows:

1) Particle state involves 1) thermal and 2) kinetic energy. The thermal energy is related to the flowability of the particle during spreading, remelting of the underlying layer and/or availability of heat to receive the next particle. Particle kinetic energy is also related to the flowability (viscous spreading) and surface formation of the splat, but mainly to the bonding strength [6]. This has been the main benefit of HV thermal spray systems where the increased contact pressure presumably has enhanced intersplat bonding. Plastic deformation often occurs during deposition in HV systems owing to the high momentum of the particles during impact. Figure 1-5 shows the plastic deformation of a stainless steel substrate after the deposition of a NiCr splat sprayed by HVOF.
2) Substrate counterpart requires consideration of temperature, roughness, wettability with the sprayed material, heat conduction, and plane of impact. Conduction is arguably the most important, as it determines the splat morphology, substrate melting, and diffusion phase transformations (influenced by cooling rates during solidification).

The flame of the gun also affects the substrate temperature and helps to remove absorbates and condensates during intersplat and interpass interface formation. Depending upon the chemistry of particles, oxidation can also take place after solidification in the layers exposed to the atmosphere.

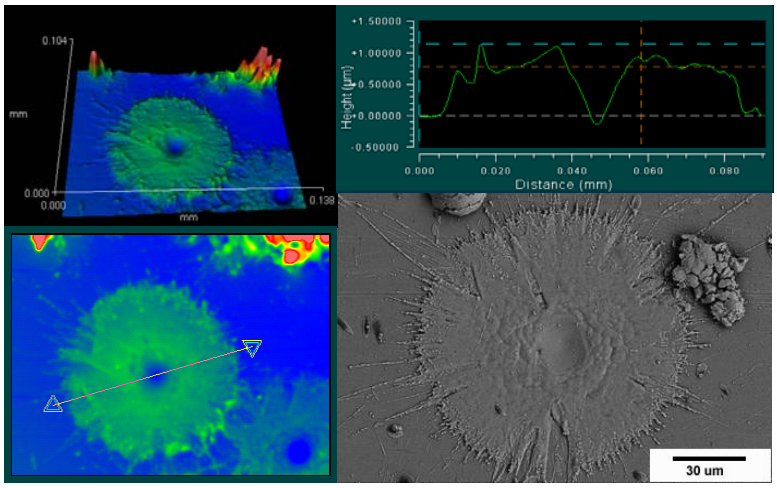

Figure 1-5. Splat of Ni-20Cr sprayed by HVOF. Plastic deformation of substrate is observed in the center of the splat. 3D profiles illustrate dimple formed due to impact.

Many of the properties of interest in thermal spray coatings (thermal, electrical, mechanical, etc.) are highly dependent on the quality of intersplat interfaces. Metallurgical bonding is preferred, although in most cases intimate mechanical contact occurs. However, the presence of oxides on the exterior of the particles at impact, and

limited lateral flow to fill up the gaps, results in defects such as globular and interlamellar pores. In addition, cracks also form within the splats owing to quenching (tensile stress buildup due to constrained volume change after solidification) which can affect the overall mechanical properties and performance. This particular architecture of thermal spray coatings reduces their property values with respect to the ones of the parent bulk materials. The latter can be advantageous for instance when decreasing thermal conductivity as in TBC's, but unfavorable when mechanical strength is required as in wear resistance applications.

Thus far, the importance of particle state and substrate temperature (or deposition temperature) in coating microstructure buildup has been discussed. The control of particle state takes place prior to actual impact (as discussed in the previous section). Now, the control of deposition temperature needs consideration of the time frame in which the impact, spreading and solidification take place. Even though the overall substrate temperature measured by non-contact pyrometers or contact thermocouples represents a reference number for the whole spraying session, this is not the actual temperature that particles experience during consolidation.

Bansal et al [7] estimated for HVOF deposition of stainless steel particles that within the same layer or pass formation, individual particles get deposited over an underlying splat at around 1/3 Tm after ~0.2 miliseconds (ms). This elapsed time between splat-splat within the same pass is controlled by the feed rate of the spray process. It is widely accepted that for traditional TS, when a second particle spreads over a splat, the first has already solidified. Spreading occurs within nanoseconds to a few microseconds (ns-μs), whereas solidification occurs from 3-10 (μs) microseconds [6]. This is due to the fact that cooling rates are extremely high for thermal spray processes (i.e., 10^6-10^8 K/s for APS [8]) and even higher for high velocity processes owing to the improved intimate contact (10^8 -10^{10} K/s for HVOF [9]). Time scale of splat-splat formation is in the range of 0.1 to a few (ms).

For a typical spray parameter used in the present research for NiCr powder and a JetKote spray torch, a feed rate of 40 g/min and a robot speed of 1 m/s could define a flux of particles of 2.1×10^8 per m^2s. The foot print diameter is around 10 mm and allows the buildup of around 0.050 mm coating thickness per pass. This represents 12 - 20 particles deposited on top of each other in one raster of the gun. The resultant elapsed time between splat-splat impact is 0.4-0.8 ms. Very likely, particles deposit after the previous splat has solidified and cooled for a few microseconds. It is important to note that 30-40% of the particles impinging on the surface bounce off after having compacted, deformed, and peened the previous deposited layer.

For process design, the consideration of deposition temperature is indispensable. Whether the goal is to tailor residual stress state, compaction, phase transformations and/or micro-cracking, variables such as feed rate, pass rates, cooling or standoff distance are key factors to control deposition temperature and the overall deposit formation dynamics.

1.1.4 Post Deposition Treatments

Thermal spray coatings are often subjected to post processing to establish final dimensions and occasionally for improving or changing microstructure. Expected improvements include [10]:

- Changed microstructure (although many high temperature treatments may detriment the microstructure, i.e. by decomposition in WC-CoCr [11])
- Enhanced bonding strength
- Relaxation of residual stress (although thermal mismatch stress will always be present after annealing)
- Closure and reduction of porosity
- Hard phase precipitation
- Improved homogeneity, among others

The following post treatments for microstructural changes are rare and only applied to very specific applications or for research purposes. Post treatments include [10]:

- Chemical/physical treatments (organic sealing, aluminizing, chrome plating)
- Thermal treatments (heat treatment, diffusion, recrystallization, laser glazing, hot isostatic pressing)
- Mechanical treatments (shot peening, hot isostatic pressing)

1.2 High Velocity Thermal Spray (HVTS) Processing

The nature of TS coatings, buildup particle-by-particle, defines a unique lamellar structure with different levels of porosity, crack, and oxidation content. The high surface area per unit volume of molten material in the particles makes this surface coating process very prone to high levels of oxidation and decomposition in-flight. In the early years of the TS industry, shrouds surrounding the plume of plasma spraying guns were used to restrict oxidation. Vacuum chambers/low pressure inert gas environments were another alternative towards restricting the oxidation and making denser coatings owing to the reduction in friction of the surrounding atmosphere for the in-flight particles.

HVTS processes allow dense coatings with limited oxidation due to the shorter residence times of the particles in a relatively lower temperature flame at competitive production costs. Among HV spraying processes, HV Oxygen Fuel (HVOF) spraying is leading the market for its versatility to deposit dense ceramic, metallic/alloy and cermet coatings. Main applications include coatings for the landing gear components, paper rolls, ball valves, bond coats for TBCs, corrosion resistant coatings in boilers, etc; as illustrated in Figure 1-6. The attempt to replace chrome-plated coatings due to environmentally deleterious conditions has brought much attention to HVTS processes in recent years [12]. The Hard Chrome Alternatives Team, HCAT, a bi-national team US-Canada validated the usage of cermet coatings (WC-CoCr) by HVOF to replace chrome plating at repair depots, and on commercial and military aircraft landing gears. Detailed performance studies (e.g., wear, fatigue, impact) were carried out to ensure equal or enhanced reliability of HVOF coatings compared to chrome-plating and others.

Figure 1-6. Traditional applications of HVOF coatings for several engineering components

However, cermet coatings such as WC-Co and CrC-NiCr have shown susceptibility to oxidation via decarburization reactions mainly due to the presence of free oxygen in the combustion reaction. A few years ago, in a new attempt to restrict oxidation, HV Air Fuel (HVAF) process emerged replacing the oxygen by compressed air in the flame. This has the dual effect of reduced particle temperature and reduced propensity for oxidation. However, the deposit quality was not equivalent to HVOF in terms of certain performance attributes. In the most recent years, cold spraying (CS), a new HV spraying process emerged as an alternative to depositing ductile materials without melting the particles, consolidating purely via kinetic energy. The CS coating is deposited by the successive impact of particles of ductile metals or alloys that plastically deform consolidating themselves over the substrate. HV plasma spraying has also emerged as a versatile technology to spray at low and high particle velocities. A convergent-divergent nozzle has been added to the traditional plasma plume to attain supersonic speeds for radially injected particles. The present dissertation will discuss results from HVOF spraying systems and HV plasma spraying and little about cold spray. Some results from atmospheric plasma spraying (APS) are discussed for reference.

1.3 Detailed Description of HV Processes

1.3.1 HVOF: High Velocity Oxygen Fuel

The synthesis and application of many dense coatings have been made possible by the high velocity oxy-fuel (HVOF) process. HVOF consists of a combustion flame of about 3000 K and gases accelerated to about 1000 m/s. Particles are injected inside the

nozzle, axially or radially into the flame, melted (or thermally softened) and accelerated towards a substrate were they deposit to form dense coatings with excellent adhesion.

There are a number of HVOF spray devices which use different methods to achieve high velocity spraying. Figure 1-7 shows examples of the most well known commercially available guns, including Diamond Jet (DJ) –from Sulzer Metco-, JP-5000 and HV2000-from TAFA-Praxair-, JetKote – from Deloro Stellite and Detonation gun or D-Gun –from Praxair Inc.

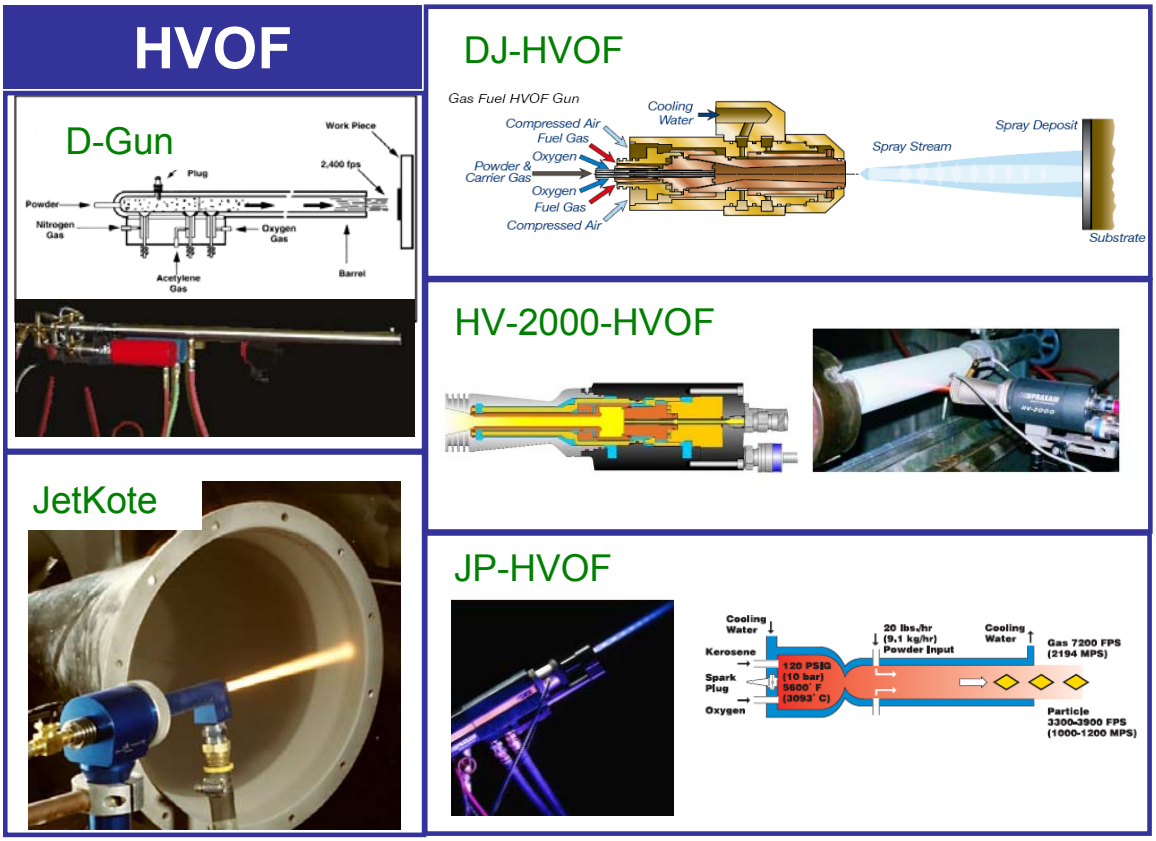

Figure 1-7. Schematics and photographs of commercial HVOF Guns; convergent-divergent nozzles (de Laval) as well as straight barrels are illustrated

Most HVOF systems use high-pressure water-cooled combustion chambers and appropriately designed nozzles. Fuel (kerosene, acetylene, propane, propylene, methane or hydrogen) and oxygen are fed into the chamber; combustion produces a high temperature, high-pressure flame which is forced to exit down a nozzle increasing its velocity. Powder may be fed axially or radially into the HVOF combustion chamber under high pressure or fed through a side nozzle where the pressure is lower. Characteristics of each system are summarized in Table 1-1.

.

HVOF Gun/System	Manufacturer	Gases / Fuel	Powder Feeding		Cooling Method	Unique attributes
			Axially	Radially		
Diamond Jet / DJ	**Sulzer Metco**	**O_2, Air/ H_2, C_3H_6, C_3H_8,**	in the combustion chamber		Air / Water	De Laval Nozzle
JP-5000 / 8000	**TAFA / Praxair Inc**	**O_2 / Kerosene,**		in the barrel	Water	Ignition by spark plug / High pressure
HV-2000	**TAFA / Praxair Inc**	**O_2 / H_2 , C_3H_6, C_3H_8, C_2H_2**	in the combustion chamber		Water	Straight barrel / Sprays dense ceramics
JetKote	**Deloro Stellite**	**O_2 / H_2 , C_3H_6, C_3H_8, C_2H_2, CH_4**	in the combustion chamber		Water	Straight barrel
Detonation Gun/ D-Gun	**Praxair Inc**	**O_2 / C_2H_2**	in the combustion chamber		Water	Ignition by spark plug / Long Straight barrel
C_3H_6 : propylene, C_3H_8 : propane, C_2H_2 : acetylene, CH_4 : methane						

Table 1-1. Commercially available HVOF systems

HVOF coatings are generally near bulk density, hard and show low residual tensile stress or, in most cases, compressive stresses, which enable the production of thicker coatings than previously possible with other processes (e.g., APS). The very high kinetic energy of particles striking the substrate surface does not require the particles to be fully molten to form coatings of high perfomance. HVOF has become the quality standard for carbide and cermet materials as gas velocities over 1000 m/s allow particle velocities over 600 m/s. The result is coating approaching bulk density with bond strengths above 60-70 MPa.

1.3.2 HVAF: High Velocity Air Fuel

As mentioned before, HVAF is a modification to the HVOF process by eliminating oxygen with air as the oxidizer. This generally tends to reduce the overall combustion efficiency and therefore the flame temperature. There is anecdotal evidence that the particle velocities are somewhat higher due to higher flow rates, but this does not appear to be particularly significant. Lowering of the flame and particle temperature reduces the propensity for decomposition/oxidation reactions of the powder, and this is a perceived benefit of HVAF. In fact previous work at Stony Brook has verified that WC-Co coatings can be deposited with no decarburization. However, the lack of thermal input also suggests that the coating performance in some cases is not as high as HVOF coating. Thicker coatings have been possible with HVAF. Technical details and illustrations of HVAF are presented in

Table 1-2 and Figure 1-8.

HVOF Gun/System	Manufacturer	Gases / Fuel	Powder Feeding		Cooling Method	Unique attributes
			Axially	Radially		
HVAF	**Unique Coat Technologies'**	**O_2, / C_3H_6, C_3H_8, C_2H_2, CH_4**	in the combustion chamber		Air / Water	Cascade combustion

Table 1-2. Commercially available HVAF system

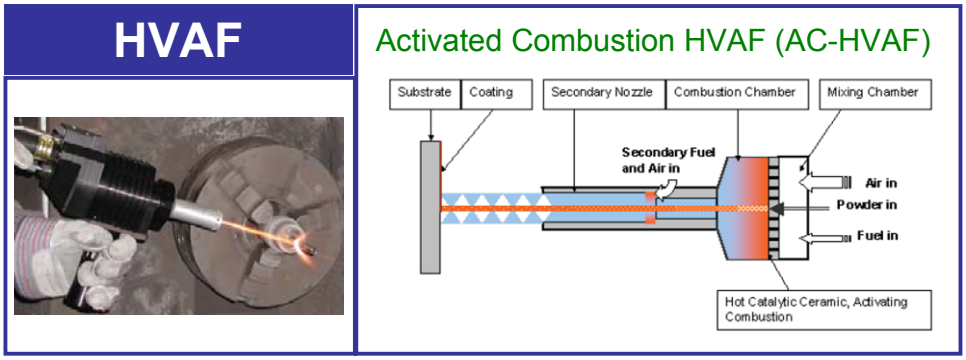

Figure 1-8. Photograph and schematic of commercially available HVAF Gun [13]

1.3.3 Cold Spray and Related Kinetic Energy Technologies

The Cold Spray (CS) or the cold gas-dynamic spraying process is the next step in the development of high kinetic energy coating processes. Similar in principle to the other thermal spray methods, it follows the trend of increasing particle velocity and reducing particle temperature as for the HVOF/HVAF processes, but to a more extreme level. There is some questions, in fact, whether CS process fits under the description of thermal spray.

The CS process uses the energy stored in high pressure compressed gas to propel fine powder particles (below 20 μm size) at very high velocities (500 - 1500 m/s). Compressed gas (usually helium) is fed via a heating unit to the gun where the gas exits through a specially designed nozzle (de Laval type mostly) at very high velocity, as described in Figure 1-9. Compressed gas is also fed via a high pressure powder feeder to introduce powder into the high velocity gas jet. The powder particles are accelerated and moderately heated to a certain velocity and temperature, where, on impact with a substrate, they deform and bond to form a coating. As with the other processes a fine balance between particle size, density, temperature and 'critical' velocity are important criteria to achieve the desired coating.

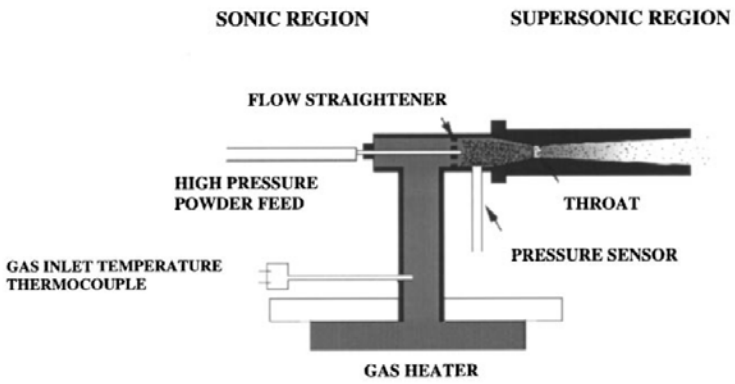

Figure 1-9. Schematic of Cold Spray System. [14]

In flight, particles remain in the solid state and are relatively cold, so the consolidation is via solid state impact. The process imparts little to no oxidation to the spray material due to its low temperature, so surfaces stay clean which is said to aid in bonding. No melting and relatively low temperatures result in very low shrinkage on cooling, plus with the high strain induced on impact, the coatings tend to be stressed in compression due to peening. Low temperatures also aid in retaining the original powder chemistry and phases in the coating, with only changes due to plastic deformation and cold working.

Consolidation (it is not clear if there is metallurgical bonding) relies on sufficient energy to cause significant plastic deformation of the particle and substrate. It is speculated that under the high impact strains and strain rates, interaction of the particle and substrate surfaces probably cause disruption of oxide films promoting contact of chemically clean surfaces and high friction generating very high localized heating promoting bonding similar to friction or explosive welding.

Efficient deposition of coatings at present is limited to ductile materials like aluminum, stainless steel, copper, titanium and alloys. Hard and brittle materials like ceramics are difficult to be sprayed in the pure form, but may be applied as composites with a ductile matrix phase. Substrate materials are also limited to those that can withstand the aggressive action of the spray particles. Soft or friable substrates will erode rather than be coated.

Advantages	Disadvantages
Low temperature process, no bulk particle melting. Very little oxidation	Limited capacity to spray hard brittle materials
Retains composition/phases of initial particles. Low defect coatings	Not all substrate materials can be sprayed
High hardness, cold worked microstructure	High gas flows, high gas consumption. Helium very expensive unless recycled
Eliminates solidification stresses, enables thicker coatings,	Retains peening stresses
Lower heat input to work piece reduces cooling requirement	Interparticle bonding is presumably weak due to lack of thermal input.

Table 1-3. Comparison of advantages and disadvantages of CS technology

1.3.4 Warm spray

There exist several anecdotal references to a concept referred to as warm spray. Examples of devices include a "heated cold spray apparatus" to promote a moderate particle temperature or tuning down the HVOF to maximize the efficiency benefit and while reducing overall temperature.

The latter technique is being developed in Japan [15]. Of key importance is to optimize the temperature of the supersonic jet immediately before injection of the feedstock powder. This is achieved by incorporating a mixing chamber where inert gas (i.e. N_2) is introduced between the combustion chamber (section which forms a supersonic jet) and barrel (acceleration zone) in a commercial high velocity oxy-fuel (HVOF) spray device, as illustrated in Figure 1-10 for a modified JP-5000 gun. The mechanism of particle deposition involves acceleration of the supplied powder to supersonic speed maintaining its temperature below melting point, and continuous deposition using mainly impact energy as the driving force.

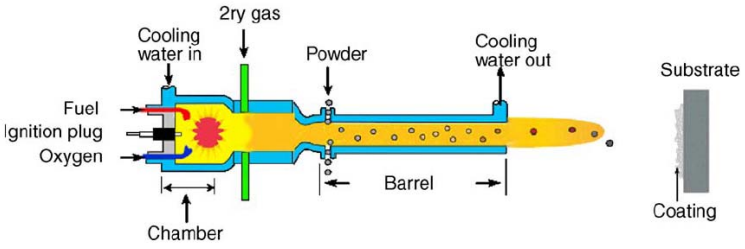

Figure 1-10. Schematic diagram of the warm spray device [15]

According to NIMS Japan, wide application of warm spray is expected in the future, taking advantage of the following features:

1) Because the temperature of the supplying particles is controllable, the structure, composition, phase, and other properties can be kept intact and deposition in accordance with the material design is possible.
2) Because the kinetic energy of the particles is controllable, it is possible to improve the physical properties of the coatings such as density andmechanical properties such as adhesion at the substrate/coating interface.

However, several challenges still remain, in terms of material properties, efficiency and performance.

1.3.5 HV plasma spraying (HVP) spraying

Sulzer Metco Inc. in recent years has launched to the market a new designed plasma gun called Triplex. The uniqueness of this system is the implementation of a triple cathode system with a cascading anode. This results in an arc of prominent length. When the arc passes through a de Laval nozzle, the speed of the plume becomes supersonic. Powder is injected externally and radially to the plume at three equidistant points. The high power of the gun, owing to the use of three cathodes (and actually three plasma plumes) allows the user to spray at three times the traditional feed rate of other plasma guns. The spray distance for HVP spraying is of 200 mm (same as traditional plasma spraying). Particles achieve supersonic velocities (more than 600 m/s) which define a very short dwell-time of the particles in the flame. The definition of particle state is a challenge under these conditions because the high enthalpy of the plume very likely melts the exterior of the particles (surface prone to oxidize, as well) but the short dwell time may limit a complete melting of the core of the particle.

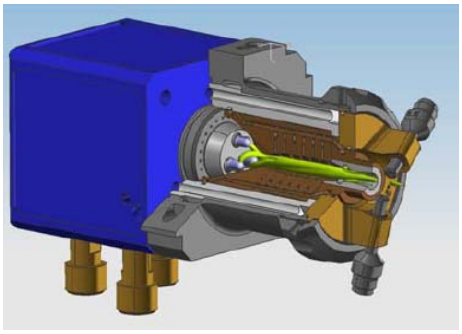

Figure 1-11. Triplex Gun: triple cathode and cascading anode with de Laval nozzle for HVP spraying [16]

Development of HVOF-like coatings is possible from such a torch while using non-combustion energy sources. However, further research is underway to investigate the process-microstructure-property relationships of coatings produced by this method.

1.4 Synthesis of the Introduction

In the present chapter, thermal spray processes and specifically high velocity processes have been described. Applicability and limitations of the processes have been discussed in the context of process control. A comprehensive understanding of all the phenomena occurring during the spray process was explained in detail. The several stages of the process applied to each of the available engineered systems are illustrated in Figure 1-12. Components and interactions can be summarized in five blocks: feedstock, heat source control, supersonic acceleration, surrounding interaction and deposition. Each component demands sufficient understanding and development to control the process and design coatings. The present dissertation will contain discussions of strategies to control the process in the blocks corresponding to heat source/supersonic acceleration (hardware-gun system control), more about deposition (particle state and deposition temperature) control, and little about the surroundings interaction and feedstock.

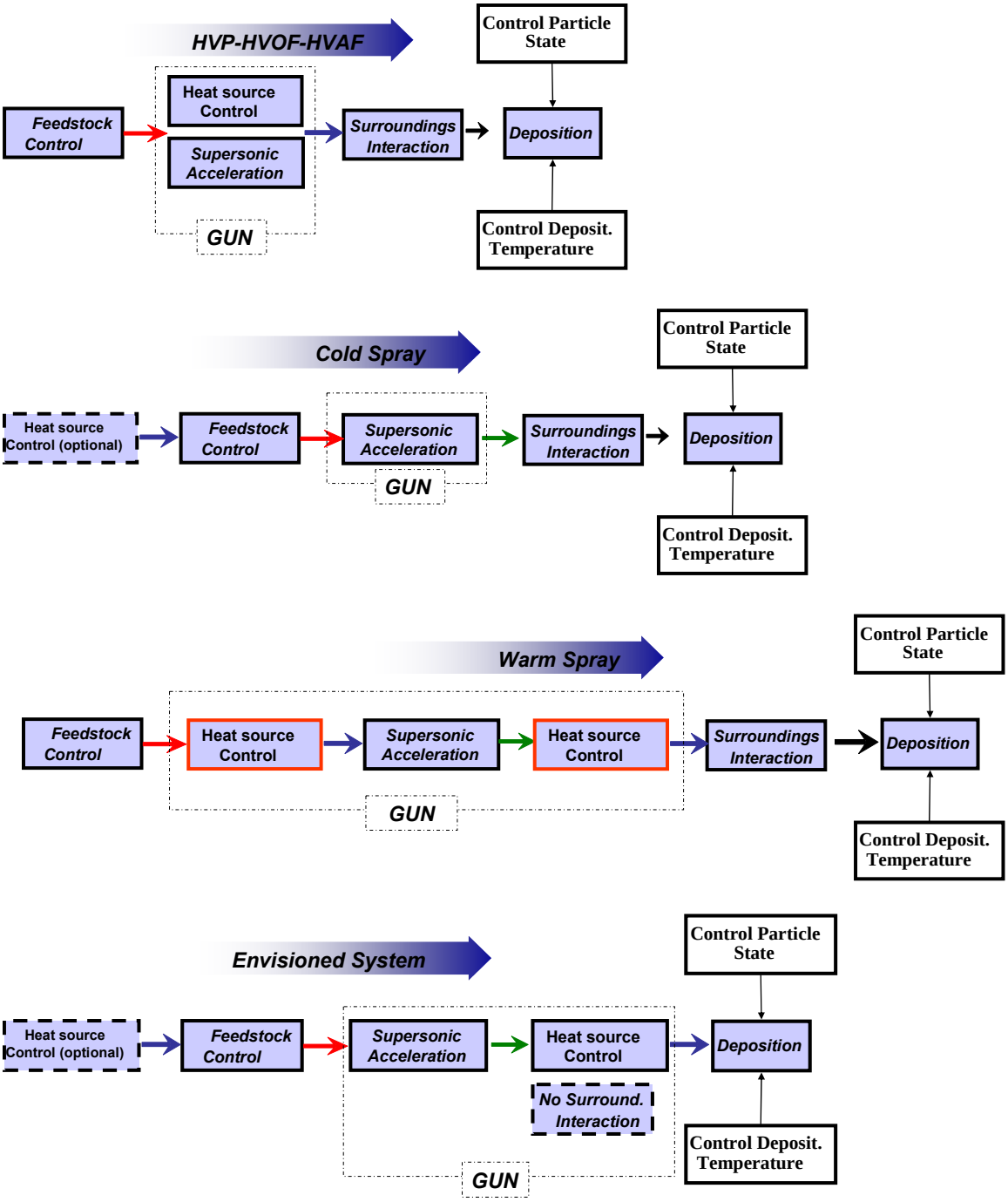

Figure 1-12. Interaction of the stages of the deposition process in HV systems, for: HVOF-HVP-HVAF, Cold Spray, Warm Spray and an envisioned system.

1.5 References

[1] M. Watanabe, S. Kishimoto, Y. Xing, K. Shinoda, S. Kuroda, Journal of Thermal Spray Technology 16 (2007) 940-946.
[2] W.-C. Lih, S. H. Yang, C. Y. Su, S. C. Huang, I. C. Hsu, M. S. Leu, Surface and Coatings Technology 133-134 (2000) 54-60.
[3] W. Zhang, Modeling of In-flight Mo Oxidation during Athmospheric Plasma Spraying, in: Mechanical Engineering Department. SUNY at Stony Brook, 2006.
[4] E. Lugscheider, C. Herbst, L. Zhao, Surface and Coatings Technology 108-109 (1998) 16-23.
[5] V. Srinivasan, M. Friis, A. Vaidya, T. Streibl, S. Sampath, Plasma Chemistry and Plasma Processing 27 (2007) 609-623.
[6] P. Fauchais, A. Vardelle, M. Vardelle, M. Fukumoto, Journal of Thermal Spray Technology 13 (2004) 337-360.
[7] P. Bansal, P. H. Shipway, S. B. Leen, Acta Materialia 55 (2007) 5089-5101.
[8] S. Sampath, X. Jiang, Materials Science and Engineering A 304-306 (2001) 144-150.
[9] L. Li, B. Kharas, H. Zhang, S. Sampath, Materials Science and Engineering: A 456 (2007) 35-42.
[10] ASM International. Thermal Spray Society Training Committee., J.R. Davis & Associates., Handbook of thermal spray technology, ASM International, Materials Park, 2004, p. vii, 338 p.
[11] S.-H. Zhang, T.-Y. Cho, J.-H. Yoon, W. Fang, K.-O. Song, M.-X. Li, Y.-K. Joo, C. G. Lee, Materials Characterization In Press, Corrected Proof.
[12] B. Sartwell, K. Legg, J. Schell, J. Sauer, P. Natishan, D. Dull, J. Falkowski, P. Bretz, D. Parker, Validation of HVOF WC/Co Thermal Spray Coatings as a Replacement for Hard Chrome Plating on Aircraft Landing Gear, in: N. R. Laboratory (Ed.) Naval Research Laboratory, 2004.
[13] A. Verstak, Baranovski, V., AC-HVAF Sprayed Tungsten Carbide: Properties and Applications, in: ASM (Ed.) International Thermal Spray Conference (ITSC07), Beijing, China, 2006.
[14] T. H. Van Steenkiste, J. R. Smith, R. E. Teets, J. J. Moleski, D. W. Gorkiewicz, R. P. Tison, D. R. Marantz, K. A. Kowalsky, W. L. Riggs, P. H. Zajchowski, B. Pilsner, R. C. McCune, K. J. Barnett, Surface and Coatings Technology 111 (1999) 62-71.
[15] J. Kawakita, S. Kuroda, T. Fukushima, H. Katanoda, K. Matsuo, H. Fukanuma, Surface and Coatings Technology 201 (2006) 1250-1255.
[16] F. Muggli, Molz, R., McCullough, R., Hawley, D., Improvement of Plasma Gun Performance using Comprehensive Fluid Element Modeling: part I, in: M. M. H. B.R. Marple, Y.-C. Lau, C.-J. Li, R.S. Lima, and G. Montavon (Ed.) International Thermal Spray Conference (ITSC 07), ASM International, Beijing-China, 2007, pp. 146-151.

Chapter 2
STATEMENT OF THE PROBLEM

2.1 Importance, need and approach to process design

The design of a process to deposit fully functional and reliable coatings is a challenge to the TS industry. By functionality, we not only mean the fulfillment of the demand of properties for an engineered surface, but also the achievement of an optimized performance in life-time at cost-effective conditions. Aiming for *prime reliant* coatings, high *performance* (wear, corrosion, electrical insulation), *repeatability* (day-to-day production of coatings) and *reproducibility* (production of coatings in different facilities) are *sine qua non* conditions. Only a thorough and integrated knowledge of all interactions during the deposition of coatings and their degradation during service could lead to a successful optimization. Therefore, the goal of designing the process to deposit optimum coatings requires both science and technology strategies.

The knowledge in TS technology developed over the past four decades and especially in the last two has added important value and reliability to this technology for many user demands. The understanding in process science, control, deposition phenomena and the unique attributes of the properties of these coatings has made possible the discernment and evaluation of variables towards optimization of coatings for applications.

Typical approaches generally optimize the number of operational variables in a Design-of-Experiments matrix in order to enhance the performance of a coating for a given application. Afterwards, properties of the "promising" coating are evaluated and specified for the application. These methods, although efficient, bring up very limited fundamental understanding in terms of commonalities of processing of different materials.

For a given application, the first step in consideration is the selection of materials and processes, based on the property requirements. If the triad process-microstructure-property relationship would be known, the designing procedure would be simplified to produce coatings of desired microstructures and properties and allow testing/verification of their performance. However, this relationship is particularly complex for thermal spray processes, given that many process variables interact during

the rapid melting and solidification of the particles. When addressing this relationship step by step, we find several questions with not many answers:

Triad *Process-Microstructure-Property*:

- What is the *process* window (particle melting state, particle kinetic energy) in which my TS process can perform? In other words, how sensitive is my process to produce different microstructures?
- What parameters should the operator manipulate to achieve a desired particle state? and, how reliable is this method?
- What is the physical description of the particle state of the selected spraying condition –molten, partially molten, oxidized, decarburized?
- What is the influence of the particle state and deposition temperature on the formation and properties of the sprayed coating? Can we depict differences during the formation of the coating?
- What is the range of properties in a spectrum of microstructures?
- What microstructural features affect the property measurements?

To address these issues, a systematic process-science approach is under development at the Center for Thermal Spray Research which has aided in identifying several fundamental issues and accredited practices for coating deposition. Diagnostics control, simulations of flames, heat transfer and mass transfer phenomena, process parameterization, residual stress analysis, property characterization and many other fields of knowledge have enhanced the opportunities to spray coatings to be fabricated with desired characteristics. Our contemporary understanding suggests that every single thermal spray coating is unique in its properties and only described by a detailed chronological control of particle state and deposition conditions.

Process maps is the adopted strategy in this dissertation to address process design with emphasis on *in situ* monitoring of coating formation via examination of residual stress evolution during deposition.

2.2 Process Design via Process Maps and *in situ* Characterization

Due to the large number of complexities and stochastic events during the deposition of thermal spray coatings, there is a need for a process science approach to link the process control to the applications by means of possible understanding of the particle state, deposition conditions and properties of the coatings and their concomitant integration. A *Process Map*, schematically described in Figure 2-1, in thermal spray can be described as a series of systematic relationships connecting the process variables to the energetic particle state (kinetic, thermal), the dynamic formation of coatings, their properties and the actual performance [1]. Process diagnostics systems and *in situ* monitoring tools will enable the parameterization of the actual process operation by particle state and stress build-up indicators.

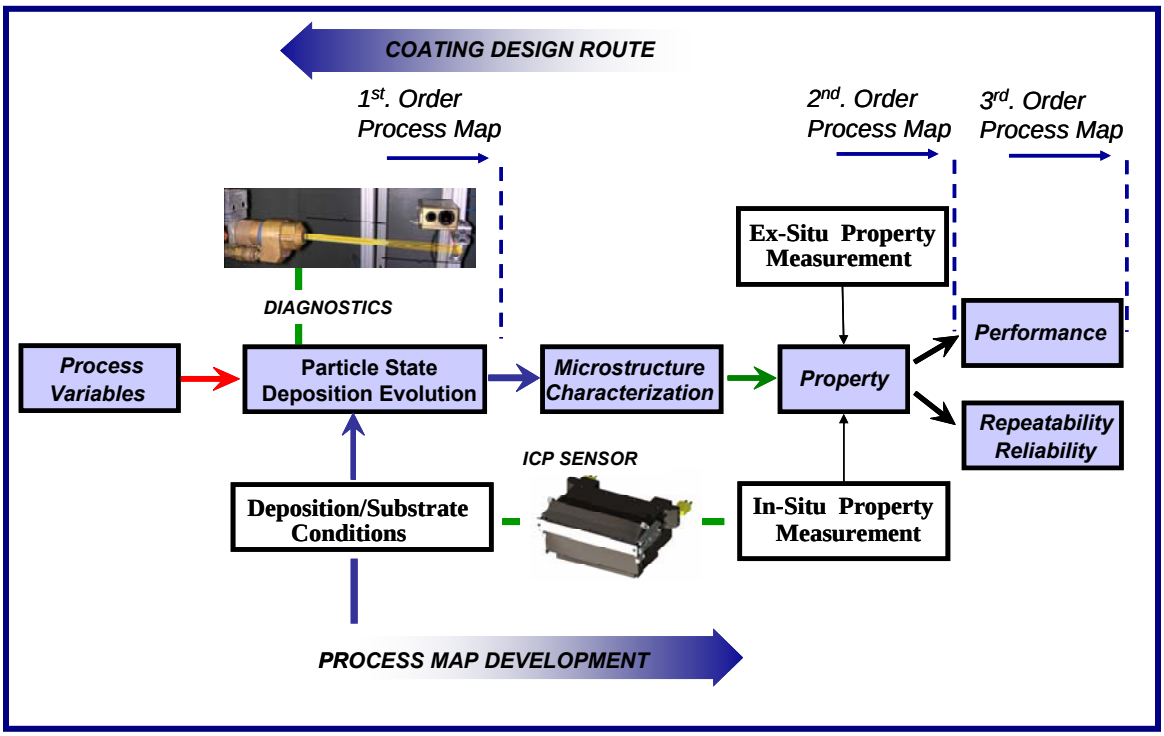

Figure 2-1. Overview of Process Maps Methodology

A first order process map is defined as the relationship between torch hardware parameters and resultant particle state (i.e., first order responses of torch variables). A first order process map, essentially will allow us to capture the versatility of spraying systems by subjecting the particles to different energy states. The latter is described by temperature and velocity of the particles or parameterized related indices like melting index and kinetic energy (or Reynolds number), respectively, either individually or as ensemble averages.

Additionally, the monitoring of the deposit build-up and evolution of stresses during spraying, is achieved via *in situ* curvature sensing [2]. Combination of these two complementary sensing devices will enable the development of a complete process picture and coating design strategies. Variables such as surface roughness, deposition rates, deposition temperature as well as particle states can be correlated to stress in real-time describing qualitatively adhesion, cohesion, peening, and microcracking, among other deposition phenomena.

Subsequently, relevant properties of coatings (obtained both *in situ* and *ex situ*) sprayed in different regions of 1st order process maps will be evaluated and visualized within the framework of a second order process map. Second order maps link the coating properties to particle states and deposition conditions. Ultimately, this allows coating designers to choose a desired combination of properties and correlate them to a particle state, and follow back through the sequence of such maps until defining the process parameters for coating deposition. Combination of microstructural

characterization, such as: micrographs and splat collection will complement the understanding of particle state, oxidation levels, flattening ratios, and pores-cracks architecture of the coating.

It is further envisioned that a third order process map can be developed when evaluating coating performance (corrosion resistance, sliding friction, wear, etc) under different loading conditions to the intrinsic properties identified in the 2nd order maps.

The benefits and throughput of Process Maps that have dramatically enhanced the knowledge of the influence of the processing on the coating properties will be used in this dissertation applied to HV spraying systems. The establishment of process-microstructure-property relationships will identify key process parameters to be controlled and recognize the need of sensor implementation for monitoring and characterization. All in the context of process design strategies.

2.3 References

[1] S. Sampath, X. Jiang, A. Kulkarni, J. Matejicek, D. L. Gilmore, R. A. Neiser, Mater. Sci. Eng. A 348 (2003) 54-66.
[2] J. Matejicek, S. Sampath, Acta Materialia 51 (2003) 863-872.

Chapter 3

PROCESS CONTROL AND CHARACTERIZATION OF METAL BASED COATINGS: A PROCESS MAP APPROACH

3.1 Introduction

Efforts are underway around the world to advance in the understanding of these complex process-material interactions; 1) to design coatings of desired properties and performance, and 2) to narrow the variability of hardware operation and supplies (powder, gases) on the reliability, and repeatability in production of coatings. In this chapter, a systematic study of the process-microstructure-property-performance relationship is presented in the context of process maps for HVOF. These maps are intended not only to be a reference material for coating designers who seek targeted property values but also a methodology for process optimization.

A guide to explore the operational process domain is suggested based on particle state (temperature, T; and velocity, V) measurements. Variations of mass flow of gases (oxygen, fuel, air) are derived into a consistent method to explore the T-V diagram. The usage of other fuel chemistries or nozzle designs, that change significantly the particle state, may be explored under a similar procedure. Coatings were sprayed at selected conditions to study differences during coating formation, property range and performance. Although several authors have attempted analogous exploration [1-6] of the HVOF thermal spray processes, the presented strategy is unique in that it connects process variables to multiple design relevant properties and integrates the various subsets of process manipulation into a unifying mapping theme.

Ni-20%Cr (weight percent) in solid solution was chosen as the representative material for this study. In addition to being representative of typical powder compositions used in HVOF thermal spray (e.g., CoNiCrAlYs, T-800 (CoCrMo)), the system offers simplicity in characterization while capturing many of the important process effects on microstructure including preferential oxidation of its components, residual stresses and heterogeneous microstructural features. Knowledge of bulk property values of NiCr also enables benchmarking process- derived variation in coating properties and connection to the contributing microstructural attributes.

HVOF coatings of Ni-20%Cr material are effective in hot corrosion applications for boilers [7] owing to the low porosity, fine grain size and lamellar structure. During service, there exists formation of oxides in splat boundaries and open pores due to

penetration of oxidizing species. Oxides protect splat material and parent substrate material from further oxidation. This evidence suggests that oxidation levels and bonding quality between splat-splat, which is part of this study, will make the coatings perform in different ways, as reported by Tang et. al [8] studying TGO growth in CoNiCrAlY-HVOF coatings.

A Hybrid Diamond Jet (DJ-Sulzer Metco) Gun with a convergent-divergent nozzle was used in this study although the proposed methodology can be applied across the spectrum of industrial HVOF processes. Particle state was monitored by two-wavelength pyrometry principle (Accuraspray sensor) and several properties (thermal and electrical conductivity, elastic modulus, hardness) were measured in the deposited coatings. The *peening intensity* of the impacting particles was monitored during spraying through a novel *in situ* curvature measurement approach (see Appendix I for details), and correlated to the microstructure, splats, residual stress and hardness of the deposits.

3.2 Process Maps

Over the last decade researchers at the Center for Thermal Spray Research along with various collaborators have vigorously pursued the development and implementation of process maps. A number of examples have been reported in the literature for air plasma spraying of Mo [9] and YSZ [10], and for HVOF spraying of dense alumina coatings [2], etc. Results from these efforts are summarized as follows.

1) Melting state and kinetic energy of the particles and deposition temperature (driven by torch heat input or particle deposition –controlling deposition rates) are the most important factors controlling the microstructure and properties.
2) Temperature and velocity measurements are not full descriptors of the particle state. There is a need to include melting indicators (i.e., melting index [11] – particularly important in ceramics) to reveal the fraction of fully molten to partially molten and unmolten particles.
3) In-sights on control of residual stress states, porosity, splat fragmentation, coating stiffness, thermal and electrical conductivity, and others have been successfully fed back to process parameter control.

Considering the aforementioned benefits of *Process Maps*, this methodology is adopted in this study to achieve optimization in process control and coating properties.

3.3 Experimental Methods.

3.3.1 First Order Process Maps – Design of Experiments

The operating space of any spraying gun can be explored by tuning the flow of gases (for plasma spraying, amperage is also considered as a variable). Thus, in plasma spraying, two gases plus current make three operating parameters and therefore, three variables in the design of experiments, that is to say: total volume flow, ratio of primary/secondary gases and current. In HVOF, two operating gases define two

variables: total volume flow of gases and the ratio between them. Examples of this treatment of variables can be found in references [2, 9].

The DJ-HVOF system used in this study provides three independent operational parameters: oxygen, fuel and air flow. The operating space in this study was explored by tuning two of them: oxygen volume flow and fuel volume flow. Air volume flow was kept constant since its participation in the flame is not clear. It is generally recognized that the oxygen quota of the air may not be fully participating in the combustion reaction while the nitrogen quota may be cooling the flame and nozzle, as well as contributing to the momentum of the particles. Spraying parameters are described in Table 3-1.

The flame energy can be computed from the heat input of the combustion of the fuel exerting a corresponding factor due to the stochiometry of the reaction. Thus, fuel/oxygen ratio, γ is calculated as:

$$\gamma = \frac{\text{fuel flow}}{(\text{oxygen flow} + 0.21 \times \text{air flow})} \quad \textbf{(1)}$$

The stoichiometric ratio for the combustion of C_3H_6 fuel in an HVOF gun is 0.23 from the reaction equation: $1C_3H_6 + 4.307\ O_2 \rightarrow 1.903\ CO + 1.097\ CO_2 + 0.382\ H + 0.432\ H_2 + 2.004\ H_2O + 0.388\ O + 0.745\ OH + 0.698\ O_2$. [12].

Coating	Condition	GAS FLOWS						Energy
		fuel	oxygen	Air	fuel/oxy Ratio	Normalized fuel/oxygen Ratio *	total	
		lpm	lpm	lpm			lpm	Kw
	1	51	207	351	0.18	0.8	621	69.5
A	**2**	60	198	351	0.22	1.0	621	82.2
	3	69	189	351	0.26	1.1	621	81.1
	4	77	181	351	0.30	1.3	621	78.5
	5	83	173	351	0.33	1.4	621	76.1
B	**6**	92	166	351	0.38	1.6	621	73.8
	7	54	225	316	0.19	0.8	619	74.1
C	**8**	63	218	316	0.22	1.0	621	85.7
	9	69	203	316	0.26	1.1	607	83.6
D	**10**	78	196	316	0.30	1.3	608	81.4

* Normalized fuel/oxygen ratios are shown with respect to the stoichiometric value (0.23).
** Nitrogen was used as carrier gas -12 lpm. DJ2700 HVOF System. Aircap: DJ2702. Spray distance 266 mm. Traverse spraying velocity 0.5 m/s. Feed rate: 23 g/min for coating deposition and splat collection, 9 g/min for diagnostics measurements. Supply pressure of gases in the console were kept constant at all times.

Table 3-1. First Order Process Map: spraying parameters of Ni-20%Cr conditions.

Energy input *E* shown in Table 1 was computed according to:

$$E = \upsilon * \frac{\gamma_{stoich}}{\gamma} * \Delta H_c \quad \textbf{(2)}$$

where v is the flow rate of fuel, γ is the ratio of fuel to oxygen, γ_{stoich} is the stoichiometric ratio, and ΔH_c is the heat of combustion of the fuel (propylene C_3H_6 = 82 KJ/(lpm*min)). If the flame is either oxygen rich or stoichiometric, the ratio $\gamma_{stoich} / \gamma = 1$.

Two sets of experiments were conducted at different total volume flow (~620 lpm and ~600 lpm) and varying the stoichiometry of the flame in each, as illustrated in Figure 3-1.

Other variables such as spray distance and deposition rates (combination of feedrate and robot speed) were not considered at this stage of the study for coating deposition but recognized that they play an important role as well. Thus, the effect of feed rate, air flow in the combustion chamber, spray distance on particle state was monitored by diagnostic sensors.

3.3.2 First Order Process Maps – Spraying Parameters

Ni-20%Cr powder (Praxair Surface Technologies, Indianapolis, IN) (particle size 5 to 45 μm) was used to spray coatings at a constant rate of 23 g/min. Powder was of spherical morphology with grain size of about 1-2 micrometers.

A water cooled HVOF DJ-Gun 2700 (Sulzer-Metco, Westbury, NY, USA), with propylene as fuel was used in this study. Average values of temperature and velocity of the spray stream of different conditions were measured with a dual fiber optical sensor device, Accuraspray G3 (Tecnar Automation LTEE, St-Bruno, QC, Canada).

From the design of experiments of a 1st order process map, Figure 3-1, four conditions were chosen to spray coatings denoted as A, B, C, and D, in Figure 3-2 – points (2) (6) (8) (10) respectively in Figure 3-1. The coatings were deposited on plate samples onto the *in situ* Coating Property (ICP) sensor [13]. Low carbon steel plates of 230 mm length, 25.4 mm width and 1.6 mm thickness grit blasted on both sides were used as substrates. Fifteen passes were sprayed in all experiments to produce coatings of 0.3 mm thickness. Thicker coatings (1 mm) were also sprayed at these conditions to be used in indentation and thermal conductivity measurements.

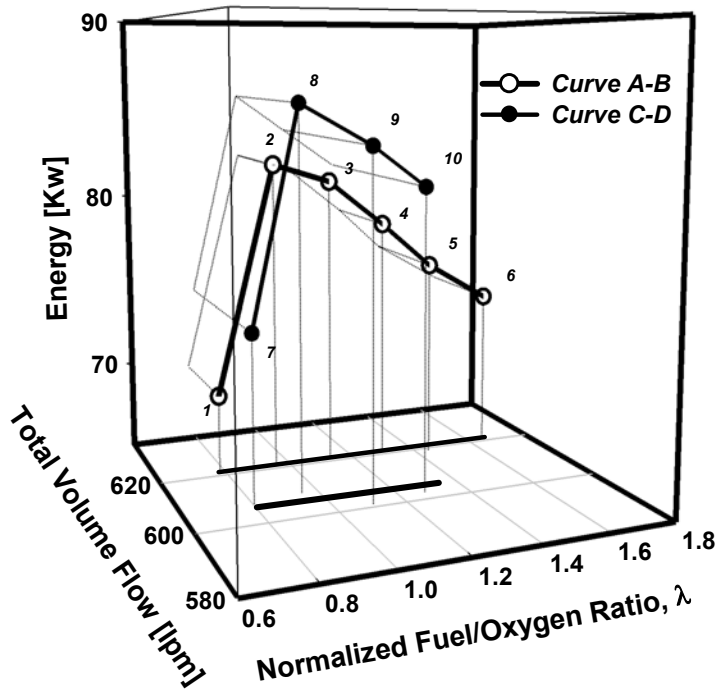

Figure 3-1. Design of experiments, including two sets of parameters at different total volume flow and different gas ratios. Flame energy as a result of the combustion of the fuel is shown in the vertical axis.

Process diagnostics with Accuraspray were carried out at a relatively low feed rate of 9 g/min. The effect of flame quenching due to an increment in the feed rate was investigated on the curve-trend C-D. A feed rate of 23 g/min was used and similar spraying conditions (7)-(10) were sprayed and measured. Similarly, the effect of an increment in air flow fed to the gun was monitored incrementing 35 lpm in all the conditions in the case of the regime represented in curve C-D. Results and trends are shown in Figure 3-3.

Particle temperatures and velocities were also measured along the trajectory of the particles from 166 mm to 266 mm every 25 mm. The gun was mounted on a six-axis robot (FANUC M-16i) which allowed for high precision displacements without bias on control volume for diagnostics. Results are shown in Figure 3-4.

3.3.3 Microstructural Examination

Coating cross-sections were examined by SEM (Leo Zeiss 1550), at 2000X magnification. Coatings were sectioned, mounted in epoxy and polished to mirror finish up to 1 um suspension solution.

Splats were collected onto polished stainless steel substrates kept at room temperature. A shuttering system consisting of a window moved by a pneumatic arm in front of the particle stream was used to collect a snapshot of particles in-flight. A *splat map* (at the same spraying feed rate of 23 g/min) was qualitatively characterized by SEM.

Phase analysis was investigated with X-ray diffraction and conducted on coatings and feedstock powder using K_α Cu radiation (λ=1.54059Å) at 40 kV and 25 mA in a SCINTAG/PAD-V instrument. EDAX on SEM was also used to identify the oxides present.

3.3.4 Property Measurements

3.3.4.1 Thermal Conductivity Measurement

Thermal conductivity measurements were carried out on 12.5 mm diameter and 1 mm thickness free standing coating disks, coated with carbon, using Holometrix laser flash thermal diffusivity instrument. Measurements were made on two samples of each condition for nine times each.

3.3.4.2 Elastic Modulus Measurement

Microindentation testing was carried out on polished top-surfaces of thick coatings bonded to the substrates. Experiments were conducted in an instrumented indenter (Microtest 600, Micro-Materials Limited, Wrexham Technology Park, Wrexham, UK), using a WC-Co Berkovich tip and an incremental load up to 5 N, at room temperature. Elastic modulus was calculated from the unloading portion (elastic recovery portion) of the load-depth records according to Oliver and Pharr method [14]. Hardness was also extracted from this experiment.

3.3.4.3 Stress Evolution and Residual Stress Measurements by ICP (in situ Coating Property Sensor)

A Stony Brook developed *in situ* coating property sensor (ICP) [15] was used to monitor the curvature and temperature while spraying of four plates at the four spraying conditions A,B,C, and D. Calculation of stresses from the curvature measurements are shown in Chapter VI.

3.3.4.4 Electrical Resistivity

Electrical resistivity was measured using a four point probe (Miller FPP-5000) resistivity instrument. It consists of four equally spaced metal tips, with each tip supported by springs on the other end to minimize sample damage during probing. High impedance direct current is provided during the measurement through the outer two probes and the voltage across the inner two probes is measured to determine the sample resistivity. Geometrical factors have to be considered due to the finite size and thickness of the specimen. In this work, the correction factors dependent on sample shape and dimensions were calculated based on the work of Topsoe [16] and Smits [17]. Measurements were made on one sample of each condition for nine times each in different orientations.

3.4 Results and Discussion

3.4.1 Synthesis of a First Order Process Map

As mentioned earlier a *first order process map* represents the relationship between gun parameters and the particle state. Such a map can be represented as a Temperature-Velocity space of the traveling particles with identification of specific operational regimes. Figure 3-2 represents a first order process map of the present study of HVOF NiCr. Several important features are identified on this map.

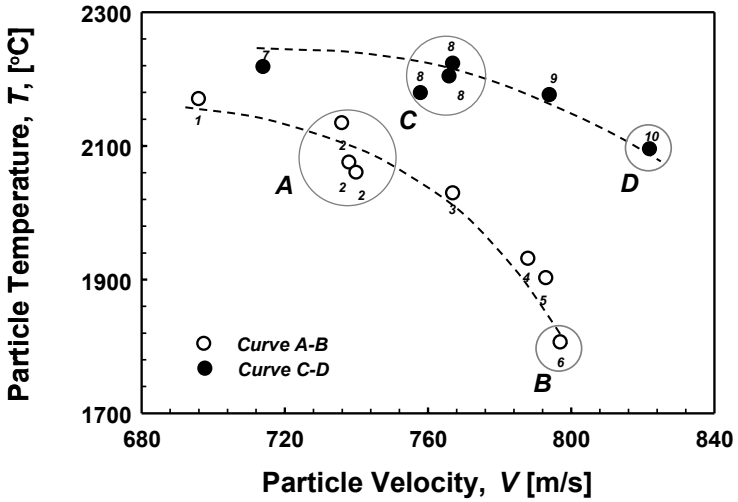

Figure 3-2. First order process map in a DJ-HVOF gun. From left to right, curves A-B and C-D represent particle states of Ni-20Cr particles sprayed at oxygen-rich towards fuel-rich conditions. Three measurements in random order at conditions (2) and (8) were done for repeatability control. Coatings for further characterization were sprayed at conditions denoted as A, B, C, and D.

A trend of particle temperature and velocity was observed when going from an oxygen rich flame to a fuel rich flame. Oxygen rich chemistry conditions cause high temperature and low velocities of particles, and when tuning towards fuel rich conditions, temperature decreases and velocity increases following a parabolic curve. The experiments carried out at higher total volume displaced the trend curves to lower temperature and velocity, which is understandable due to the lower energy input.

Analogous trends are observed in the projection of the curves of Figure 3-1 on plane Energy-Normalized fuel/oxygen ratio in comparison with 1st order process map in Figure 3-2, which suggests that prediction of T-V particle condition can be exercised by energy flame computation. Except for the oxygen-rich conditions, higher energy flames define higher particle temperature at lower velocities, and otherwise. The energy computation of these oxygen rich conditions assumes equilibrium combustion reactions that at the very fast reaction rate occurring inside the nozzle may under predict the energy input at this condition. Gas input enthalpies and dissociation of not only fuel (C_3H_6) but other species like CO_2 and H_2O also contribute to the energy of the flame and

are not considered here. The values proposed here are not intended to be exact, but a relative framework to identify the kinetic and thermal energy transferred to the particles.

An independent increment of air flow to the flame results in decrease of the temperature and increase of the speed of the particles, as in Figure 3-3. This suggests that the main effect of the air flow was not to increase the energy input by adding extra oxygen to the flame but, to increment the drag force to the particles, shortening their dwell time. The magnitude of the temperature and velocity change is relatively small in comparison to what can be achieved by tuning the fuel-oxygen mixture. Feed rate was also found to play a role in the temperature and velocity of the ensemble of particles. The typical flame quenching effect was observed when increasing the flow rate from 9 to 25 g/min. The parabolic trends to scan the T-V space were found not to be susceptible to change to either linear increment of air flow or flame quenching.

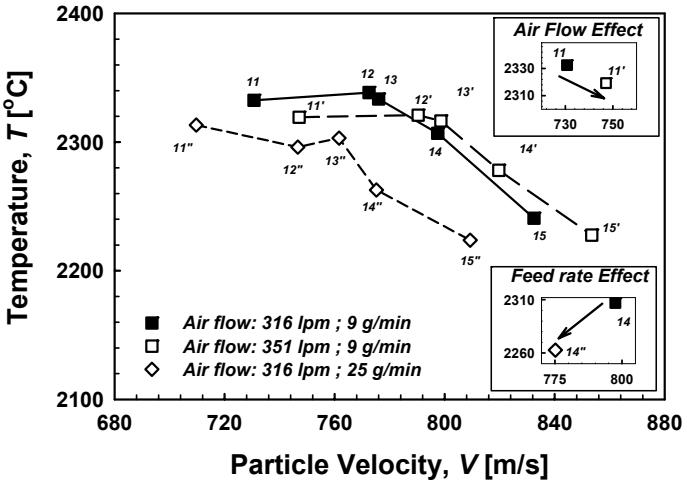

Figure 3-3. Effect of air flow and feed rate increment on the particle state. Note conditions (11) to (15) correspond to conditions (7) to (10) of curve C-D in Figure 3-2, after hardware renewal. Inset –top right- illustrates the magnitude of T-V change in particle state due to air flow increment for condition 11. Inset –bottom right- illustrates the same for condition 14 due to and increment in feed rate.

3.4.2 Particle State Monitoring along the axial trajectory

Particles accelerate within the divergent section of nozzle and the first ~100 mm outside the nozzle [12]. Afterwards, the gas-flame decreases in velocity and temperature and simultaneously, more and more retarding force acts on the particles due to air entrainment. For this reason, particles decelerate as observed in conditions A, B in Figure 3-4.

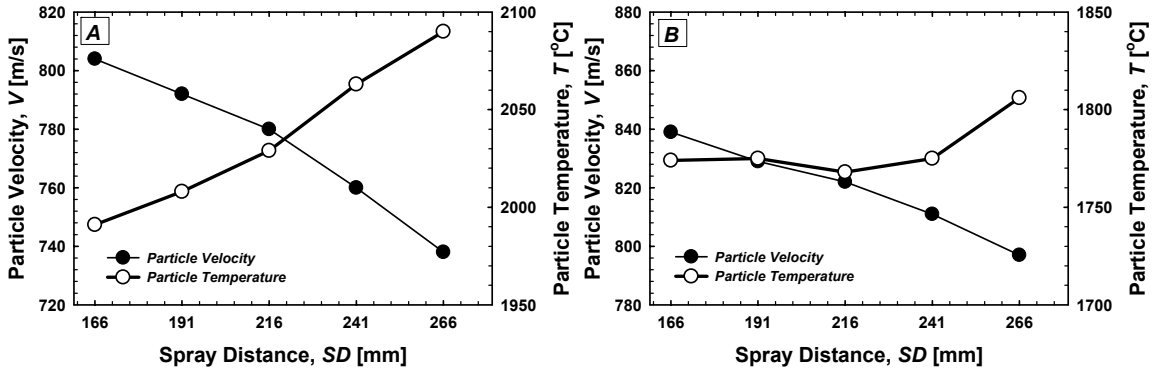

Figure 3-4. Particle temperature and velocity for conditions A and B, at different spray distances.

The plume jet core changes substantially from oxygen-rich to fuel-rich conditions. The higher amount of fuel extends the combustion to the outside of the nozzle. As a result, longer flames are observed. It is expected that longer flames reduce the resistance of the surrounding air due to the low density of the gases at high temperature. For this reason, particles decelerate less in B condition compared with A for the same trajectory.

The temperature trends are also notable. Temperature was found to increase as the particles fly away from the nozzle. Although particles are in a colder atmosphere as they travel, the oxidation is enhanced in this downstream region due to extensive air entrainment within the combustion flow field.

The enthalpy of the exothermic reaction of formation of chrome oxides, Cr_2O_3 is around -925 kJ/mol, and can input sufficient heat as to increase temperature significantly in the depleted NiCr of the particle. Moreover, measurements are consistent with the fact that a longer flame (B) would protect the particle from oxidation by means of shortening the interaction with the surroundings downstream of the flame. This is enhanced by the fuel burning the oxygen of the surroundings upstream. As a result, B shows a small increment in particle temperature and only at the deposition distance (266 mm) where the flame is essentially extinguished. Microscopy analysis indicates highest oxidation of particles sprayed at stoichiometric conditions whereas fuel rich conditions (longer flames) show less oxidation.

Note that scanning the temperature drop or increment along the spray stream may be a useful tool (when the oxide formation is an exothermic reaction in the feedstock) to optimize the torch parameters with respect to designing coatings with appropriate oxide content. Similar results where observed by Lih et. al. [6] when spraying CrC on a matrix of NiCr, and Lugscheider et. al. [3] spraying NiCoCrAlY.

3.4.3 Microstructure Characterization

Figure 3-5 shows the cross-sectional microstructures of the various deposits. Overall coatings show high density and no apparent porosity. Coalescence of intersplat

boundaries is expected to contain metallurgical bonding owing to the high temperature of the particles. However, the presence of interlamellar oxide can also modify intersplat interfaces. Significant differences are observed in the four cases. High resolution micrographs support the observations, however not all are presented here.

1) A and C conditions show a lamellar structure with apparently no interlamellar porosity but oxides. A structure of thin flattened splats can be observed. Relatively, longer residence times in the flame for particles at A and C conditions resulted in greater oxidation. Image analysis results are presented in Figure 3-6, C being a higher temperature condition shows slightly higher oxide content than A.

2) B shows a lumpy microstructure due to lack of liquid flow. Very few globular pores are observed and no interlamellar pores were observed at the magnification used. Oxidation on the splat is very low owing to the shorter residence time and the shielding effect of the reducing flame.

3) D condition shows combined attributes of A-C with B features. Although D experienced a shorter residence time, it clearly experienced a larger heat input in the flame which promoted the oxidation of the particles in contrast with B.

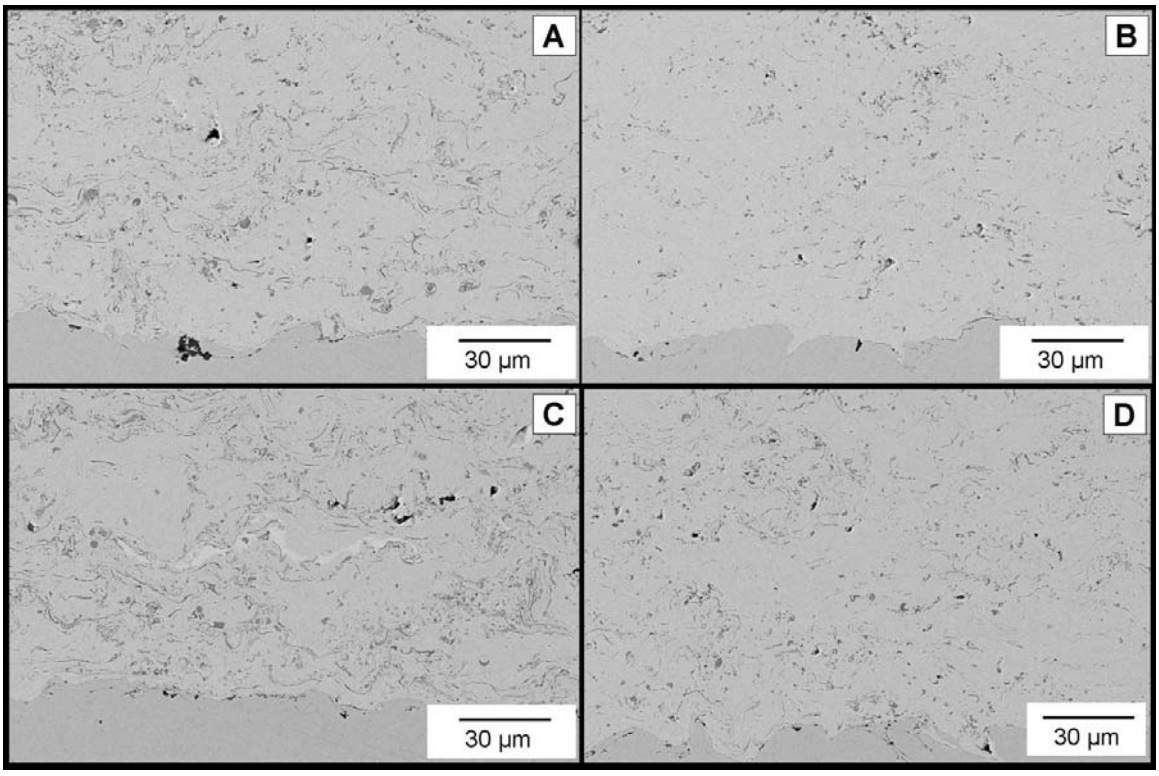

Figure 3-5. SEM images (2k X) of four Ni-20Cr coatings sprayed at different particle state conditions shown in Figure 3-2.

In the literature, authors have reported the presence of NiO as the oxide present when spraying Ni-20Cr [4] with a Jetkote system with propylene as fuel at different spraying conditions. On the other hand, Sidhu et al [7, 18] have reported that Cr_2O_3 is

prone to form during the spraying of Ni-20Cr wired feedstock by HVOF. In the present study, EDAX has suggested that the oxide present in the as-sprayed coating shows high content of Cr, and likely is Cr_2O_3. XRD diffraction patterns did not identify diffraction peaks of chrome oxides, probably due to the low content of the oxide, texture in the coatings, and/or roughness effects.

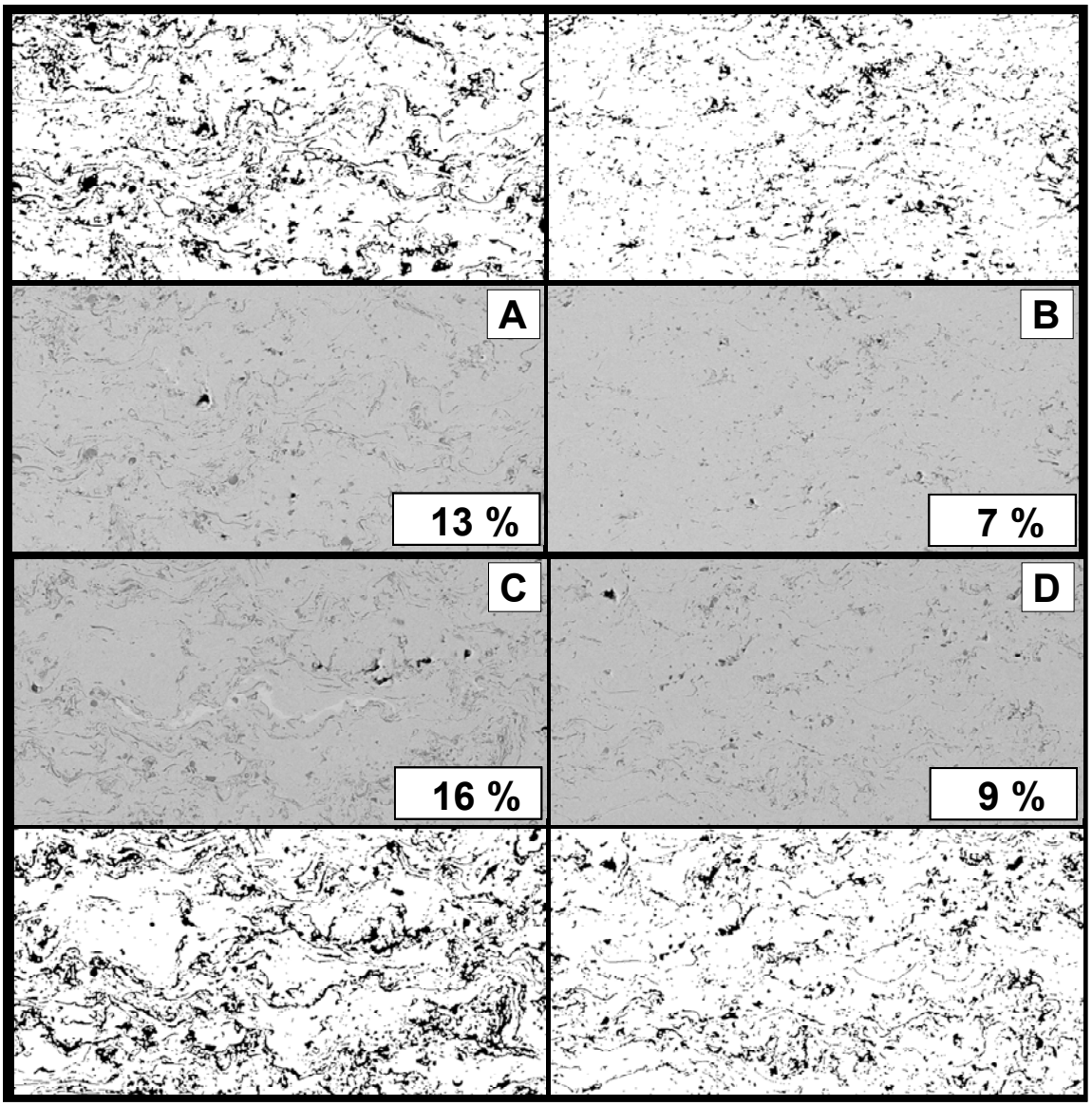

Figure 3-6. Oxide content analysis via image analysis for deposited coatings.

3.4.3.1 Splats – splat maps

Splats represent the building blocks of a thermal spray coating and as such provide an excellent visual representation of processing effects. Splats were synthesized at the four identified process conditions (A, B, C and D and are shown in Figure 3-7). All the

samples showed an assortment of molten and partially molten particles in the center-populated and scattered areas.

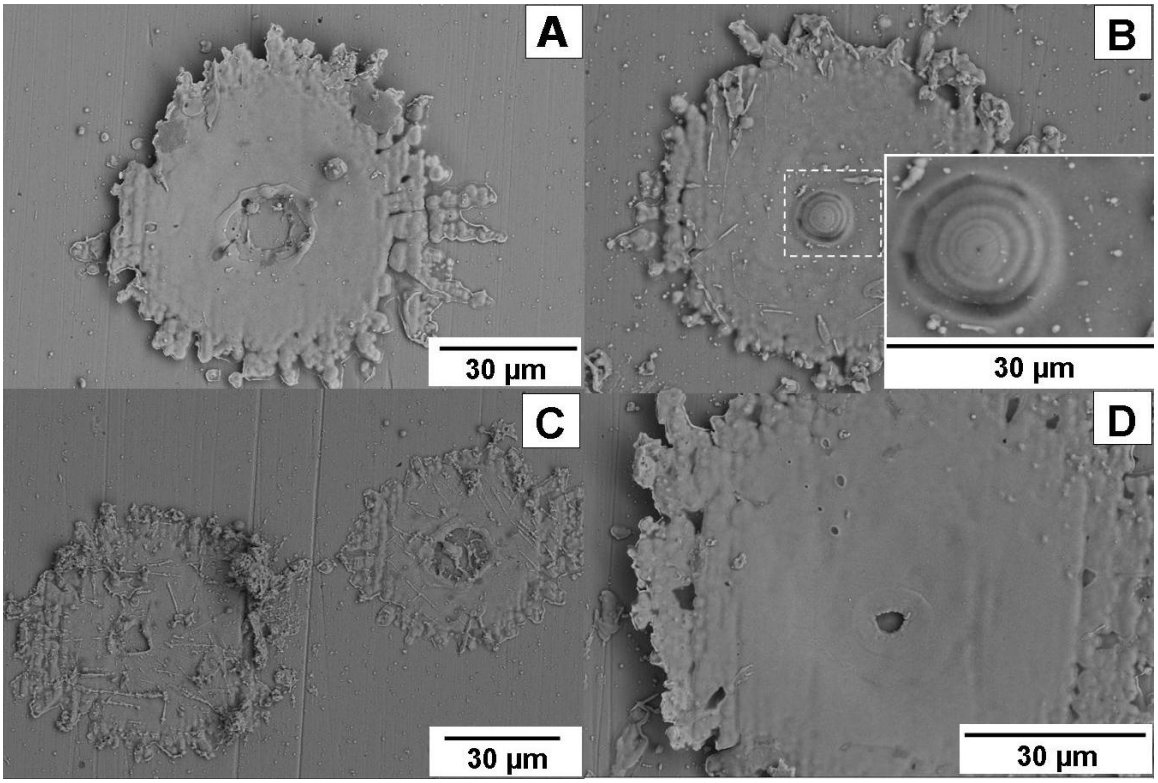

Figure 3-7. Individual splats collected from the four different conditions, showing craters in the center point due to release of gas trapped during impact. B condition shows gas trapped. Inset shows magnifications of dome formed on top of gas pocket.

By analyzing scattered splats some discrimination can be made about their in-flight history and deposit formation dynamics. It was found that smaller particles experience more oxidation in conditions of high particle temperature, such as A and C, whereas B particles of the same scale-size are not as oxidized. This is in agreement with the microstructural features reported in the cross-sections. In terms of morphology, Figure 3-7 also illustrates typical splats of different melting states. In A, C, and D, the air pocket that usually gets trapped when spraying particles at high velocity [19] was freed after the spreading of splat, but in B, the higher viscosity due to a lower melting state retains the air pocket. Columnar grain growth was observed on the splat surface and following the dome that trapped the air (see inset condition B). It should be noted that splats show much smaller grain size than the original particle grain size seen in the feedstock, which is an indicator of the full melting state of the particles when the impact occurred.

3.4.4 Second Order Process Maps

3.4.4.1 Thermal Conductivity

In reference [20], it was found that thermal conductivity (*k)* of Ni-5%Al by different thermal spray processes is enhanced by a combination of high kinetic energy and high thermal energy. As a result, metallic HVOF coatings showed higher thermal conductivity than air plasma, arc spray and cold spray processes. Thus, it is expected that improved interaction of the interlayer/intersplat interfaces by intimate contact or metallurgical bonding will result in high thermal conductivity. Expanding on this principle, in the second order process map of thermal conductivity, Figure 3-8a, it can be observed that the region of high kinetic energy (enhancing compaction), and high thermal energy (enhancing wetting and metallurgical bonding) show the highest thermal conductivity (D zone) –right hand side of the map[1]. In addition, the high substrate temperature during spraying, observed in Figure 3-9b. improved the cohesion of the particles. Towards lower velocity and high temperature regions (A, C zones), the presence of oxide on the interface drives the thermal conduction. The more the oxide content the lesser the thermal conductivity[2].

3.4.4.2 Indentation Elastic Modulus

The elastic modulus for thermal spray coatings provides a quantitative descriptor of the integrity of coatings by combining the typical elastic response of splats (constituted by alloy and oxide) with bonded and un-bonded interfaces. In this study indentations sampled a reasonable volume of material (including a number of splats and interfaces) to cross-compare the consolidated elastic behavior of the coatings incorporating all microstructural effects. In Figure 3-8b, the region of low oxide content (high velocity, low temperature) shows the highest elastic modulus (B-zone) owing to the presence of less depleted Ni-20Cr alloy with good intersplat bonding, as discussed in map of Figure 3-8a. D-zone, although of the highest intersplat bonding, as it shows oxidation its elastic modulus decreases. Similarly, as the NiCr alloy losses Cr to the oxide, and the latter affects the interfaces, elastic modulus decreases in A- and C-zones. In conclusion, the highest elastic modulus can be obtained by spraying conditions of high velocity and low temperature. However, in practice one should be careful since this kind of conditions may fall in the regime of unmolten particles.

[1] Contour plot shows similar trends on the right bottom corner and left bottom corner of Figure 9a. The trend in the bottom-left hand side of the map is an artifact and it is disregarded.

[2] Thermal conductivity of APS Cr_2O_3 coating = 2.7 W/mK , densified coating = 3.7 W/mK [21] ASM International. Handbook Committee., Properties and selection : nonferrous alloys and special-purpose materials, AMS International, [Metals Park, Ohio], 1990, p. xv, 1328 p.

3.4.4.3 Electrical Resistivity

Similarly to the thermal conductivity, the electrical resistivity *(ρ)* of thermal spray coatings responds to the extent of contact between splats and the content of oxide and defects present in the microstructure [22]. The lowest thermal and electrical resistivity was measured in B, owing two the low oxide content and high intimate contact between splats. However, the highest ρ was observed in A and not in C (as expected from the thermal conductivity measurement) probably due to a higher dependency of ρ to the metallurgical bond (obtained at higher particle temperature in C) and not to the oxide content. It should be noted that *k*-measurements were carried out through the thickness of the microstructure, whereas the ρ-measurements were in-plane measurements. The anisotropy of ρ in-plane versus through thickness was found to be negligible for HVOF Ni-5Al coatings ($\rho_{in\text{-}plane}/\rho_{through\ thickness} = 1.1$) by Sharma et al [22], so it is considered that the trends of thermal and electrical resistivity are comparable.

3.4.4.4 Hardness and Peening Intensity

The hardness in HV sprayed coatings reflects the strain hardening caused by the peening effect. Hardness can also be showing differences due to residual stress. However in the present case, differences in plastic stress (hardness indent) are much higher than the differences in residual stress. In Figure 3-8d, the trend of higher particle momentum to higher induced compressive stresses (peening intensity) in the microstructure is observed. The slope of the curves curvature vs. time during deposition in Figure 3-9a, and b, reflect the intensity of the peening of the impacting particles (refer to Appendix I for more details of peening intensity). Figure 3-8e almost reflects a similar trend for hardness, except that C is slightly harder than B. The mechanical behavior of these coatings (hardness, elastic modulus, peening intensity) was found to be closely related to the intensity of impact of the particles. Therefore, assertions from the monitoring of particle velocity can be directly correlated to stiffness and hardness – higher velocity, higher hardness, higher modulus), except for condition C in which the particle temperature may have played a more dominant role in the evolution of the microstructure.

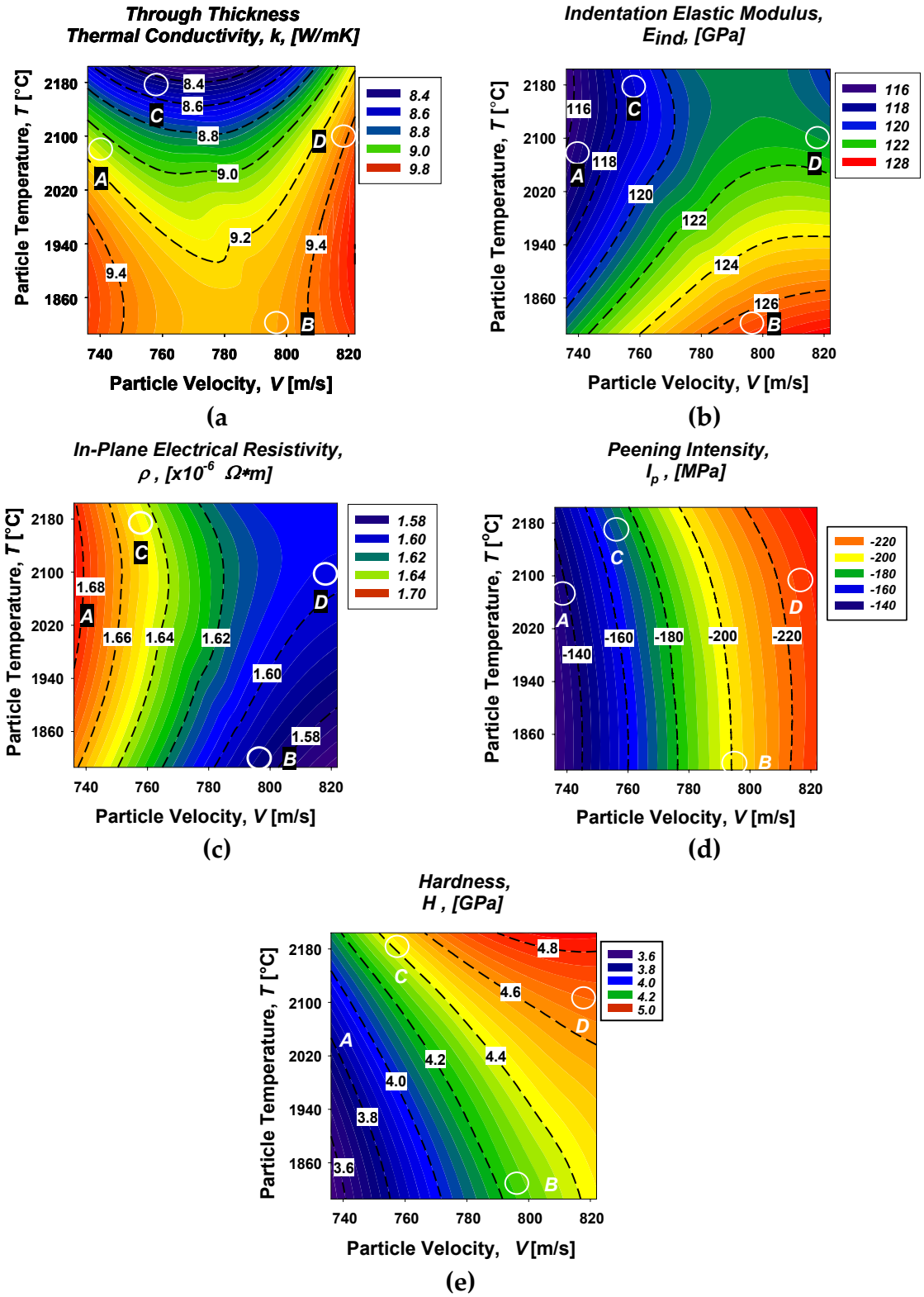

Figure 3-8. Second Order Process Maps: Thermal Conductivity, Elastic Modulus, Electrical Resistivity, Hardness and Peening Intensity.

3.4.5 Evolution of Stresses and Residual Stress

Plots of temperature versus time and curvature versus time for sprayed conditions are presented in Figure 3-9a, and Figure 3-9b.

Condition B and D reached high surface deposition temperature, even though the particle temperature was not the highest. This is because a more reducing condition (high fuel content) elongates the torch flame heating the substrate. This may have effects in the microstructure of the coatings due to annealing or sintering. Furthermore, this high substrate temperature defines a larger cooling gradient to room temperature which imposes more tensile stress due to thermal contraction.

Upon analyzing curvature curves, it is evident that in all conditions, in the first pass quenching stresses prevail due to limited plastic deformation of the steel substrate. Subsequently, each pass contributes to input compressive stresses owing to the peening effect on the deposited NiCr. Particles with higher velocity contribute more to compressive stresses as can be seen comparing the slopes of the curvature curves during spraying and shown in Figure 3-8d.

The stresses in the coatings at the end of the deposition stage are all compressive with higher values for conditions B and D, as observed in Figure 3-10. These two conditions also present higher substrate temperatures and as a result, thermal stresses are also higher due to the larger thermal gradient.

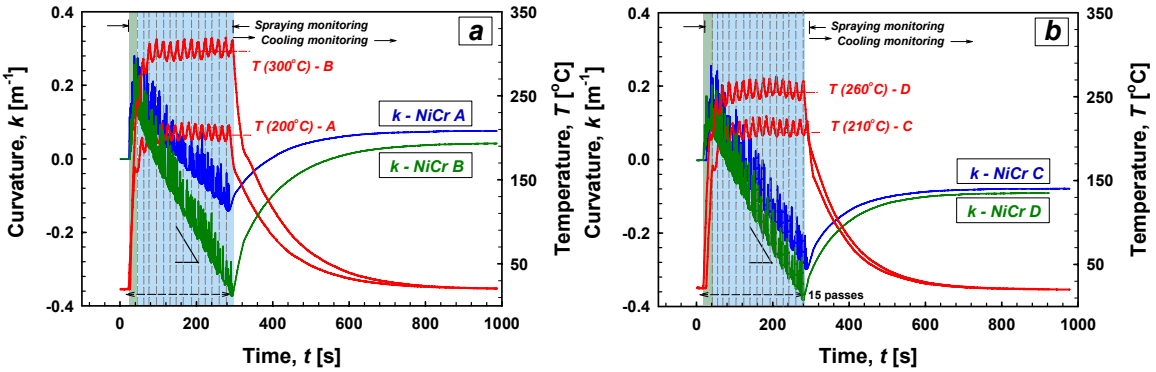

Figure 3-9. Curvature and temperature evolution during spraying (shaded region) and cooling of NiCr coatings. Peening intensity is evaluated considering the slope of the curvature curves during the spraying stage.

The final residual stress of coatings is a combination of the stress developed during deposition (dependent on particle state, substrate temperature, others) and the thermal stresses (dependent on the coefficients of thermal expansion, temperature gradients, coating/substrate stiffness). Particularities of the combinations of these two are only seen during the monitoring *in situ* of the stress evolution. For instance, in Figure 3-9a, A and B are of quite different particle state but both end in similar curvature, but different residual stress state (Figure 3-10). In Figure 3-9b and Figure 3-10, D shows higher

peening intensity and also higher thermal stress, so the final curvatures for C, D are coincidentally in compression at similar stress value. Residual stress profiles two of these coatings are discussed in Chapter VI.

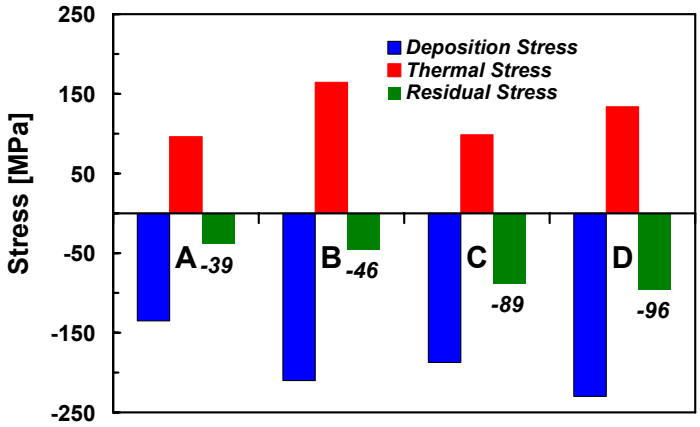

Figure 3-10. Stress developed during deposition, during cooling (thermal mismatch) and after cooling (residual stress) for A, B, C, D coatings.

3.4.6 Property Range

Researchers and engineers are all interested in the process induced range in property values that any material-processing system displays. Whether they are seeking for a broad range or trying to minimize the process effect on resulting properties, the process-microstructure-property relationship has to be carefully established. In the present study, this relationship for a DJ-System spraying NiCr powder was explored. In Table 2, property values as well as standard deviations of measurements are presented. The overall property range is relatively tight (less than 10%), except for the hardness measurements, which shown to be very sensitive to the peening intensity. This demonstrates one relation between stress and properties, perhaps indicating the measurement of stress to have potential as a descriptor or even predictor of properties.

It is also observed in Table 3-2, that the properties are lower with respect to the bulk values for thermal/electrical conductivity and modulus due to presence of intersplat interface and oxides, but higher for hardness owing to strain hardening and compressive stress. Also, the standard deviation of measurements (i.e., modulus and hardness for coating B) indicates the degree of heterogeneity of the microstructures when testing different areas of the samples. It is noted that although differences between property values may fall within their standard deviation for two different coatings the range of the standard deviation is smaller compared to the range of property values. This assures that the differences are real statistically.

Property	Units	Prop/bulk Prop	Property Measurements +/- SD*				Property Range (max-min)/bulk	SD Range (Aver SD/bulk)
			A	B	C	D	%	%
Thermal Conductivity	**W/mK**	**0.50-0.58**	8.96 ± 0.28	9.32 ± 0.27	8.25 ± 0.29	9.47 ± 0.33	***7.4***	***1.8***
Elastic Modulus	**GPa**	**0.56-0.62**	115.7 ± 3.4	126.9 ± 7.3	119.9 ± 3.1	121.1 ± 4.4	***5.5***	***2.2***
Electrical Resistivity	**μΩ*m**	**1.28-1.36**	1.47 ± 0.05	1.38 ± 0.02	1.41 ± 0.10	1.39 ± 0.02	***8.3***	***4.4***
Hardness	**GPa**	**1.37-1.61**	3.9 ± 0.3	4.2 ± 0.7	4.6 ± 0.3	4.7 ± 0.3	***24.2***	***13.4***

Bulk properties
Themal conductivity : 16.4 W/mK [23]
Elastic Modulus: 215 GPa. [21]
Electrical Resistivity : 108 μ ohm/cm [24]
Hardness: 2.5 – 2.9 GPa [21]
* SD: Standard deviations are computed from repeated measurements of the same sample or sampling of different areas of the specimen.

Table 3-2. Range of properties values of NiCr coatings sprayed at different spraying conditions. Property values, standard deviations, and coating property/bulk property ratios are presented. Individual measurements of thermal conductivity, elastic modulus, electrical resistivity and hardness correspond to the second order process maps of Figure 3-8

3.5 Conclusions

Process Maps were used in the present study to examine the effect of spraying parameters on the formation, microstructure and properties of Ni-20%Cr coatings by HVOF on a DJ-System. Concurrent analysis of melting state, oxide content of splats and microstructures and properties proved that HVOF formation of coatings is sensitivity to changes in particle state.

Careful manipulation of the spraying parameters allowed us to build a first order process map (a T-V diagram), in which the characteristics of the flame could be correlated to the particle state (temperature, velocity) and the substrate temperature. There exists a direct correlation between flame energy and particle temperature, and flame chemistry (fuel/oxygen ratio) and particle velocity. Thus, when spraying with flames richer in fuel, the particle velocity increases and as the flame energy decreases, the temperature also decreases. These two variables (flame energy, and fuel/oxygen ratio) would allow the operator two explore the T-V diagram within his discretion.

The monitoring of T-V along the spray stream-downstream showed that the exothermic reaction of formation of the oxide inputs heat during flight. Particles get hotter as they travel away from the core of the flame due to the interaction with the air (oxygen) entrained. In fuel rich conditions, some oxygen of the surrounding gets consumed by the fuel that did not burn effectively in the plume upstream. As a result, particles are sprayed through an ambient with low oxygen content resulting in lower oxidation.

Second order process maps revealed the following trends:

To enhance thermal conductivity high kinetic energy with high thermal energy is required; as long as, the oxide content is relatively low as to avoid affecting the interfaces significantly.

Stiffer (in-plane) coatings resulted at high particle speed and low melting state.

Electrical resistivity responds similarly to thermal transport with lower values at high thermal-kinetic energy of the particles. Its response to oxide content is probably less important providing an electron path exists in the splat/splat interfaces.

Differences in particle state also reflected different evolution of stress buildup during spraying in the coatings. Higher induction of compressive stresses due to peening was identified at higher particle velocities.

It is highlighted that the monitoring of the stress developed during spraying can depict differences in the actual formation of the coating at different particle states. Peening intensity and substrate temperature are key factors when considering strain hardening of substrate and coating, compaction, and *in situ* annealing and oxidation, respectively. Furthermore, knowledge of the sources of stress permits the manipulation of the spraying conditions to obtain desired residual stresses and/or restrict the distortion of sprayed parts due to residual stress.

Although microstructures of coatings were dissimilar, such feature differences were not significantly representative in property values. The maximum difference in property values among the tested coating is less than 8.3% for electrical resistivity, 7.4% for thermal conductivity and 5.5% for elastic modulus (–percentages are higher than the resolution of the measuring techniques). Nonetheless, further research should clarify whether these differences are substantial when subjecting the coatings to in-service conditions or the material/processing window in this study represents a "forgivable" range.

The *Process Map* methodology is an excellent tool to address the effects of spraying parameters in production of coatings. The applicability of the method is universal for any thermal spray technology. In this regard, the present results constitute a guideline to explore other HVOF-systems and materials.

3.6 References

[1] E. Turunen, T. Varis, T. E. Gustafsson, J. Keskinen, T. Falt, S.-P. Hannula, Surface and Coatings Technology 200 (2006) 4987-4994.

[2] E. Turunen, T. Varis, S.-P. Hannula, A. Vaidya, A. Kulkarni, J. Gutleberg, S. Sampath, H. Herman, Materials Science and Engineering: A 415 (2005) 1-11.

[3] E. Lugscheider, Herbst C., and Zhao L., Surface and Coatings Technology 108-109 (1998) 16-23.

[4] R. Knight, R. W. Smith, HVOF Sprayed 80/20 NiCr Coatings - Process Influence Trends, in: C. C. Berndt (Ed.) Proceedings of the International Thermal Spraying Conference & Exposition, ASM International, Orlando, FL, USA, 1993, pp. 159-164.

[5] J. A. Hearley, Little J. A., and Sturgeon, A. J. , Surface and Coatings Technology 123 (2000) 210-218.
[6] W.-C. Lih, S. H. Yang, C. Y. Su, S. C. Huang, I. C. Hsu, M. S. Leu, Surface and Coatings Technology 133-134 (2000) 54-60.
[7] T. S. Sidhu, S. Prakash, R. D. Agrawal, Scripta Materialia 55 (2006) 179-182.
[8] F. Tang, L. Ajdelsztajn, J. M. Schoenung, Scripta Materialia 51 (2004) 25-29.
[9] S. Sampath, X. Jiang, A. Kulkarni, J. Matejicek, D. L. Gilmore, R. A. Neiser, Mater. Sci. Eng. A 348 (2003) 54-66.
[10] A. Vaidya, Srinivasan, V., Streibl, T., Friis, M., Chi, W., Sampath, S., Process Maps for Plasma Spraying of Yttria Stabilized Zirconia: An Integrated Approach to Design, Optimization and Reliability, in: SUNY Stony Brook University, Stony Brook, 2008.
[11] H.-B. Xiong, L.-L. Zheng, L. Li, A. Vaidya, International Journal of Heat and Mass Transfer 48 (2005) 5121-5133.
[12] M. Li, P. D. Christofides, Chemical Engineering Science 60 (2005) 3649-3669.
[13] S. Sampath, J. Matejicek, Method and Apparatus for Determining Process-Induced Stresses and Modulus of Coatings by in-situ Measurement. US Patent 6478875
in.
[14] W. C. Oliver, G. M. Pharr, Journal of Materials Research 7 (1992) 1564-1583.
[15] J. Matejicek, S. Sampath, D. Gilmore, R. Neiser, Acta Materialia 51 (2003) 873-885.
[16] H. Topsoe, Geometric Factors in Four Point Resistivity Measurement, in: Bridge Technology, 1968.
[17] F. M. Smiths, Measurement of Sheet Resistivities with the 4-Point Probe, in: Bell System Technical Journal, 1958, pp. 711-718.
[18] T. S. Sidhu, Prakash S., Agrawal, R.D., Surface and Coatings Technology 200 (2006) 5542-5549.
[19] L. Li, B. Kharas, H. Zhang, S. Sampath, Materials Science and Engineering: A 456 (2007) 35-42.
[20] S. Sampath, X. Y. Jiang, J. Matejicek, L. Prchlik, A. Kulkarni, A. Vaidya, Materials Science and Engineering A 364 (2004) 216-231.
[21] ASM International. Handbook Committee., Properties and selection : nonferrous alloys and special-purpose materials, AMS International, [Metals Park, Ohio], 1990, p. xv, 1328 p.
[22] A. Sharma, R. Gambino, S. Sampath, Acta Materialia 54 (2006) 59-65.
[23] T. Yoshihiro, O. Kenji, M. Tetsuo, S. Tomoo, Journal of Applied Physics 81 (1997) 2263-2268.
[24] A. A. Al-Aql, Materials and Design 24 (2003) 547-550.

Chapter 4
GLOBAL PROCESS MAP OF Ni-20Cr COATINGS

4.1 Introduction

Thermal spray is known in industry for its ability to produce relatively thick coatings with unique properties to solve a large number of application problems from corrosion protection to thermal barriers. In each of these applications, optimization procedures need to be carried out to implement coatings of the highest performance in service. There is a need for coating designers to know the potential spectrum of properties and microstructures that can be achieved by optimization of process parameters across a spectrum of thermal spray torches or within the same torch.

For instance, in bond coats that support TBC's, the composition and resultant oxidation due to spraying significantly affects the oxide scale formed after heat treatment. Low oxidation in as-sprayed coatings favors the formation of protective α-alumina scale (TGO) which is indispensable during service [1]. Similarly, NiCr coatings also experience elemental diffusion during service forming oxides that protect against corrosion [2]. A property-based understanding of the process control (particle state and coating formation) across the different processes used in such applications emerges as an important need for both materials designers and applicators.

It is generally appreciated that protecting metallic feedstock composition from oxidation during thermal spraying will promote good splat-splat bonding. Although mesoscale and microscale oxide features can be easily characterized through image analysis and elemental mapping, the effect of oxidation on splat to splat bonding is difficult to characterize microstructurally. In metal/alloy coatings, thermal conductivity and electrical conductivity have been observed to be highly dependent on the nature of the intersplat interface and the oxide content [3, 4]. Mechanical properties such as elastic modulus or hardness are also dependent on the nature of these interfaces. Thus, investigation of property range over a broad range of coating microstructures will enable the understanding of the sensitivity and discrimination of different phenomena occurring during the application of the measurement technique. This is one goal of the present study.

Sensor implementation for process design and control are essential to determine the effect of process parameters in particle state and coating formation. The use of process diagnostics, such as measuring the particle velocities and temperatures, has aided understanding of how thermal spray enables the production of coatings with a wide array of physical characteristics, as well as to map the particle conditions to the end coating results. Currently most diagnostic measurements are considered with respect to the particles prior to, or at the point of, impact onto a substrate, or with the process plume itself that provides the particle energy (thermal and kinetic). The next logical step is to measure conditions at the substrate itself as the particles deposit, which is enabled by the monitoring of stress formation. The final goal is to promote the understanding of processing effects on the microstructure and properties of the coatings by a correct interpretation of the information produced by the sensors.

The particle state, microstructures, induced stresses and properties by using several HVOF and plasma systems: two High Velocity Gas Fuel (HVGF) guns -DJ and JK-, two Liquid Fuel (HVLF) guns –JP5000 and WokaStar-, and High Velocity Plasma (HVP) gun –Triplex Pro200- with the high velocity nozzle are compared using *Process Maps* approach and *in situ* characterization of stress evolution. Coatings were sprayed with these five process guns (see Chapter I) and with the same material feed stock (Ni-20Cr) resulting in different coating structures and properties. HVGF, HVLF and HVP processes induce similar particle kinetic energy states at high velocity regimes as measured with particle diagnostic tools during spraying but due to the differences in particle history are expected to result in different coating structures with different levels of residual stress, oxide content and property values.

The understanding of these differences presented in this chapter leads to an improved methodology for mapping coating processes from one another along with a more in depth understanding of coating formation by recourse to studying stress buildup. Correlation of property evaluation, microstructure, spray stream control (thermal soaking, melting state, and viscous state, etc) and stress evolution highlights key parameters to be controlled during processing.

4.2 Experimental Methods

4.2.1 First Order Process Maps – Spraying Parameters

Five different thermal spray processes were used to deposit coatings at different particle states:

4.2.1.1 HVGF guns:

- DJ-2700 - two different conditions were selected at two different flame chemistries (stoichiometric and fuel rich) at constant total volume flow of gases (similar conditions A and B from Chapter III).
- JK-3000 – one condition was sprayed with hydrogen fuel.

4.2.1.2 HVLF guns:

- WOKA Star 600 - NiCr was sprayed at similar parameters used for carbides (named medium energy condition, Med E). The flow of gas and fuel was reduced by 30% to deposit coatings at a lower flame energy condition (named, Low E).
- JP-5000 – commercial parameters were chosen to spray NiCr with kerosene as fuel.

4.2.1.3 HVP gun:

- Triplex Pro 200 - an entire spectrum of particle velocities were investigated, from APS regime ~100 m/s, to ~350 m/s using a 9 mm nozzle, and even further to HVOF regime ~600 m/s using a 5 mm de Laval nozzle. Of the entire spectrum three sets of data were chosen for this chapter representing low, medium, and high speed conditions.

Spraying parameters are described in Table 4-1 to 4-5.

HVGF: DJ-2700					
Coating	GAS FLOWS				
	Propylene	Oxygen	Air	Fuel/oxy	Total
	slpm	slpm	slpm		slpm
A	60	198	351	0.22	621
B	92	166	351	0.38	621
Nitrogen was used as carrier gas. Water cooled DJ2700 HVOF System. Aircap: DJ2702. Spray distance 266 mm. Traverse Spraying velocity 22.8 m/min. Feed rate: 23 g/min for coating deposition.					

Table 4-1. DJ-2700- Spraying parameters of Ni-20%Cr coating

HVGF: JK-3000			
Coating	GAS FLOWS		
	Hydrogen	Oxygen	Carrier
	slpm	slpm	slpm
Standard	590	212	27
Argon was used as carrier gas. JK-3000. Spray distance 203 mm. Sample were air cooled. Traverse Spraying velocity 76.2 m/min. Feed rate: 41 g/min for coating deposition.			

Table 4-2. JK-3000- Spraying parameters of Ni-20%Cr coating

HVLF: WOKA Star 600			
Coating	FLOWS		
	Kerosene	Oxygen	Carrier
	l / h	slpm	slpm
Low E	13.2	613	11
Med E	18.9	875	11
Nitrogen was used as carrier gas. WokaStar600. Spray distance 355.6 mm. Traverse spraying velocity 48 m/min. Coating samples were air cooled. Feed rate: 40 g/min for coating deposition, and diagnostics measurements.			

Table 4-3. WokaStar600 - Spraying parameters of Ni-20%Cr coating

HVLF: JP-5000			
Coating	FLOWS		
	Kerosene	Oxygen	Carrier
	l / h	slpm	slpm
Standard	19.3	800	60
Nitrogen was used as carrier gas. JP-5000. Spray distance 355.6 mm. Traverse spraying velocity 22.8 m/min. Coating samples were cooled with CO_2. Feed rate: 80 g/min for coating deposition. Barrel length: 102 mm.			

Table 4-4. JP-5000 - Spraying parameters of Ni-20%Cr coating

HVP: TRIPLEX PRO200					
Coating	POWER			GAS FLOWS	
	Current	Volts	Power	Argon	Helium
	A	V	Kw	slpm	slpm
Low speed	500	93.5	47	20	20
Med speed	480	134	64	40	120
High Speed	450	200	90	160	200
Nitrogen was used as carrier gas. Triplex Pro200. Spray distance 102 mm. Traverse spraying velocity 60 m/min. Coating samples were air cooled. Feed rate: 90 g/min for coating deposition, and diagnostics measurements.					

Table 4-5. Triplex Pro200 - Spraying parameters of Ni-20%Cr coating

Low carbon steel plates (grit blasted on both sides to balance out the peening stresses induced during blasting) were evaluated with ICP sensor. Due to differences in feed rate capacity and deposition efficiency of the different spray torches, different number of passes was sprayed in all experiments to produce coatings of around 0.2 mm thickness. Thicker (1 mm) coatings were also sprayed at these conditions to be used in indentation and thermal conductivity measurements.

Ni-20%Cr powder from Praxair Surface Technologies, and Sulzer Metco (particle size 5 to 45 μm) was used to spray the coatings. Powder was of spherical morphology with grain size of about 1-2 micrometers. Accuraspray was used to collect particle temperature and velocity of coatings sprayed with DJ and WokaStar systems, and DPV2000 for Triplex conditions. Particle states of JK and JP-5000 were not measured.

4.2.2 Microstructural Examination

Coating cross-sections were examined by SEM (Leo Zeiss 1550), at 2000X magnification. Coatings were sectioned, mounted in epoxy and polished to mirror finish with up to 1 μm suspension solution.

4.2.3 Property Measurements

4.2.3.1 Thermal Conductivity Measurement

Thermal conductivity measurements were carried out on 12.5 mm diameter and 1 mm thickness free standing coating disks, coated with carbon, using Holometrix laser flash thermal diffusivity instrument. Measurements were made on two samples of each condition for nine times each.

4.2.3.2 Elastic Modulus and Hardness Measurement

Microindentation testing was carried out on polished top-surfaces of thick coatings bonded to the substrates. Experiments were conducted in an instrumented indenter (Microtest 600, Micro-Materials Limited, Wrexham Technology Park, Wrexham, UK), using a WC-Co Berkovich tip and an incremental load up to 5 newtons, at room temperature. Elastic modulus was calculated from the unloading portion (elastic recovery portion) of the load-depth records according to Oliver and Pharr method [5]. Hardness was also extracted from this experiment.

4.2.3.3 Stress Evolution and Residual Stress Measurements by ICP (in situ Coating Property Sensor)

A Stony Brook developed *in situ* coating property sensor (ICP) [6] was used to monitor the curvature and temperature while spraying. Calculation of stresses from the curvature measurements are explained in Appendix I.

4.2.3.4 Electrical Resistivity

Electrical resistivity was measured using a four point probe (*Model FPP-5000*) resistivity instrument. It consists of four equally spaced metal tips, with each tip supported by springs on the other end to minimize sample damage during probing. High impedance direct current is provided during the measurement through the outer two probes and the voltage across the inner two probes is measured to determine the sample resistivity. Geometrical factors have to be considered due to the finite size and thickness of the specimen. In this work, the correction factors dependent on sample shape and dimensions were calculated based on the work of Topsoe [7] and Smits [8]. Measurements were made on one sample of each condition for nine times each in different orientations.

4.3 Results

4.3.1 Synthesis of a First Order Process Map

Figure 4-1 shows the results of average particle temperature and velocity of a total of seven spraying conditions with high velocity (HV): -plasma (Triplex), -liquid fuel (Woka), and -gas fuel (DJ) spray systems. A broad spectrum of particle energy conditions are considered in the T-V map: temperature ranges from 1800°C to 2400°C,

and velocity from ~100 m/s to 800 m/s. Triplex low speed is a representative condition of APS, whereas Triplex high speed, DJ, and Woka high E fall in the regime of HVOF systems. Triplex med speed and Woka low E fall in the transition from APS to HVOF regime. Overall substrate temperature of all coatings ranges between 100°C -200°C, with the exception of DJ-B condition that reached 350°C.

Diagnostics measurements were carried out at the spraying distance.

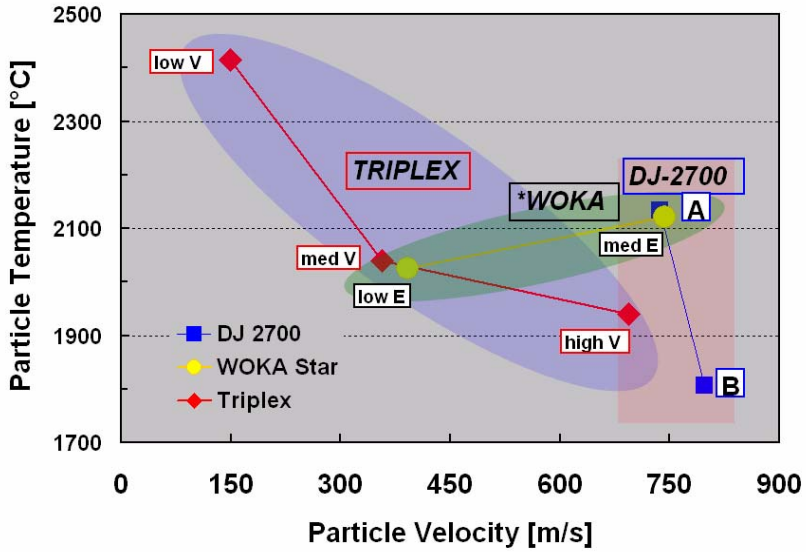

Figure 4-1. First order process map: temperature-velocity map for the sprayed coatings. Three systems are represented: Triplex, Woka Star 600, and DJ-2700 at different spraying conditions

4.3.2 Curvature-temperature and stress evolution of sprayed coatings

Figure 4-2 to 6 show the evolution of the stress during spraying monitored by the ICP sensor. Differences in compressive induced stress can be identified during the first pass and subsequent passes as the peening effect depends on the characteristic strain hardening of underlying layer, the substrate or coated material.

Salient results are:

- In most cases, except for HVLF guns, quenching predominated at the onset due to the limited deformation of the substrate by the impacting particles. Other issues may affect this initial bending such as adhesion, stress relief of the substrate, among others (as discussed in Chapter V: part I)
- In all subsequent passes, a negative and steady change in curvature was observed suggesting the predominance of peening stresses on the NiCr deposited layers.
- During cooling, the change in curvature imparts tensile stress in the coating (coefficient of thermal expansion: $\alpha_{NiCr} > \alpha_{steel}$), and is more pronounced for higher gradients of temperature (from spraying- to room-temperature.).

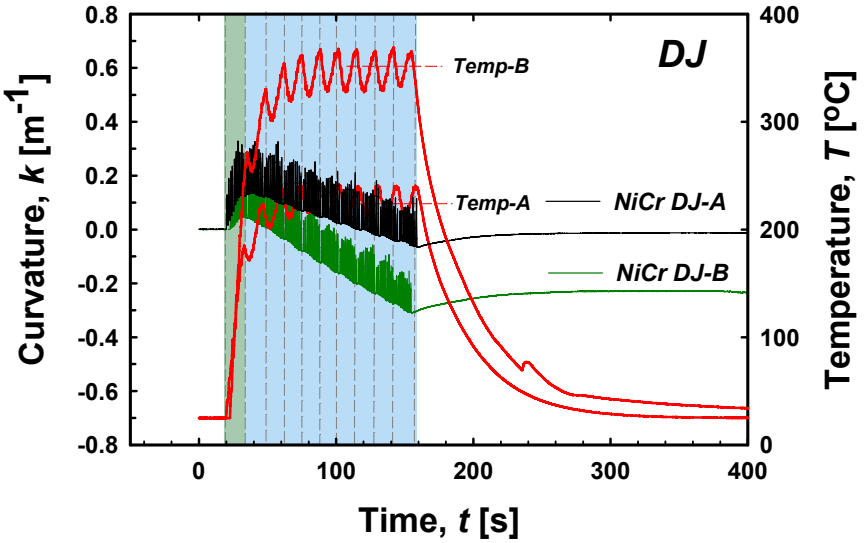

Figure 4-2: Curvature-temperature evolution of two spraying conditions with DJ-2700 (propylene fuel): A is stoichiometric and B is fuel rich. Details of these conditions are published in [3]. Ten passes were deposited. Shaded region shows spraying session.

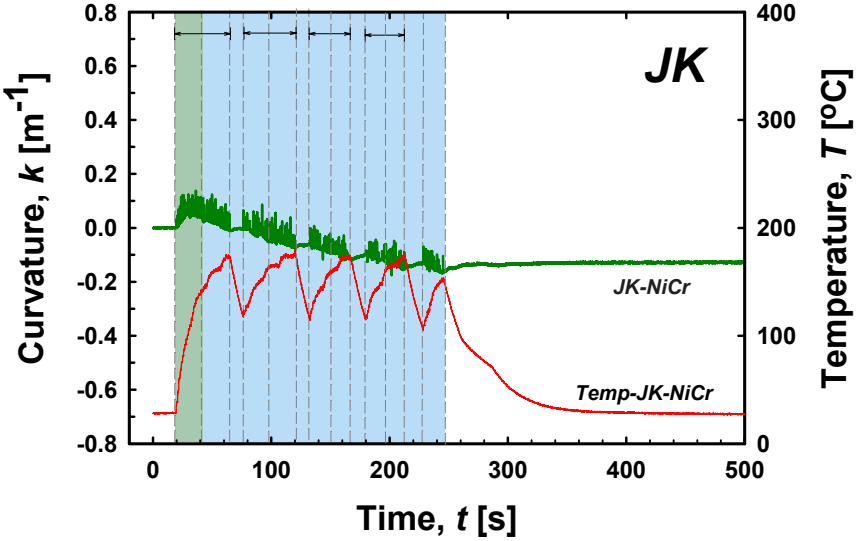

Figure 4-3. Curvature-temperature evolution of spraying condition with JK-3000 (hydrogen fuel). Nine passes were deposited. Shaded region shows spraying session

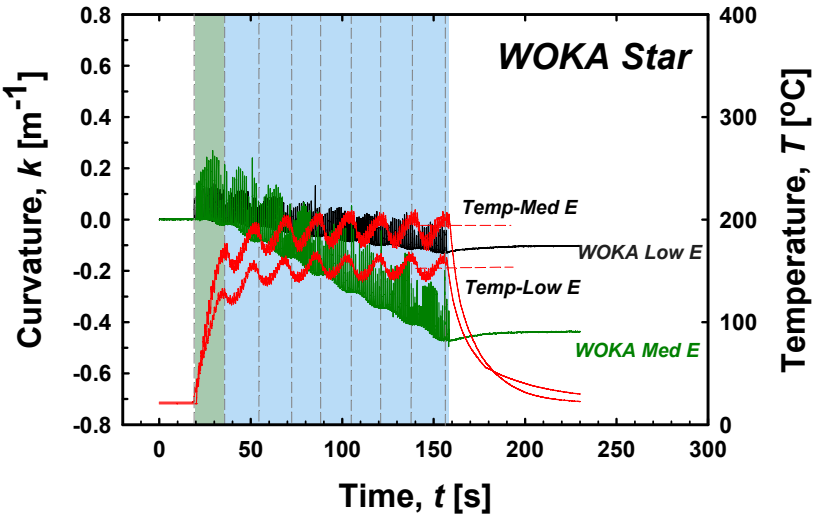

Figure 4-4: Curvature-temperature evolution of two spraying conditions with HVLF WokaStar600: low energy condition and medium energy condition. Eight passes were deposited.

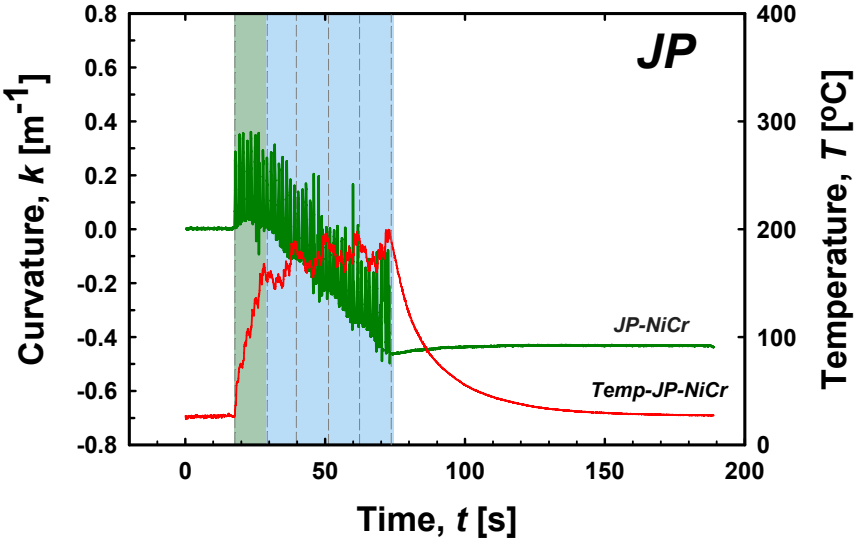

Figure 4-5. Curvature-temperature evolution of spraying condition with JP-5000. Five passes were deposited.

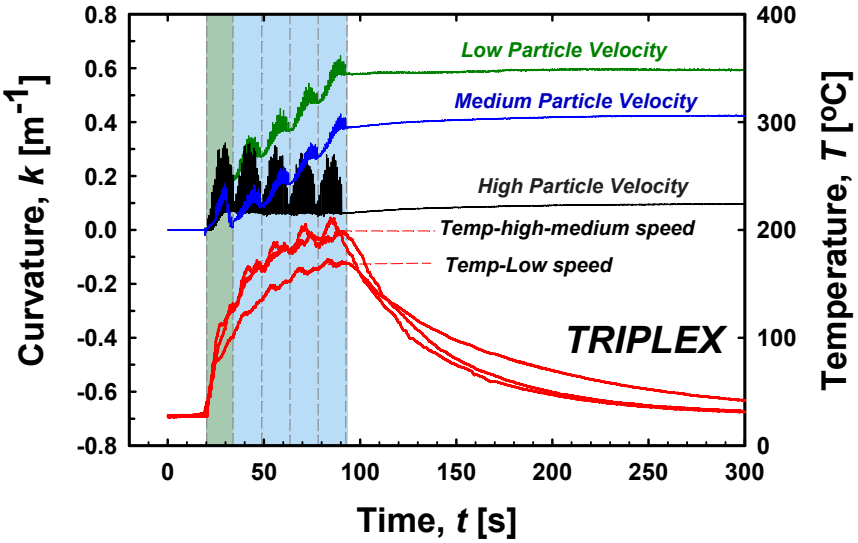

Figure 4-6: Curvature-temperature evolution of three spraying conditions with Triplex Pro 200: Low, medium and high speed. Five passes were deposited.

The stress developed during spraying (deposition stress) is calculated from the slopes of curvature evolution from Figure 4-2-6. This calculation takes into account the deposition per pass of the coating, thickness and stiffness of the substrate. It is noted that after the first pass, each layer develops a steady stress level. The thermal stress is calculated from the curvature gradient during cooling, and later added to the deposition stress to obtain the residual stress at the end of deposition. Results are presented in Figure 4-7.

Stress states vary from compressive (-400 MPa) to tensile (+400 MPa). The overall stress in the coating did not reach the yield strength of the bulk material (~860 MPa) [9], which indicates that (i) deformation was purely elastic; strains combined with coating stiffness did not generate high enough stress to activate inelastic mechanisms or (ii) a lower stress inelastic mechanism, such as splat sliding or microcracking occurred. Dominance of peening effect was observed in almost all the high velocity conditions. Thus, in the regime of HVGF guns, stress values ranged from -100 MPa to -250 MPa; for HVLF guns, they exceed -250 MPa, except for the low energy condition with Woka gun. The latter condition –Woka low E- shows compressive stress, ~ -75 to -90 MPa, in contrast with the Triplex med. speed condition which showed similar readings of T-V but instead develops tensile stress in the range of ~+230- +250 MPa. Triplex conditions show dominance of tensile stresses due to quenching at low particle velocities. As the particle velocity increases, the total tensile stress decreases as the peening effect increases. Hence, Triplex med. speed develops less tensile stress than the low speed condition, and likewise, Triplex high speed develops less tensile stress than med. speed as to reach an almost neutral development of stress.

Thermal stress was always tensile for all conditions which indicates that the thermal strain was positive ($\alpha_{coating} > \alpha_{substrate}$). The oxidation during in-flight can change the composition of the coating and so, its properties including α. However, the nature of the

thermal stress indicates α of coating (14.7 μm/m°C) is still higher than the α of steel (12 μm/m°C).

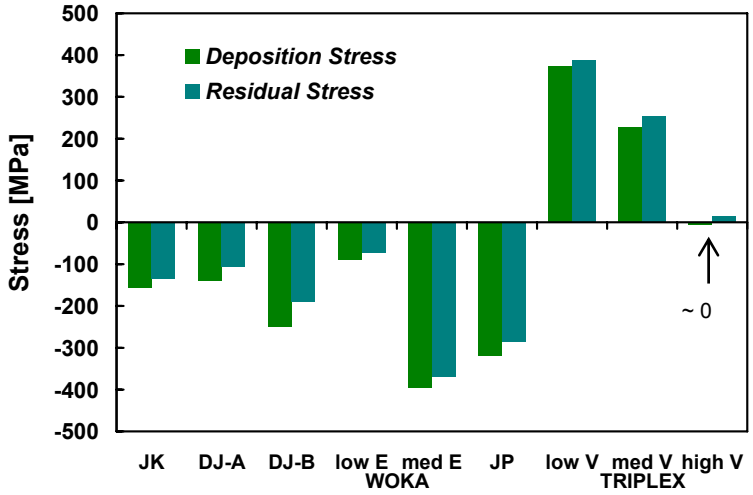

Figure 4-7: Deposition and residual stresses for various NiCr coatings via curvature measurements

4.3.3 Microstructure Characterization

Figure 4-8 shows the cross-sectional microstructures of the various deposits. Overall coatings show high density. Darker features in the microstructures are chrome oxide mainly, identified by EDAX. Small amounts of Ni oxide were found in the microstructures that experienced higher temperature flames (Triplex low and medium speed).

In consideration of the oxide content, 1) coatings sprayed by DJ-B, JK, and JP-5000 conditions show minimal oxidation during in-flight; 2) DJ-A, Woka, and Triplex med speed conditions show disperse oxide in the particles; and 3) all Triplex conditions show mainly oxide in the exterior of the particles.

In consideration of flattening of the particles, 1) Triplex low speed condition shows a typical plasma sprayed microstructure with flattened splats and interlamellar oxides whereas 2) Triplex med-high speeds as well as Woka low E conditions show less flattening and "lumpy" (partially melted particles) microstructures; 3) the rest of microstructures do not show clearly intersplat interfaces and so, flattening of the particles can not be observed.

4.3.3.1 *HVGF coatings*

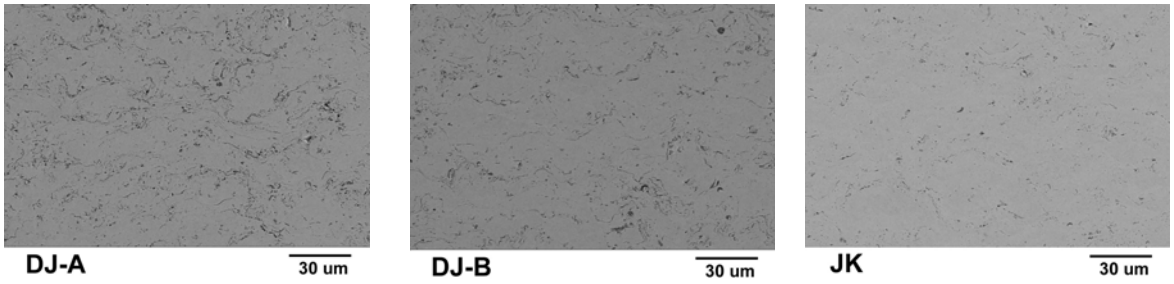

4.3.3.2 *HVLF coatings*

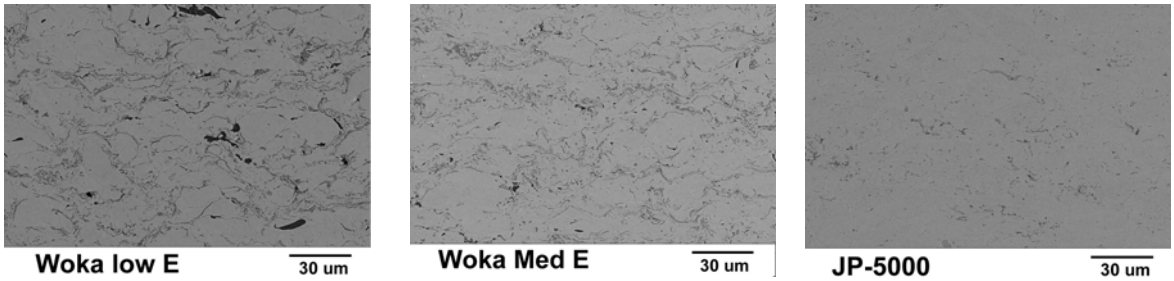

4.3.3.3 *HVP coatings*

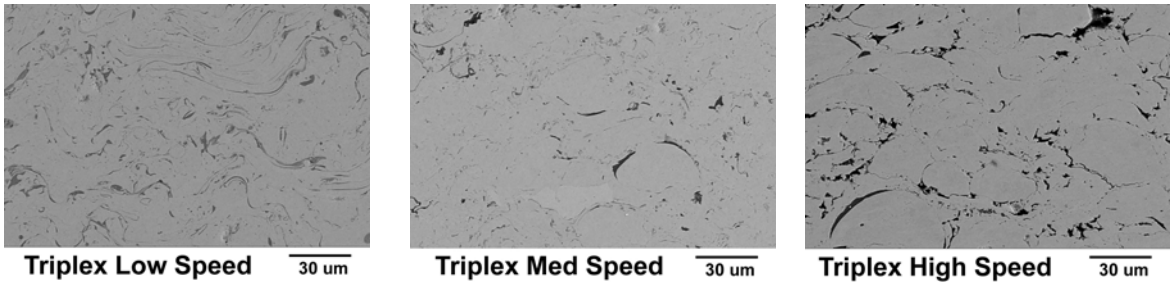

Figure 4-8: SEM images of Ni-20Cr coatings sprayed with different guns and conditions.

4.3.4 Property Evaluation

4.3.4.1 Mechanical Properties

In

Figure 4-9a, hardness is plotted as a function of deposition stress. As the peening effect dominates the compressive stress buildup increases, the hardness also tends to increase.

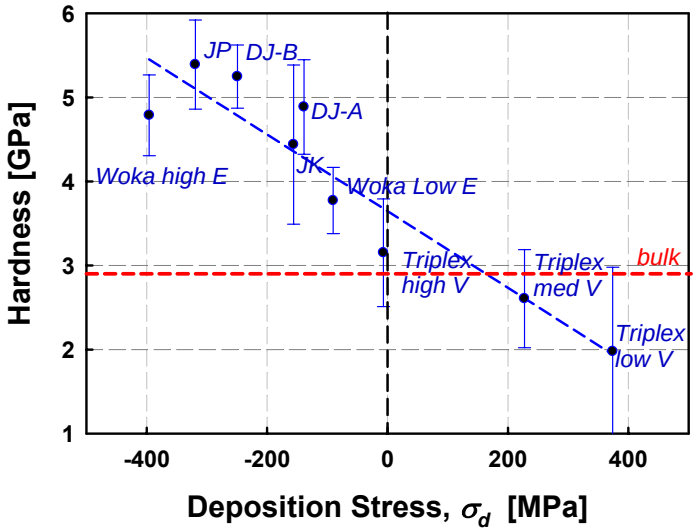

(a)

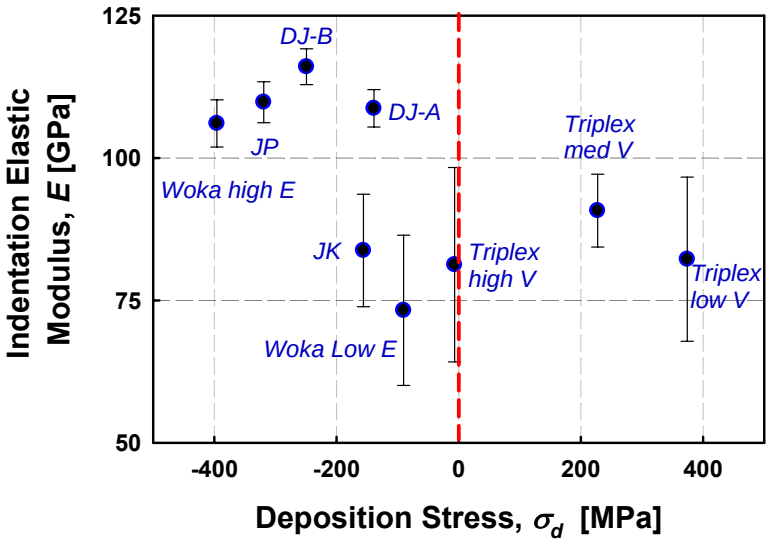

(b)

Figure 4-9. Hardness and indentation elastic modulus as a function of deposition stress

As the quenching dominates the hardness of the coatings drops below the bulk value. It can be argued that the hardness responds almost linearly to the strain and strain rate hardening caused by the impact of particles, assuming that the deposition stress directly relates work-hardening with the plastic deformation that causes residual stress by peening. Variations in hardness cannot simply be attributed to splat-splat interface behavior, because a number of the values fall above bulk.

In Figure 4-9b, indentation elastic modulus of coatings is plotted as a function of deposition stress as well.

The elastic behavior of coatings can be grouped in two sets. 1) coatings with elastic modulus higher than 100 GPa, and 2) lower than 100 GPa.

Stiffer coatings show less deviation in the measurement of modulus which could represent a more homogeneous microstructure. The second group shows higher deviation in the measurements probably caused by a heterogeneous presence of pores, oxides or unmolten particles. The characteristics of the JK coating may not fall within this description according to its microstructure, as it will be discussed in the discussion section.

4.3.4.2 *Thermal and Electrical Properties*

Figure 4-10 shows the thermal conductivity of the coatings as a function of their electrical conductivity. It was found that the higher the electrical conductivity is, a higher the thermal conductivity is also measured. The pairs of coordinates almost fall in a linear trend with exception of JP condition. This is perhaps not surprising for a metallic material, as the transport in both cases is dominated by electrons. The mechanisms slowing electron transport may be similar as well in both in-plane and through the thickness cases. It is noted that thermal measurements are of the through-thickness conductivity whereas the electrical measurement is the in-plane conductivity of the coatings.

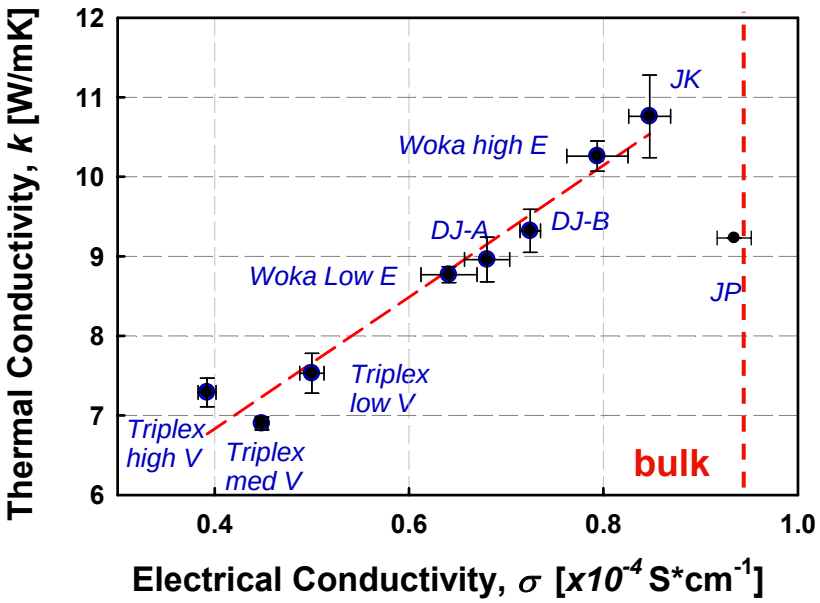

Figure 4-10. Thermal and electrical conductivity of NiCr coatings by various processes.

4.4 Discussion

4.4.1 Particle state and microstructure

The particle interactions between the feed stock and the various flames and conditions considered in this study are quite different as shown by the formation, microstructure and properties of the coatings. The enthalpy, heat density and gas dynamics of the flames determine unique particles states in regard to their kinetic energy, melting state, and distribution of oxide. The kinetic energy of the particles depends on the drag forces given by the gas dynamics of the flame which define the velocity of the particles and so, their residence time in the plume. A combination of heat transfer mechanisms and dwell time define the thermal soaking (transient heat transfer to a particle immersed in a hot flame) of particles and the oxidation mechanism taking

place. In Figure 4-11, the abovementioned considerations are illustrated for the HVP, HVGF, HVLF systems.

Dwell time ($\Delta t_{fly} = 2s/V$, s=spray distance, V=average particle velocity) was calculated for the conditions monitored by diagnostics sensors. It is highlighted that the conditions of plasma spray regime (~150 m/s) –Triplex low V- and HVOF regime (~600-800 m/s) –DJ and Woka Med. E.- all show similar dwell time but fairly different particle melting state and oxidation. Therefore, the answer to the dissimilar particle state is in the differences of heat transfer and the interactions of the particles upstream (with the flame chemistry) and down stream with the air entrained. Considering the microstructures presented in Figure 4-8, the oxide content and the distribution of the oxide in a particle have been illustrated in Figure 4-11 showing presence of oxide mainly in the exterior of the particles for Triplex, oxide distributed in the particle for DJ and almost no-oxide for JP.

The formation of an oxide shell in plasma spraying (Triplex conditions) is commonly observed due to the high temperature of the flame, easier air entrainment and stronger gas mixing [10]. .

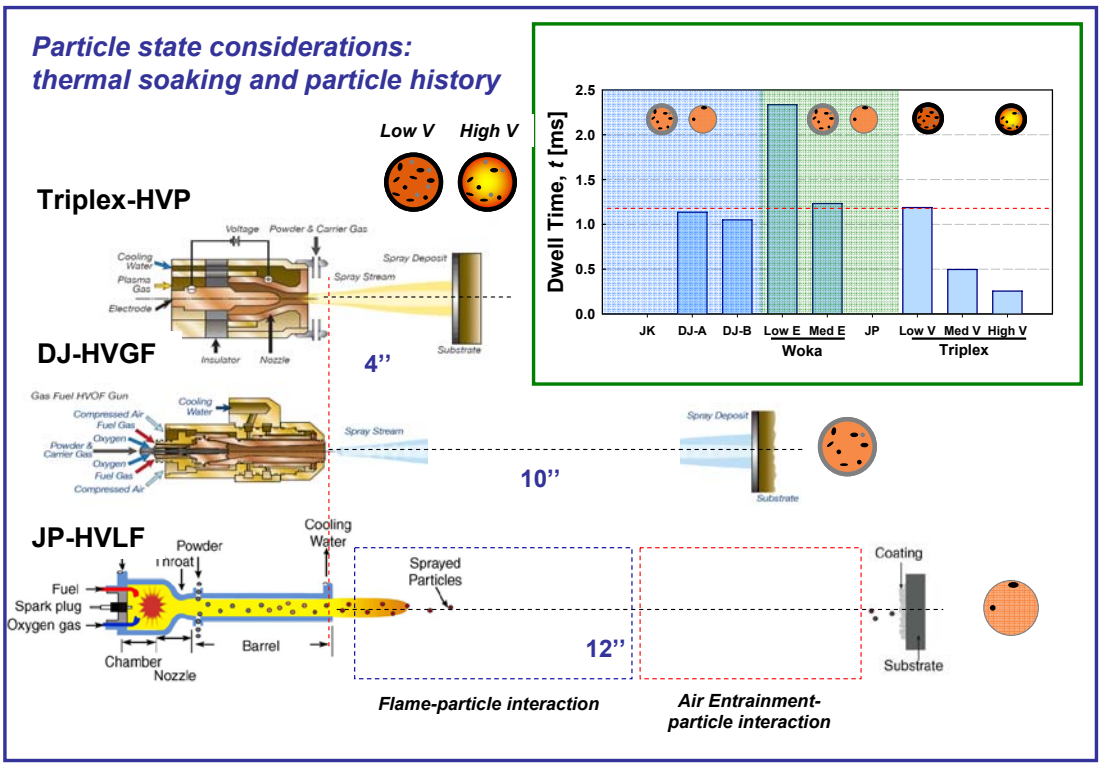

Figure 4-11. Schematic of differences in particle state due to differences in particle-flame interactions considering thermal soaking, and dwell time.

As seen in Figure 4-8, with exception of -Triplex low V- condition, it is noted that particle temperature measurements do not reflect that particles sprayed with the plasma plume had experienced either interaction with higher temperature flames or further oxidation along the trajectory. Particle temperature and velocities were carried out at the spray distance and do not necessary reflect the thermal history. Additionally, the

emissivity of the oxide shell formed in the particle can cause bias in the temperature measured by the diagnostics sensor.

Conditions with shorter dwell times than the average (~1.2 ms) –Triplex med V, high V- showed lumpy microstructures with presence of unmolten particles. This suggests that particles did not have enough time to heat up and melt, especially for larger particles. Thermal soaking was particularly limited for -Triplex high V- due to its extremely short dwell time that unmolten particle cores are observed in the microstructure. A gradient temperature distribution in the particle is expected in this condition, with the exterior molten and oxidized, and the core unmolten. This effect is also present mainly in particles of larger sizes. Particle injection in the plasma torch is radial and not axial as in all the other systems. This difference may affect the residence time of the particles in the flame as the acceleration of the particles occur in an open flame and not in a constrained one as within the HVOF nozzles. Also, the injection angle and carrier flow does not necessarily assure uniform heating of all the particles injected.

Condition –Woka low E- presents the longest dwell time for the particles to heat up. However, its microstructure is composed of unmolten particles. In comparison with the microstructure of –Woka med E- in the former, particles got heated up by a low energy flame during longer time, which resulted in low melting but further oxidation. The latter instead experienced a higher temperature flame during a shorter period of time, which determined lower oxidation and no-unmolten particles in the microstructure.

All the previous results suggest that unless there exists a detailed knowledge of the flame characteristics (temperature, heat transfer, gas dynamics) and its interaction with the particles (acceleration-deceleration, oxidation, heat transfer, residence time), the measurements of T-V hardly can be correlated to the 'true' particle state and resultant microstructure.

In an attempt to entail the particle history during in-flight into the analysis, melting index was used to parameterize differences in dwell time and thermal energy of the flames. Results are present in Figure 4-12. Melting index, first introduced by Vaidya et al [11] and expanded by Xiong et al [12] is defined as the ratio between the dwell time (Δt_{fly}) and the time needed to melt a particle in a flame (Δt_{melt}) The latter is characterized considering the thermal conductivity of the particle, its latent heat and the heat transfer coefficient with the flame, thus:

$$MI = \frac{\Delta t_{fly}}{\Delta t_{melt}} = \frac{6k}{\rho L} \times \frac{1}{1+\frac{2}{Bi}} \times \frac{(T_f - T_m)\Delta t_{fly}}{r_p^{\,2}} \quad [12]$$

where MI is melting index; k is thermal conductivity of liquid, L is the latent heat of fusion, and ρ is the density. Bi is Biot number defined as hd/k, where d is particle diameter, h is heat transfer coefficient. T_f is flame temperature, T_m is particle melting point; and r_p is the radius of the particle.

For the present study, an individual particle of average diameter 25 μm was considered to fly through the different flames HVP, HVGF-DJ and HVLF-Woka at the

respective measured T-V (Figure 4-1). Thermophysical properties used in the calculation are summarized in Table 4-6.

By comparing Figure 4-1 and Figure 4-12, it is observed that the melting state of the particles before represented by the temperature is drastically changed when using melting index. Now, partially molten versus molten states can be differentiated. Particles states lower than melting index of 1 are considered in partially molten state (HVGF, HVLF, and HVP -high V) whereas higher than 1 would represent fully molten particles (HVP, -low and med V). Melting index as it is related to the melting state can also indicate extent of oxidation of the particles. Thus, -DJ-A is more oxidized than DJ-B as its melting index is higher; similarly cases are presented between Triplex –low V- versus –med V- and –Woka low E- versus- Woka med E. HVLF conditions are less molten than HVGF conditions, which is commonly seen when comparing coatings sprayed by these two processes.

The use of kinetic energy versus velocity only accentuates the differences since the mass of the particle considered is the same

Melting index: Thermophysical Data					
Processes	**Ni-20%Cr**				
	k	***L***	ρ	***h***	T_m
	W/mK	J/kg	Kg/m^3	W/m^{2}K	°C
HVP-triplex	90	3x10^5	8.4	35.000	1400
HVGF-DJ				10.000	
HVLF-JP*				4.000	
* Coefficient of heat convection, h , for –Woka low E- condition was decrease in 30% since torch energy was reduced in 30%					

Table 4-6. Physical data used for calculation of melting index.

The above approach is an approximation of the true particle state. Deviations arise from uncertainty in coefficients of heat convection from different flames at different spraying parameters (fuels, gas flows, hardware, etc), limited availability of properties at high temperature and lack of integrating the interaction of particle along the spray stream).

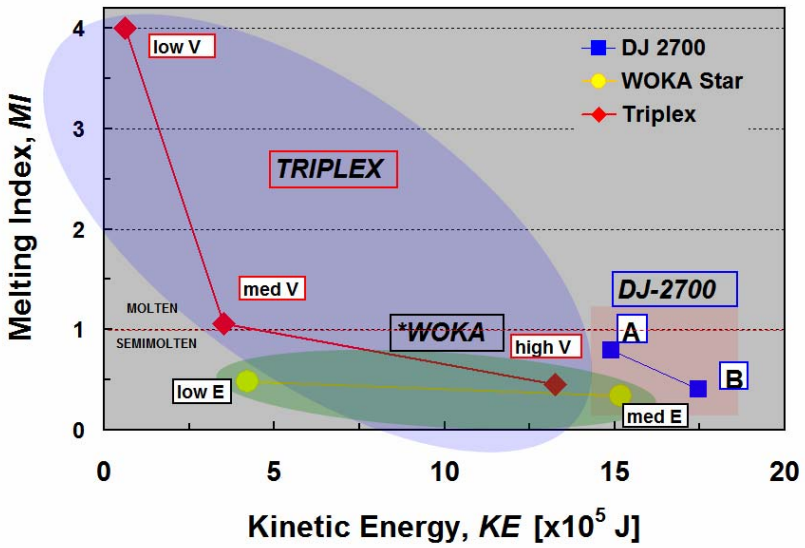

Figure 4-12. First order process map: melting index- kinetic energy of particles sprayed by different processes. Conditions correspond to T-V values of the systems presented in Figure 4-1.

4.4.2 Stresses and mechanical properties

It is clear from the results of Figure 4-2 through 6 that the evolution of stresses between the conventional HVOF processes (HVFG and HVLF) and the HVP process represented by the Triplex plasma gun are very different and unique. Most notably is the lack of compressive stress buildup in the HVP coatings.

Regarding the deposition stress, the instantaneous deflection of the plate during the raster of the spray stream and the resulting properties, coatings were grouped in four sets, thus:

Group	Peening Intensity	Spray Cond/Process	Depos. Stress MPa	Impact Factor *	HV Category
I	Highest	JP	-319	1.4	HVLF
		Woka Med E.	-396	2.3	HVLF
II	High	DJ-A	-139	1.0	HVGF
		DJ-B	-249	1.0	HVGF
III	Medium	JK	-156	0.1	HVGF
		Woka Low E	-90	1.1	HVLF
IV	Neutral	Triplex high V	-7	0.9	HVP
	Low	Triplex med V	228	negligible	HVP
	Lowest	Triplex low V	374	negligible	HVP

*$\Delta k_{peak}/(F.R/d^2)$ where, Δk_{peak} = Instantaneous curvature change during spray stream rater (include effect of impacting particles and stream of gases); F.R. = feed rate; d = nozzle diameter (or diameter of the spray stream footprint).

Table 4-7. NiCr sprayed coatings grouped by deposition stress, impact factor and overall peening intensity.

- Group I is characterized by the highest peening stress. Likely, the particle state in these conditions is of partially molten particles and low particle temperature.
- Group II considers particles with high peening stress as well, but likely with higher particle temperature.
- Group III includes –JK- condition with low impact factor but higher deposition stress, and –Woka Low E- with higher impact factor but low deposition stress. It is believed that the combination of particle state and deposition temperature (likely –JK- high velocity, low deposition temperature; and –Woka low E- low velocity, high deposition temperature) may create intersplat interfaces of similar strength, as characterized by the elastic modulus.
- Group IV includes the three coatings sprayed with a plasma plume. Commonalities among them are the high tensile stress quota owing to the higher melting state and the presence of oxide shells in the particles. As the particle velocity increases the peening effect also increases; thus, the resultant deposition stress are neutral for -high V-, tensile for –med V- and more tensile for –low V-.

4.4.2.1 Elastic Modulus

The elastic modulus of thermal spray coatings mainly responds proportionally to the amount of contact of the intersplat interfaces. Process induced phenomena that can affect this are metallurgical bonding, compaction, intimate contact, friction at the interfaces, and mechanical interlocking. Many of them occur during deposition of particles at high velocity and are evidenced by the analysis of the stress evolution. Compressive stress buildup is usually related to improved contact and compaction of these interfaces. This would explain the reason why groups I and II show higher elastic modulus.

On the other hand, factors that adversely affect the strength of the interfaces are: the presence of oxide, globular or interlamelar pores, lack of metallurgical bonding, among others. Group IV falls within this description with presences of oxides in the intersplat boundaries, more for -low and high V- conditions and a little less for –med V- condition which shows slightly higher modulus. Besides, the heterogeneity of the microstructures with unmolten particles, core-unmolten particles, and dispersed oxides determine high deviation of the modulus measurements.

In group III, the lowest elastic modulus of condition –Woka low E- responds mainly to three factors: the lack of metallurgical bond due to low particle temperature, presence of oxides in the interfaces and the low peening intensity. For –JK- condition the first two factors are ruled out as seen in the microstructure and conductivity properties but the peening intensity still remains relatively low.

4.4.2.2 *Hardness*

Hardness of the coatings responds linearly with the peening intensity, that is to say that likely, the higher the peening quota is related to a higher strain/strain rate hardening and results in a harder coating. At the scale size of the indentation, a number of interfaces are plastically deformed and their nature (e.g. oxide-oxide, interlamelar pore, etc) must affect the size of the imprint as well. Nevertheless, as many values fall above bulk, the overall hardening of splats does contribute significantly. Groups of sample I, II, III, IV fall aligned as their hardness reduces with lower peening intensity, as seen in Figure 4-13. Compressive stress is also known to affect hardness measurements, and could be significant in this case.

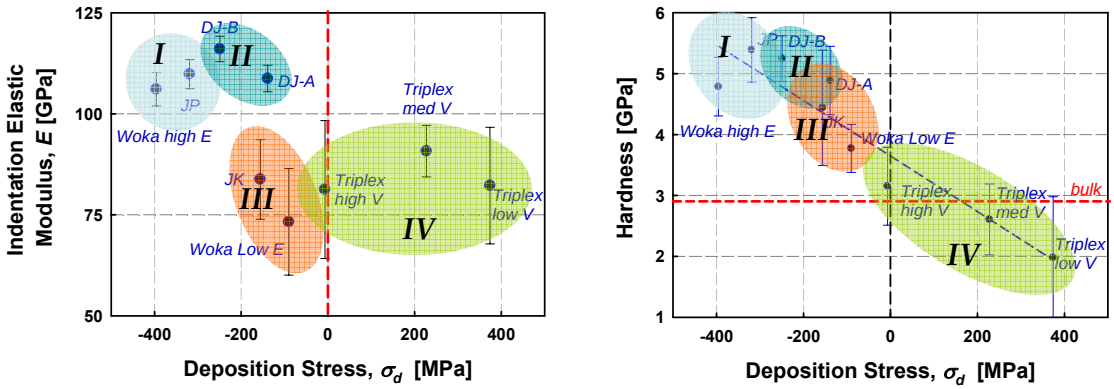

Figure 4-13. Elastic Modulus and Hardness of NiCr coatings grouped by process parameters.

4.4.2.3 *Residual Stress*

In Figure 4-2 to 6, at higher relative kinetic energy the slope of compressive stress buildup is steeper. The same trend holds true for the Triplex in that the stress is less tensile as the particle velocity is increased and particle temperature is decreased.

These differences are captured by the melting index in a second order process map illustrating the correlation between particle energy state (kinetic energy and melting index) and stress development (Figure 4-14).

Triplex low V- and med V- are more thermally soaked (molten-high melting index) with little or no internal temperature gradient. HVOF on the other hand is expected to have partially molten particles (or thermally softened). Related to the difference in stress are these differences between processes in terms of particle history.

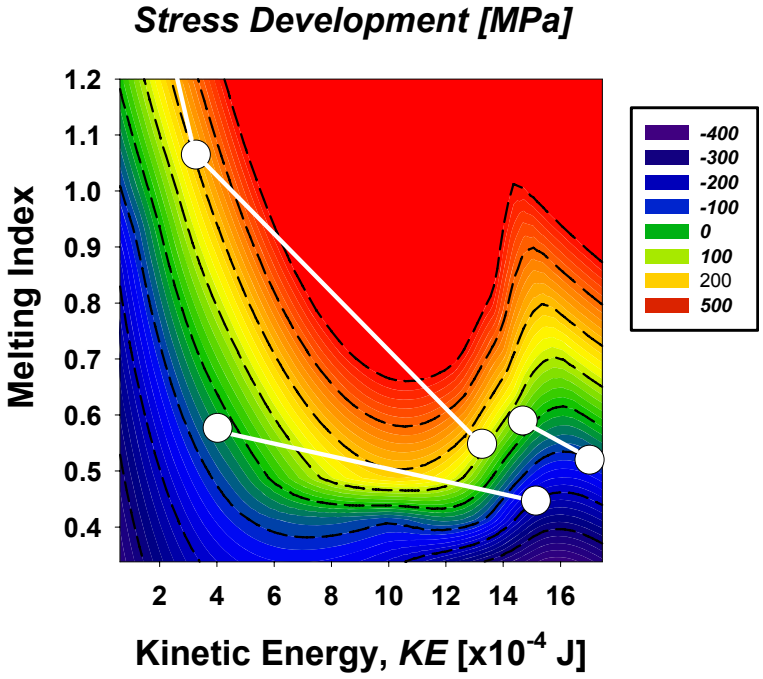

Figure 4-14: Second order process map of NiCr coatings sprayed at multiple particle states. Contour lines delineate the stress developed during deposition of coatings. Melting index and kinetic energy coordinates are presented in circles. Refer to Figure 4-12 for details of process and conditions

As expected for any conventional high velocity thermal spray process there exists buildup of compressive stress that increases as the particle energy state in terms of kinetic energy vs. the thermal energy is increased. Namely, as the particle velocity rises and/or the particle temperature decreases the compressive conditions in the coating rises:

$$\text{Peening}_{\text{compressive}} \propto \frac{\text{Particle Kinetic Energy}}{\text{Particle Thermal Energy}} = \frac{KE}{TE}$$

The ratio of particle KE/ TE are higher for HVLF, followed by HVGF and the lowest is for HVP. The higher the ratio the higher the induced compressive stresses.

On the other hand, as the thermal energy of the particles increases, the quenching effect is favored. Therefore, in the overall stress development during coating deposition, there exists a process condition at which transition between compressive, neutral, and tensile stress occurs. Triplex high V- plasma condition falls in this transition. As seen in Figure 4-14, this condition produces an inflexion of the contours. The lack of a smooth transition is probable an implicit error in the melting index computation of this condition. Some reasons can be consider, such as: the non-uniform melting state within individual particles, broad distribution of molten, partially molten, and core-unmolten particles, and the intrinsic error calculating residence time of the particles since they are highly affected by the acceleration and deceleration

For all the guns, the overall temperature of the substrate/coating system was similar, except for DJ-B condition. A hotter substrate temperature eventually would decrease the peening effect. However, the differences found may not be substantial in the stress-strain behavior of the coating [13]. This would indicate that the total thermal input is roughly identical and the thermal stresses do not play a significant role on the final residual stress for this coating/substrate system, as seen in Figure 4-7. Furthermore, the α mismatch between coating and substrate (~$\Delta\alpha$ = 2.7 μm/m°C) is relatively small defining thermal stresses on the order of 20-30 MPa. Only DJ-B shows higher thermal stress (~60 MPa). The overall residual stresses of all these coatings respond primarily to the intrinsic build up of stress during deposition.

4.4.2.4 Thermal and Electrical Conductivity

The thermal transport and electrical conduction in thermal sprayed metallic coatings depends on the existence of free paths for the movement of electrons. In thermal spray coatings, grain boundaries, porosity, but mainly intersplat interfaces act as barriers against the flux of electrons. True contact given by metallurgical bonding or intimate contact given by high impact deposition improves conductivity properties. On the contrary, the presence of oxides especially in the interfaces lowers the properties.

In the present study, the trend of thermal and electrical properties is discussed but not the particular micro-scale mechanisms acting in each of the microstructures. In Figure 4-10, the thermal conductivity of the coatings was plotted as a function of the electrical conductivity. Except for condition –JP- a linear relationship can be established between thermal and electrical conductivities, with higher property values for microstructures free of oxide (-JK-DJ-B-Woka high E). As the presence of oxide increases in the microstructure, there is a decrease in the property values (DJ-A, Woka low E). Coatings sprayed with the plasma torch show the lowest properties due to the enhanced presence of oxides in the interfaces.

The slope of the curve can be related to Wiedemann-Franz law that correlates the thermal and electrical conductivities at temperature of metal materials. At room temperature the value of Lorenz number from the experimental results approximates to 2.7 x10 $^{-8}$ [WΩK^2] which is comparable to the theoretical value of 2.44 x10 $^{-8}$ [WΩK^2] for various metal materials. This suggests that probably the bulk properties of the alloy Ni-20Cr that retained its structure after spraying behave proportionally but are reduced by the presence of barriers in the free paths, especially oxide in the interfaces. It is noteworthy that this detriment in thermal and electrical properties is also proportional in each individual property.

The bias of the behavior of –JP- condition is uncertain at the moment.

4.4.3 Property Range

In Chapter III, the property range found in a process map for a DJ-system spraying NiCr was of 7.4% for thermal conductivity, 5.5% for elastic modulus, 8.3% for electrical

conductivity and 24% for hardness. In this chapter, property range was also studied for the same properties and results are presented in Table 3-2. Similarly to Chapter III results, elastic modulus measurements showed the lowest sensitivity, followed by thermal conductivity, electrical conductivity and hardness. The overall property range is relatively small for thermal conductivity and elastic modulus (less than 25%), substantially larger for electrical conductivity (~60 %), and significantly more pronounced for hardness measurements (118%). It is also highlighted in this chapter, the highest sensitivity of hardness measurements and the direct proportionality of them to the peening intensity. Therefore, the monitoring of the stress evolution can be of great insight when depicting coating formation differences in real-time.

It is also observed in Table 3-2, that the thermal conductivity and elastic modulus properties are lower with respect to the bulk values. 70% and 60% of the bulk property respectively could not be exceeded, mainly due to the presence of intersplat interfaces and oxides. Electrical resistivity is shown to be more sensitive to changes in the microstructure (property range of 60%). However, reaching bulk properties is possible owing to the fact that electrons are able to find conducting free paths despite the microstructures are not free of defects. Finally, hardness is shown not to be significantly dependent on microstructural features but on the impact and the strain fields created by high velocity particles during deposition. The broad range of kinetic energies used in the present study also determined a broad range of peening intensities and therefore, strain hardening conditions. As a result, the hardness measurements can vary from 70% of the bulk to 190% in the structures of the highest strain hardening.

Property	Prop/bulk Prop	Property Range (max-min)/bulk	SD Range (Aver SD/bulk)
		%	%
Thermal Conductivity	**0.4-0.7**	***24***	***1.4***
Elastic Modulus	**0.3-0.6**	***20***	***3.9***
Electrical Conductivity	**0.4-1.0**	***58***	***4.2***
Hardness	**0.7-1.9**	***118***	***21.1***
Bulk properties: Thermal conductivity : 16.4 W/mK [14] Elastic Modulus: 215 GPa. [9] Electrical Resistivity : 108 μ ohm/cm [15] Hardness: 2.5 – 2.9 GPa [9]			

Table 4-8. Range of property values of NiCr coatings sprayed at different spraying/process conditions. Standard deviations and coating property/bulk property ratios are presented.

4.5 Conclusions

Process Maps methodology across different spray processes was applied to study the process-microstructure-property relationships of NiCr coatings. Five different spray torches and a total of nine process conditions were investigated. The T-V window was explored from low velocity conditions at high temperature (APS like) towards supersonic velocity and lower temperature (HVOF like) with conditions in between (around 350 m/s). The spray streams displayed an assortment of particles states and oxidation levels as seen in the coating microstructures. Particle states varied from fully molten to partially molten and core-unmolten particles depending upon their thermal soaking on the flames during in-flight.

In an attempt to characterize the melting state of the particles across different processes, melting index was used to represent a first order process map. Melting index helped in the understanding of the true particle states among the processes by including the differences in dwell times and heat transfer from the flames. Particles sprayed at high velocities showed to be in partially molten state, whereas only the particles interacting with plasma plumes reached a fully molten condition. Microstructures indicated that as the melting state was increased more oxide was present in the coating, and as the kinetic energy of the particles increased more oxide was dispersed within the particles. A singular particle state was identified during plasma spraying at supersonic velocities. This condition although in the regime of supersonics spray streams is fairly different than traditional HVOF particles. It is characterized by a non-uniform melting state within the particles with core unmolten regions and molten and oxidized particles shells.

The residual stress evolution was studied by measuring the curvature change of sprayed substrate plates. It was found that the nature of the residual stresses when molten or partially molten particles impact a substrate at low and high velocities lies in the quenching of the particle and the peening over the underlying splat. The lower the particle melting state (melting index) and the higher momentum (kinetic energy) rule the dominance of peening over quenching effect. The differences in particle history, captured by melting index, explained the overall differences in resulting stress conditions for the coatings in a second order process map.

Elastic modulus of coatings was found to be sensitive to the strength of the intersplat interfaces. Thus higher elastic modulus was measured when the interfaces were formed by high velocity impact and relatively high melting states. Hardness, instead responded to the peening intensity and strain hardening of the coating microstructure. Electrical and thermal conductivities were found to be dependent linearly to each other. Conductivity values were dependent on the true contact between splat-splat, and so, reduced by the presence of oxides or poor contact. In general, property ranged from 20% up to 190% among all the coatings.

4.6 References

[1] F. Tang, L. Ajdelsztajn, G. E. Kim, V. Provenzano, J. M. Schoenung, Materials Science and Engineering: A 425 (2006) 94-106.
[2] T. S. Sidhu, S. Prakash, R. D. Agrawal, Scripta Materialia 55 (2006) 179-182.
[3] A. Valarezo, W. B. Choi, W. Chi, A. Gouldstone, S. Sampath, Proceedings of International Thermal Spray Conference (2007).
[4] S. Sampath, X. Y. Jiang, J. Matejicek, L. Prchlik, A. Kulkarni, A. Vaidya, Materials Science and Engineering A 364 (2004) 216-231.
[5] W. C. Oliver, G. M. Pharr, Journal of Materials Research 7 (1992) 1564-1583.
[6] J. Matejicek, S. Sampath, D. Gilmore, R. Neiser, Acta Materialia 51 (2003) 873-885.
[7] H. Topsoe, Geometric Factors in Four Point Resistivity Measurement, in: Bridge Technology, 1968.
[8] F. M. Smiths, Measurement of Sheet Resistivities with the 4-Point Probe, in: Bell System Technical Journal, 1958, pp. 711-718.
[9] ASM International. Handbook Committee. Properties and selection : nonferrous alloys and special-purpose materials, AMS International, [Metals Park, Ohio], 1990, p. xv, 1328 p.
[10] S. Deshpande, S. Sampath, H. Zhang, Surface and Coatings Technology 200 (2006) 5395-5406.
[11] A. Vaidya, G. Bancke, S. Sampath, H. Herman, Influence of process variables on the plasma sprayed coatings: an integrated study, in: K. A. K. C.C. Berndt, E.F., Lugscheider, E., Herbst C., and Zhao L. (Ed.) International Thermal Spray Conference (ITSC 2001): New Surfaces for a New Millenium, ASM International, Materials Park, Ohio, 2001, pp. 1345-1349.
[12] H.-B. Xiong, L.-L. Zheng, L. Li, A. Vaidya, International Journal of Heat and Mass Transfer 48 (2005) 5121-5133.
[13] P. Bansal, P. H. Shipway, S. B. Leen, Acta Materialia 55 (2007) 5089-5101.
[14] T. Yoshihiro, O. Kenji, M. Tetsuo, S. Tomoo, Journal of Applied Physics 81 (1997) 2263-2268.
[15] A. A. Al-Aql, Materials and Design 24 (2003) 547-550.
[16] R. Molz, McCullough, R., Leach J., Schmid, R., Niessen, K. von., An Evaluation of High Velocity Deposition Processes, in: HVOF colloquium, 2006.
[17] R. Molz, McCullough, R., Hawley, D., Development of Process Maps for Coating Evaluation of High Velocity Plasma, in: International Thermal Spray Conference (ITSC'07), Beijing, China, 2007.
[18] R. Molz, Schmid, R., Triplex Pro 200 Plasma Gun Carbide Coatings approach HVOF quality for Specialty Applications, in: A. C. S. (Ed.) International Cocoa Beach Conference on Advanced Ceramics and Composites Daytona Beach, Florida-USA, 2007.

Chapter 5
ANALYSIS OF STRESS DEVELOPMENT DURING COATING FORMATION

5.1 Importance of residual stress in thermal spray coatings

It has been widely recognized that residual stress and the stress developed during spraying TS coatings affect the adhesion-cohesion strength, micro- and macro-cracking, fatigue crack growth and shape distortion of sprayed components.

Interfacial and intersplat crack growth (associated with adhesion-cohesion strength) can occur when high residual stresses are held in the coating-substrate system. The former is affected by stress concentrations and sharp shifts of the stress profile in the coating-substrate interface. In both cases, the stored energy can lead to debonding and/or scuffing of coatings during service. Therefore, to seek reliability, the fracture toughness of these interfaces and the residual stress state of the coatings need to be tailored by an appropriate assessment of deposition parameters.

The large magnitude of stresses during solidification leads to micro-cracking of splats of brittle materials and yielding or creep of elastic-plastic solids. This phenomenon is almost unavoidable given the large thermal mismatch to which particles are subjected during the rapid solidification. The presence of micro-cracks relieves stresses during deposition and adds compliance to the structure. This can be an advantage in the case of thermal barrier coatings. Materials such as YSZ, Cr_2O_3, and others, are deposited by plasma spraying with very little stress during deposition at the macro-scale; whereas on the micro-scale, the isles of material after micro-cracking still retain a small amount of residual stress, depending on their aspect ratio. On the other hand, current trends in TS-YSZ deposited coatings on turbine blades show the usage of coatings with macro-cracks running vertically in the microstructure. These efforts have been put to achieve strain tolerance during high temperature cycling where thermal expansion mismatch flexes cracks, and does not allow elastic stress to develop much in the ceramic. It will be discussed in this chapter, the processing strategy to achieve macro-cracking, as well as, the analysis of the stress developed during deposition to achieve such microstructure.

In terms of fatigue life, design engineers are concerned with crack initiation in the coating/substrate interface of sprayed components. Literature does not report an important detriment of fatigue life in sprayed components due to crack initiation in TS coatings. For instance, in applications such as turbine blades, cracks do initiate in the

surface of YSZ coatings but they end in delamination or spallation and not in catastrophic failure of the blades. Another example is landing gear in the aircraft industry. Large components are generally protected with wear resistant coatings (e.g., WC-CoCr) deposited by HVOF spraying. Although the specified fatigue life has been achieved, there exists concern when experiencing with thicker coatings. In all these cases, tailoring the stress state can help to extend the life of the coatings, and compressive stresses are required to act perpendicularly to the direction of crack growth. The assessment of the residual stress state of coatings can also be used to prevent undesired distortion of sprayed components. This is an issue when spraying over relatively thin substrates. An adequate combination of spraying parameters can lead to reduce any distortion.

In the present study, several considerations are discussed to tailor the stress state of coatings regarding the materials involved and the spraying processes. First, fundamentals about the origin, magnitude and relief mechanisms of residual stresses in TS coatings are discussed to understand their nature and response to the thermo-mechanical conditions at which particles are subjected during buildup. Opportunities for tailoring the stress evolution via process parameters (essentially, particle state and deposition temperature) are discussed with to goal to achieve desired microstructures, properties, and stress states. Second, stress evolution is studied in the first deposited layer of coatings. The phenomena of adhesion, peening, stress, stress relief and others are discussed on a broad range of feed stock materials, spraying processes and substrate conditions. Finally, the stress evolution is studied in various metal/alloys and cermets. The influence of processes parameters are reflected in the evolution of the stress and then linked to the resultant properties and microstructural characteristics of the coatings.

5.2 Origin of stresses during deposition of TS coatings

In the literature the following sources of stress generation during spraying have been reported:

1. The constrained volume change that takes place during cooling and solidification of the molten droplet in intimate contact with the relatively cold substrate results in large residual stresses known as *quenching stress* [1]. Quenching stresses are tensile since reduction in volume takes place from liquid to solid, and then from contraction of solid.
2. The subsequent cooling of substrate and coating bonded together from spraying temperature to room temperature determine a second order of residual stresses originating from the contraction mismatch due to the difference in coefficients of thermal expansion (α) between the layers. This is referred to as *thermal mismatch stress*. Thermal stresses can be tensile or compressive depending on the thermal mismatch between the coating and the substrate.
3. A third source of residual stress has been identified during spraying of high kinetic energy particles such as HVOF or cold sprayed. The so called *peening*

stress originates due to the plastic deformation of an impacted layer ensuing the surrounding material's resistance against it [2]. This stress is compressive.

4. A constrained volume change associated with any solid state phase transformation also induces residual stresses in the microscale.

At the end, the summation of all the effects defines the final residual stress state of the coating.

5.3 Mechanism of Stress Relief

While "stress formation mechanisms" act during deposition; simultaneously, stress relief mechanisms alleviate part of the induced stress. Kuroda and Clyne [1], have proposed the following stress relaxation mechanisms present during spraying :

1. Edge relaxation
2. Through-thickness yielding
3. Interfacial sliding
4. Micro-cracking, and
5. Creep

Figure 5-1 illustrates schematics of stress distributions in splats subjected to stress relaxation mechanisms. Due to the fact that a single splat may be subjected to many of the relaxation mechanisms, the measurement of quenching stress can only be an averaging effect of all of the stresses put together. The estimation of the stress buildup minus the relaxation results even more difficult for sprayed coatings. The aforementioned mechanisms, 2) to 5) are potentially able to be tailored by particle state and deposition temperature, and this constitutes part of the goal of the present study. It should be noted that as all mechanisms occur concurrently it is difficult to segregate the effect of each one in the overall stress of the coating.

5.4 Quenching stress

In its simplest form, quenching stresses can be evaluated considering the contraction of the splat from the undercooling temperature to deposition temperature. Thus, quenching stress can be described by the following formula:

$$\sigma_q = -\alpha_d * \Delta T * E_d$$

Where σ_q is the quenching stress, α_d is the coefficient of thermal expansion of deposited splat, ΔT is the difference between splat final temperature (substrate temperature) and initial temperature (splat undercooling temperature) and E_d is the elastic modulus of the splat. Note the following:

1. This approach does not take into account the large volume change associated with transition from liquid to solid.
2. In most thin film cases, E_d is considered the biaxial modulus.
3. ΔT is negative, but the negative sign imposes a positive quenching stress.

4. The *strain* is imposed on the splat, via the substrate. In this approach, the *stress* arises via Hooke's law. This describes the highest possible stresses that may be obtained for such a case.

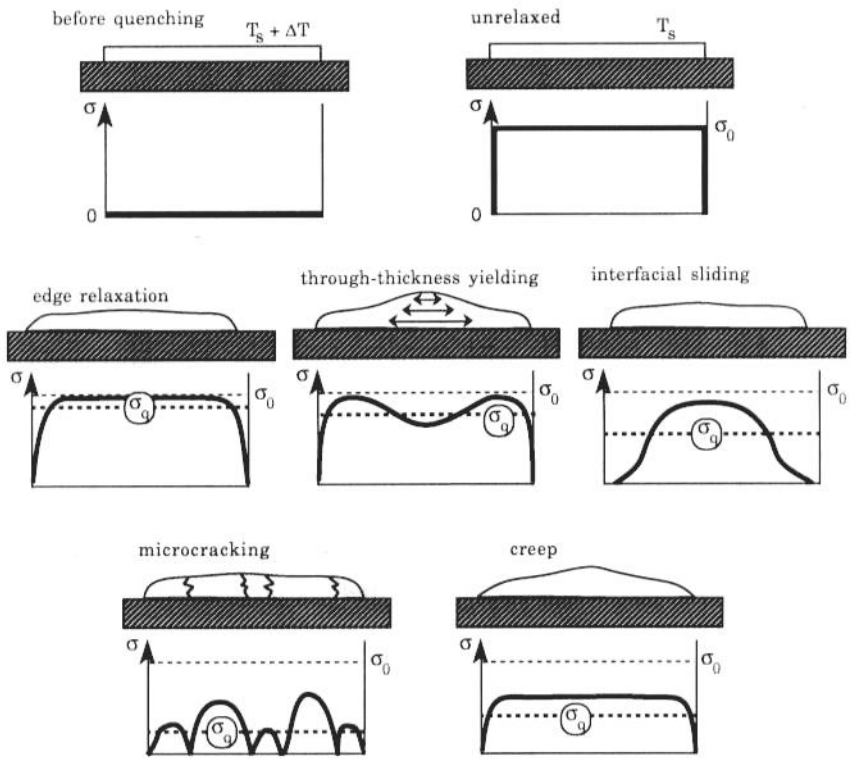

Figure 5-1. Schematic illustration of the stress distributions within a single splat before and after various stress relaxation phenomena have taken place. [1]

Simple calculations can show that for TS, the stress values reach hundreds of megapascals (MPa). For a real material with inelastic mechanisms, the stress will be limited by yielding, cracking, etc. However, for some materials with small grain size, this 'flow stress' could be of similar order to that calculated assuming only elasticity. Any analytical or modeling evaluation approach of quenching stresses, considering inelasticity is a complicated task [3, 4].

The work of Kuroda [5] to measure quenching stress by monitoring the bending of a thin strip during spraying, and followed by other researchers Matejicek et al [6], Tricoire et al [7], Hugot et al [3], Bianchi et al [8] revealed important considerations.

- The magnitude of the quenching stress depends on the relief mechanism acting during the deposition. In this regard, brittle and porous materials develop low stress; brittle but dense materials develop higher residual stress and almost comparable to metal/alloy materials
- The magnitude of quenching stress responds to variations in deposition temperature. It has been suggested that as the deposition temperature increases the cohesion between splats is improved [9-12] owing to the formation of

contiguous splats, improved wetting, more rapid heat transference, reduced amount of adsorbates and/or organics in the surface [13], etc. Therefore, *as the cohesion strength is improved at higher deposition temperatures, the level of stress buildup is also higher*. (-reduced effect of "interfacial sliding mechanism"). This is illustrated in Figure 5-2 for several coating materials.

- In the case of metal/alloys coatings, generally, the quenching stress increases with substrate temperature. This shows that at the lower temperatures, improved bonding (and thus improved 'constraint') dominates over the effect of decreased quenching strain. At some threshold temperature, quenching stress starts to decrease, indicating perhaps that bonding is no-longer as temperature sensitive. Specifically: [14]:
  - NiCr has a threshold at around 800 K.
  - Al, Ni never show the incremental portion of the curve, presumably because of yielding or creep.
  - A threshold for Mo has not been identified. The quenching stress keeps increasing with temperature. This is interesting as it suggests (a) a delay of inelastic mechanisms and (b) importance of liquid-solid phase transition or (c) consistent improvement in bonding with temperature increase.
- On the other hand, in dense ceramic coatings (e.g. Al_2O_3 produced by HVOF) quenching stress increases as the deposition temperature increases because of the improved cohesion among splats. However, the stress can increase until a maximum value where macro-cracking occurs. Vertical cracks would appear in the microstructure. This is also possible in cermet coatings when high content of the ceramic phase is present (e.g. WC-12Co).
- In the case of porous ceramics coatings (i.e., YSZ by APS), the values of residual stresses are relatively low during deposition. But, in principle, as the deposition temperature increases, the cohesion is improved and the coatings become denser. The quenching stress eventually will exceed the fracture toughness of the coating and open up cracks vertically. This is the case of dense vertically cracked (DVC) thermal barrier coatings (TBC), also called pre-cracked TBCs or segmented TBC's.

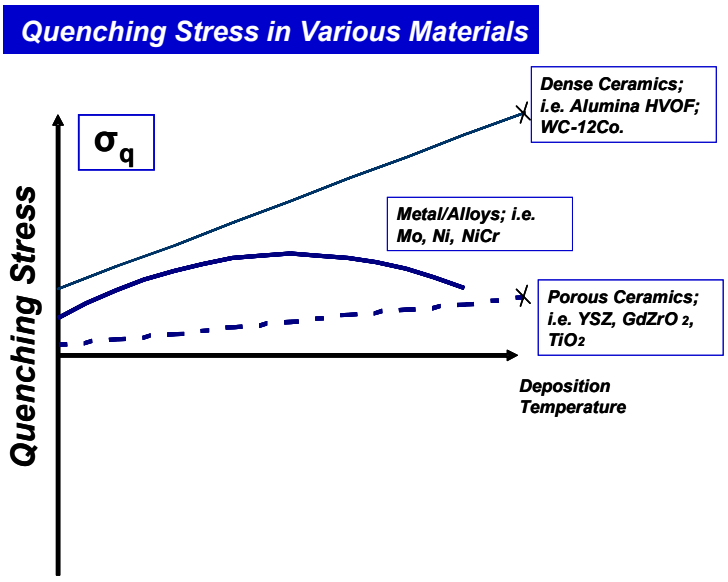

Figure 5-2. Development of quenching stress for different materials with variation of deposition temperature

It must be noted that deposition temperature not only refers to the substrate temperature as such, but indeed to the temperature of the substrate layer at the instant of spreading of the depositing particle. Therefore, from the point of view of the design of the process, several process parameters define the deposition temperature, including:

- Feed rate
- Rastering speed (together with feed rate, they constitute one variable – deposition rate)
- Substrate preheating/Forced Cooling
- Spray distance
- Particle state

5.5 Peening stress

Itoh et al. [15] and Kuroda et al [16, 17] reported for the first time the generation of compressive stress during HVOF spraying by using a cantilever deflection method and a knife edge curvature measurement technique, respectively. This continuous build-up of compressive stress has been explained by the peening effect of partially molten particles similar to the shot-peening process. As a result, the total contribution to the stress induced in a high velocity thermal sprayed coating layer during deposition is obtained by summation of compressive stress due to peening and tensile stress due to quenching.

It should be noted that the peening effect is understood to be caused by depositing particles and rebounding particles, as well. Differences in compressive induced stress have been identified during first pass, subsequent passes and the last pass of spraying since the peening effect depends on the characteristic strain hardening of the substrate

and the underlying coated layer. In this perspective, the last deposited layer is free of peening effect. Note that X-ray residual stress measurements have failed to confirm residual stresses measured by traditional curvature methods (as it will be discussed in Chapter VI) because X-ray measurements are carried out over the last deposited layer that it is not representative of the whole coating. Coated materials such as CoNiCrAlY, NiCrAlY, stainless steel and WC-Co have all presented similar behavior [15-17].
Peening action in HVTS process can be approached by investigating the dynamic impact of individual particles. The impacting particle and the underlying substrate (deposited coating or substrate) under loading are strongly affected by the strain, strain rate, deposition temperature and the characteristic strain hardening of the material (microstructure) [18]. Several researchers [18-20] have attempted to model the impact of sprayed particles by HVOF or cold spray using the Johnson-Cook (J-C) model [21]. This model takes into account the influences of strain hardening, strain rate hardening, and thermal softening during impact of unmolten particle. J-C model is presented in Appendix A.

Regarding the cited model, the following aspects directly related to process control can be inferred:

1. Particles impacting with higher momentum will increase the plastic stress *(i.e., the stress that is associated with plastic strain, or that persists after unloading)* acting on the substrate – more peening stress [17].
2. Higher deposition temperature will induce lower plastic stress and thus lower peening stress.
3. Presumably, molten particles tend to deform less the peened surface –less peening stress.

These observations are illustrated in Figure 5-3. Depending upon the characteristic strain hardening of the coated materials, they develop peening stress at different magnitudes. In the present study, it has been found that hard alloys such as T-800 or cermets with high content of ceramic phase do not get peened as much as other alloys such as Ni, NiCr or cermets with higher metallic based matrix content.

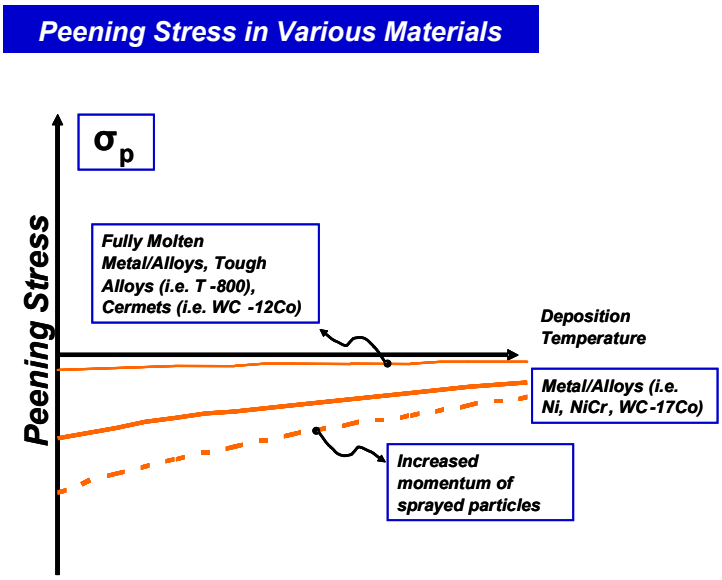

Figure 5-3. Development of peening stress for different materials with variation of deposition temperature

5.6 Quenching, Peening and Thermal Stresses

The final stress state of a deposited coating requires the summation of all the effects: *quenching and peening* (that constitute the *deposition stress*) and the *thermal stress*. The magnitude of the imposed thermal stress is directly proportional to the thermal mismatch for linear elastic materials. It is tensile in the coating when the substrate contracts at higher rate ($\alpha_s > \alpha_d$) and compressive when otherwise ($\alpha_d > \alpha_s$). Typical balance of stress in plasma spraying (quenching+thermal) is illustrated in Figure 5-4. The occurrence of the three sources of stresses in an as sprayed coating is illustrated in Figure 5-5.

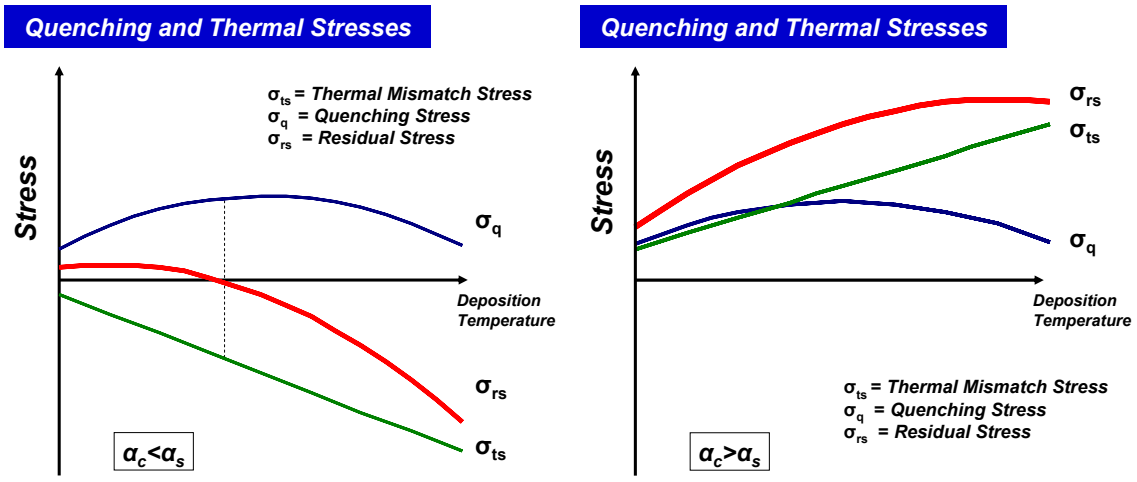

Figure 5-4. Schematic diagram of the variation of the final residual stress with deposition temperature, including quenching and thermal mismatch (typical for APS). After [1].

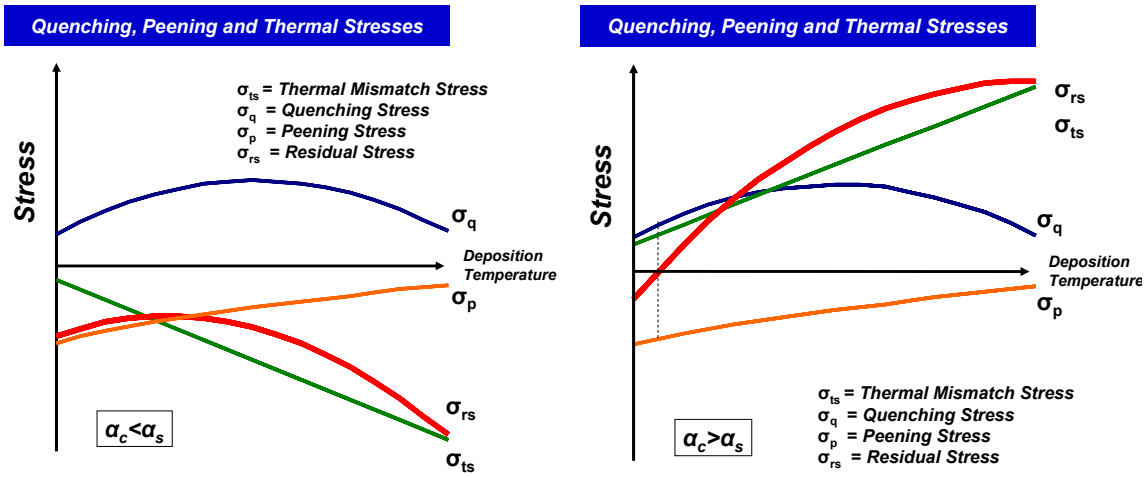

Figure 5-5. Schematic diagram of the variation of the final residual stress with deposition deposition temperature, including quenching, peening and thermal mismatch (typical for HVOF). For cold spray disregard quenching.

5.7 Synthesis

The design of a TS process requires basically the control of two main variables: particle state and deposition temperature. For instance, tuning fully molten particles can enhance quenching stress, accelerating them would increase peening of the underlying layer, and adding cooling to the whole system would eventually decrease thermal stresses. This suggests that a proper assessment of process parameters, assisted by stress evolution monitoring can lead to design stress states in coatings. Moreover, the understanding of the implications of the stress developed leads to estimate the microstructure integrity (e.g. cohesion, microcracking) and properties.

In the next section, the interactions of the first deposited layer and substrate, as well as, the interactions of deposited layer by layer coatings are studied by means of stress evolution analysis. Implications in adhesion/cohesion, compaction, hardening, among others are presented for several materials systems and processes.

5.8 PART I.

Coating-Substrate Interaction: Stress Evolution Approach

5.9 Introduction

Over the years, many researchers have studied the deposition of single splats on different substrate conditions. There has always been interest in the interaction between the particles/splats (coating units) impacting, spreading and solidifying over the substrate in the look for insight in the formation of bonds and the evolution of the microstructure of the sprayed coating. Several remarkable findings are summarized as follows:

- Fukumoto et al [12] found the existence of a threshold substrate temperature (transition temperature) above which splats spread without fragmentation.
- Jiang et al [13] demonstrated that the presence of adsorbates and condensates on the surface of the substrates played the dominant role on the fragmentation phenomena and consequent detriment of the adhesion; the substrate temperature effect being an artifact of surface desorption and not a direct physical contributor.
- Li et al [22] discussed the possible metallurgical bond of splats to the substrates by melting of the interface in select particle –substrate systems.
- Fauchais et al [23] described the quality of contact of the interface related to the impact pressure, wetting, and also reaffirmed the adsorbates/condensates.

All these findings at the micro-scale of the TS deposition have been correlated to the macro-scale operation, where for instance: 1) preheating reduces adsorbates/ condensates prior to the spraying; 2) increasing substrate temperature during deposition (above transition temperature) has been found to improve the cohesion between splats and reduce the number of defects [9], 3) materials such as Mo have been used as bond coats owing to the improved adhesion resulting from substrate melting.

5.10 Description of Principles

In the present study, an attempt to observe the interactions at the mesoscale level (first deposited layer and substrate) by *in situ* monitoring of curvature and thus stress is presented. During the deposition of the first pass several are these interactions, including: stress relief on the substrate due to heating, plastic yielding of the top layer of

the substrate or coating, residual stress build-up, among others. This can be done by the observation of the evolution of the stress during the onset of spraying session.

Fauchais referred in his work [23] that the contact between piled-up splats is controlled by the relief of quenching stress and that the stored elastic strain energy depends on the degree of relaxation mechanisms taking place during the spraying. The residual stress would thus conceivably represent the quality of the bonding occurring individually in each splat but measured at the mesoscale range – if splats bond better, they can pull harder.

Apparently, this principle to evaluate adhesion could be used flexibly between different materials and processes, but the occurrence of *stress build-up* mechanisms together with other *stress relief* mechanisms limits its use. For instance, interfacial sliding, micro-cracking and yielding all can reduce the strain energy accumulated within the splat. Therefore, different materials will undergo different stress relief mechanisms, examples: YSZ (micro-cracking) or Ni (yielding).

In this section, we first examine the described adhesion principle by evaluating the stress in thin layers of Mo-coatings sprayed by APS on substrates of different roughness (expected differences in adhesion strength). Later, similar experiments are carried out in APS-Ni, and HVOF - NiCr, NiCrAlY and WC-CoCr on different substrate materials, processes and roughness. Results are presented and discussed.

5.11 Principle Validation: Adhesion of Molybdenum thin coatings by APS

Single layers of Molybdenum coatings were sprayed onto grit blasted and then vacuum heat treated steel substrates of different roughness. Curvature evolution was monitored via ICP-sensor. APS process was chosen to separate the contribution of peening of HV processes.

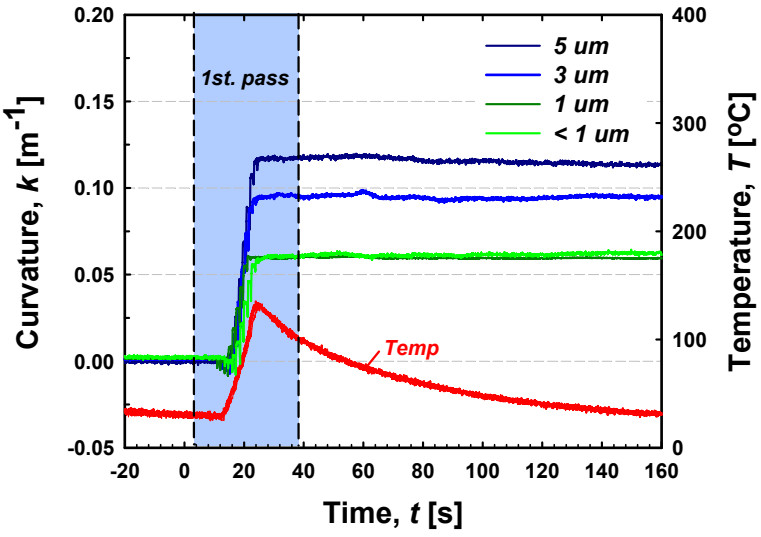

Figure 5-6. Curvature evolution during spraying of Mo single layer coatings on steel substrates of different roughness. Substrates were preheated to eliminate adsorbates/condensates.

A significant difference in curvature due to different quenching effect is observed in Figure 5-6. The higher the roughness in the substrate, the higher the residual stress developed by the coating..

Locally, as splats get strained in tension, the top layer of the substrate experiences a balancing strain of the opposite nature, compressive. Provided that substrates were heat treated and no differences in residual compressive stress are expected, the differences found are strictly related to deposit stress buildup and relief mechanisms.

Top view observations were carried out by SEM at two different magnifications 200X and 500X. Low magnification images, in Figure 5-7 show slight differences in the areal coverage of the splats, likely due to differences in deposition efficiency. Image analysis was carried out to find out the percentage of area covered versus uncovered after the first raster of the gun. Only the coverage of surface of *Ra* 1 μm appears significantly different. Such differences were accounted in the evaluation of the curvature assuming a periodic array of splats spread on the surface. Correction factors ranging from 1.05 – 1.1 were found applying analytical models for biaxial curvature due to the film arrays and cracks [24].

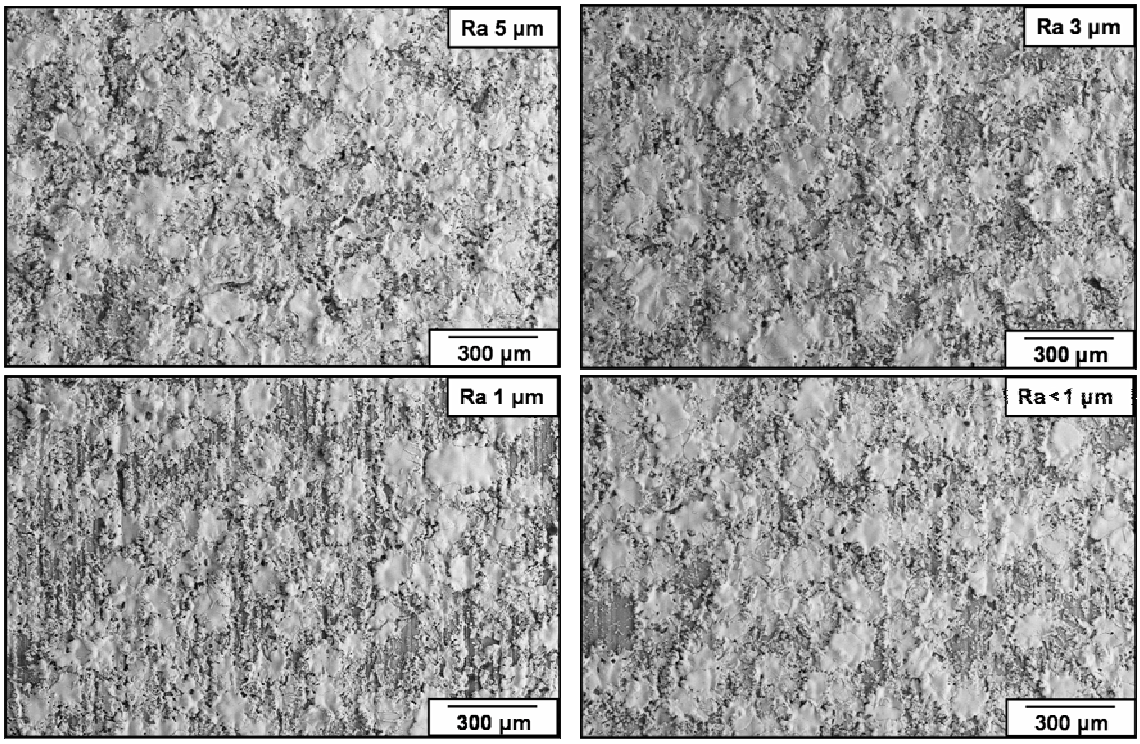

Figure 5-7 . Top view of single-layer Mo coatings on steel substrates of different roughness. Reduced deposition efficiency is observed in sample of Ra 1 μm roughness.

Stresses were evaluated using Stoney formula [25]. Results are presented on Figure 5-8. The variability of film thickness, due to overlapping splats or uncoated regions, was ruled out by adopting a fixed thickness of 25 μm for all coatings.

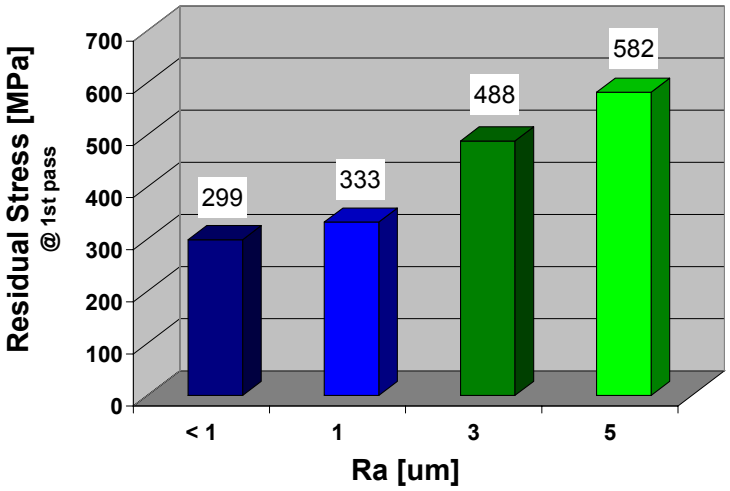

Figure 5-8. Residual stress in single layer deposited Mo coatings on steel substrates of different substrate roughness.

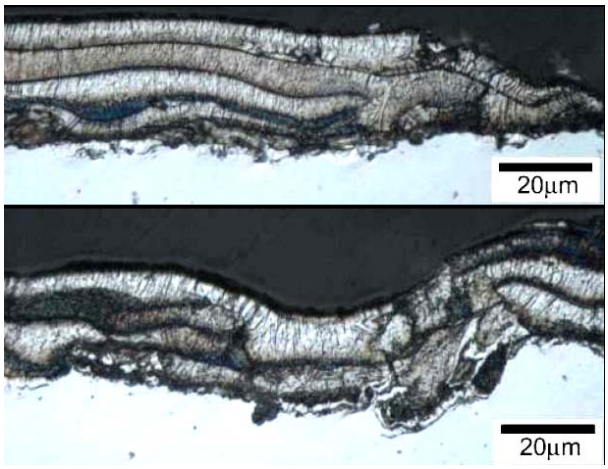

Figure 5-9 . Cross-section micrographs of Mo single layer coatings. Samples were etched. Top is substrate roughness of ~0.1 um (named as Ra < 1 um) and bottom is 5 um roughness.

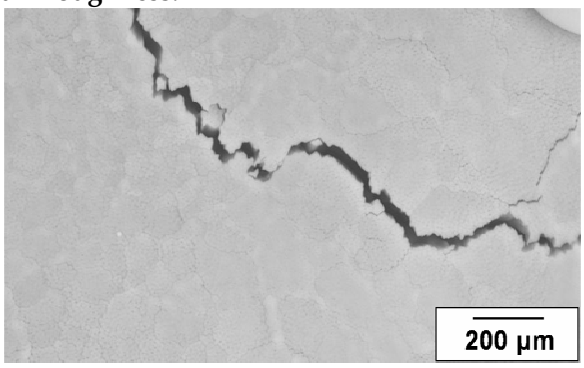

Figure 5-10. Surface of a Mo splat. Size of the columnar grains is estimated between 100-150 nm. Micro-cracks are observed across the splat and grain boundaries

Cross-section images support this consideration as presented in Figure 5-9 (Typical grain growth with preferential orientation is observed in contiguous splats). Residual stress values were in the range of 300-600 MPa, and higher than the yield strength of bulk Mo. This is expected for thermal sprayed coatings, as the yield strength is high owing to the small grain size. Matejicek et al [26] reported a possible yield strength for Mo-APS coatings of ~1300 MPa using the Hall-Petch relationship for small grain sized materials. High magnification images showed that in the splats, grain sizes vary from 100 nm to 150 nm as observed in Figure 5-10. The yield strength would range between ~1000 to ~1300 MPa. Based on this consideration, the stress values evaluated via curvature are acceptable

Li et al [22, 27] have reported substrate melting during the deposition of molybdenum particles on stainless steel substrates, characterized by the formation of flower-shaped splats and craters on the steel. In this regard, no substantial differences would be observed depositing splats on substrates of different roughness. Nonetheless, further observations by Vaidya et al [28] revealed that particle state influences substrate melting. Particles of low kinetic-thermal energy did not melt the substrate, whereas particles of high energy state showed substantial melting and spreading of the splat into flower shapes. Thermal conductivity of low-carbon steel is about one third of the stainless steel, and in this regard, substrate melting might not be prone to occur since the temperature at the interface drops.

SEM micrographs are shown in Figure 5-11. SEM - Top view of single-layer Mo coatings on steel substrates of different roughness.Figure 5-11 revealed splats of contiguous morphology and no apparent substrate melting. Microcracks are dispersed in almost all splats (Figure 5-10-Figure 5-11) which are evidence of stress-relief mechanisms occurring during the deposition. The particular roughness profile of condition *Ra* = 1 μm seems to limit the particle spreading. The dynamic flow of the particle spreading is obstructed by the corrugated surface. Splats show less number of microcracks in their surfaces and the flattening ratio has been reduced.

Condition *Ra* = 1 μm could have held higher residual stress but the lower deposition efficiency determined a reduced curvature.

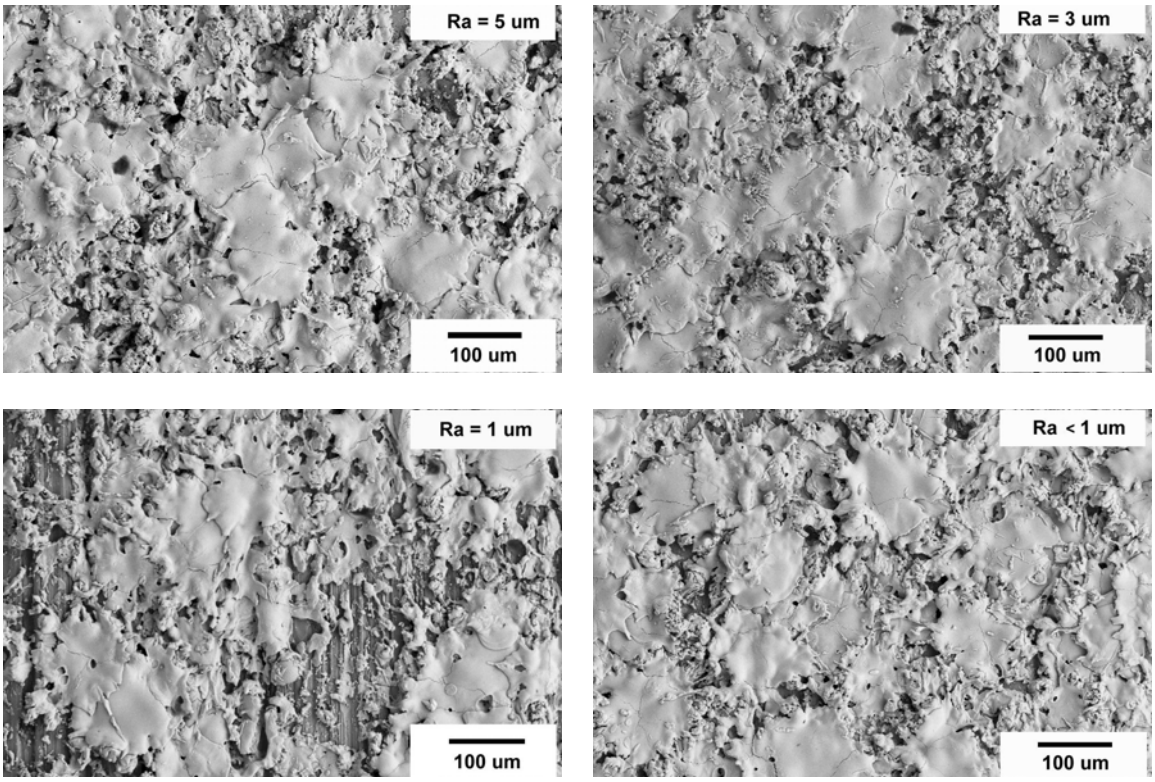

Figure 5-11. SEM - Top view of single-layer Mo coatings on steel substrates of different roughness.

5.12 Parameterization: Quenching Intensity Factor

A new indicator, first defined by Kuroda et al [17] related to the initial curvature change in the first pass is proposed. Referred here as the *quenching intensity factor* (*Iq)* [N/m] indicates the quality with which particles solidifying from the melting point transmit the force –inherent to their constrained volume change- through the points of adhesion, to the substrate.

Provided that during the deposition of the first pass, the thickness of the layer affected by the induced stress is relatively smaller than the substrate, the following approach based on Stoney formula [25] can be adopted:

$$I_q = \int_{z_1}^{z_2} \sigma dz = \frac{1}{6}\left(\frac{E_s}{1-\nu_s}\right) t_s{}^2 \kappa$$

Where Iq is the quenching intensity factor in [N], σ is the stress in the top layers (coating and peened region), κ corresponds to the curvature induced by the strained top layers, E_s is the elastic modulus of the substrate, υ_s is the Poisson's ratio of the substrate, and t_s is the thickness of the substrate.

The stress is integrated over the distance from the surface of splats assuming that the depth of stress distribution is sufficiently small as compared to the substrate thickness. Schematics of strained layers for quenching only and quenching+peening effect are illustrated in Figure 5-12.

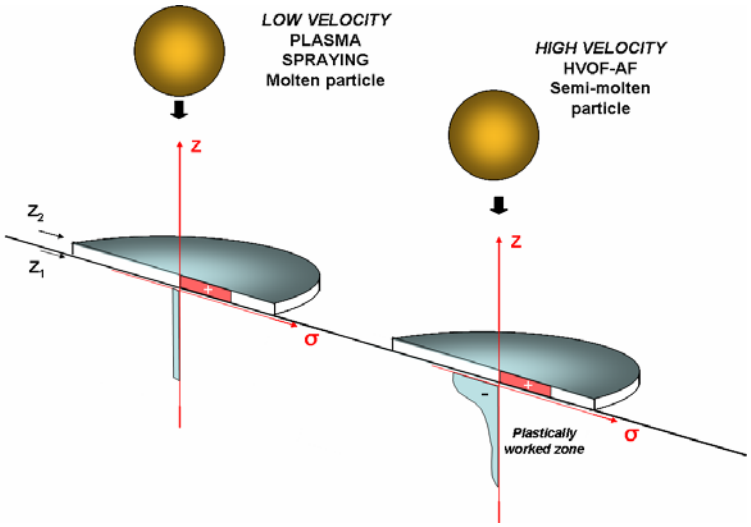

Figure 5-12. Schematic of stress generation by a thermally sprayed particle (a) molten particle, and (b) partially molten particle

5.13 Experimental Procedures

Table 5-1 summarizes the variables considered for the experimental exploration. A range of materials and processes provided insight to understand the interaction of the first layer and the coating. Several roughness conditions were tested. Vacuum annealing of roughened substrates allowed studying the effect of substrate roughness discarding the strain hardening due to the peening during substrate preparation.

Variables	Details
Coating Materials	Mo, Ni, WC-CoCr, Ni-20Cr, NiCrAlY
Processes	APS, HVOF-DJ, HVOF-JP-5000
Surface preparation	• Grit-blasting at different pressures (Ra = 1 μm (as received), 3 μm, 5 μm, < 1 μm (polished)) • Vacuum annealing-stress relieve • Rust
Substrate Material	Steel AISI 1018, Al, SS316, Ti_6Al_4V

Table 5-1. Description of variables considered in the experimental design

Table 5-2 summarizes the experiments carried out combining various processes and coating/substrate materials. Various substrate preparation conditions are investigated.

Coating	Process	Vacuum Annealing of Substrate*	Substrate Roughness - *Ra*					Substrate Material
			5 μm	3 μm	as recvd. 1 μm	Polished < 1 μm	Rusted** (5 μm)	
Molybdenum	APS	Yes	X	X	X	X	-	Steel
Nickel	APS	Yes	X	X	X	-	-	Steel
WC-CoCr	HVOF DJ	Yes	X	X	X	-	-	Steel
WC-CoCr	HVOF DJ	No	X	-	X	-	X	Steel
WC-CoCr	HVOF DJ	Yes***	X	-	X	-	-	Aluminum
WC-CoCr	HVOF JP-5000	No	X	-	-	-	-	SS316/Ti_6Al_4V/ Steel/Al
Ni-20Cr	HVOF DJ	Yes	X	-	X	-	-	Steel
Ni-20Cr	HVOF DJ	No	X	-	X	-	-	Steel
Ni-20Cr	HVOF DJ	No	X	-	X	-	-	Aluminum
NiCrAlY	HVOF JP-5000	Yes	X	X	X	-	-	Steel

* Low carbon steel substrates were vacuum heat treated to anneal residual stresses from grit-blasting. Annealing conditions were 450 °C for 1.5 hours.
** Low carbon steel substrates were deliberately rusted by heat treatment in air at 300°C for 1 hour.
*** Aluminum substrates were annealed in air, at 350 °C for 1.5 hours
Samples are grit-blasted in both sides to obtain a zero initial curvature

Table 5-2. Summary of experiments carried out to study the interaction between first deposited layer and substrate material.

5.14 Results and Discussion

5.14.1 APS-Metals: Mo and Ni results

Figure 5-13. shows quenching intensity factors for two sprayed materials: Mo and Ni, by APS process. As discussed in the previous sections, molybdenum showed higher quenching residual stress as the substrate roughness increases and that is represented now by the quenching intensity factor. Nickel, on the other hand, did not show this trend. For Ni coating, roughness of 1 μm held higher residual stress.

There are several possible reasons for this behavior. As discussed previously several mechanisms of stress-relief happen during deposition including yielding and creep. These two can be acting to a greater extent than sliding during the spreading of Ni. Differences in yield strength and elastic modulus between these two materials are significant and suggest that Mo is more susceptible to show higher residual stress. The profile of substrate Ra 1 μm could have constrained the spreading of the splats as suggested by Figure 5-11. Yielding of splats could lower as less spreading was possible resulting in higher residual stress.

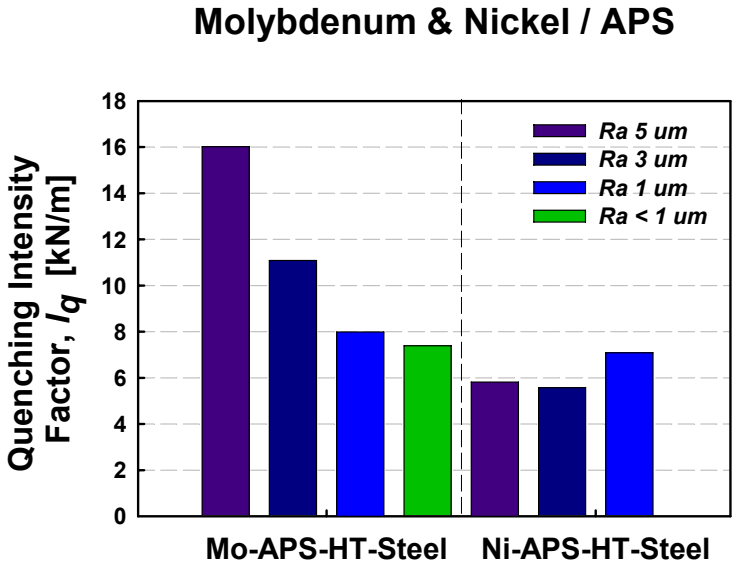

Figure 5-13. Quenching intensity factors for Mo and Ni sprayed by APS process on heat treated (HT) steel substrate of different substrate roughness.

5.14.2 HVOF Cermets: WC-CoCr by DJ2700 and JP-5000

5.14.2.1 WC-CoCr by HVOF- DJ-2700 on various substrate roughness

Figure 5-14 shows quenching intensity factors for WC-CoCr sprayed coatings on steel and aluminum substrates.

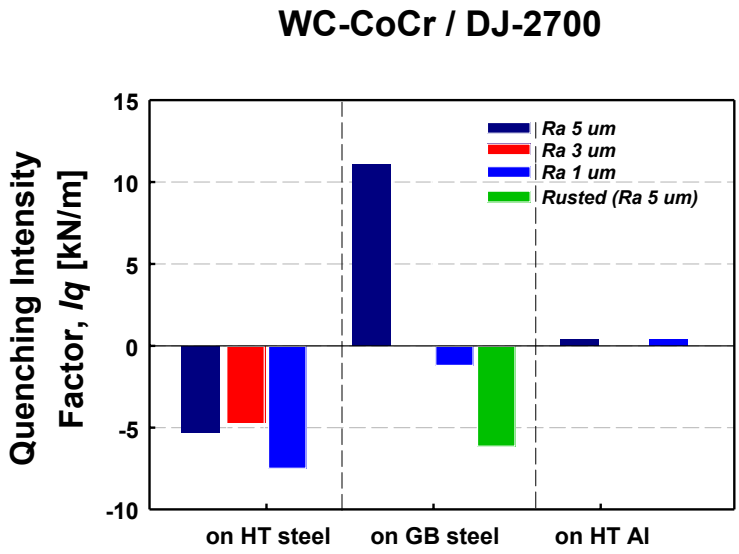

Figure 5-14. Quenching intensity factors for WC-CoCr coatings deposited by HVOF-DJ 2700 on: grit blasted and heat treated (HT) steel/Al substrates and only grit blasted (GB) steel substrates non heat treated.

The three sets of experiments are described as follows:

- A first set of experiments considered vacuum annealed steel substrates of different roughness. Values of *Iq* are negative due to the peening effect of the sprayed particles that induce compressive stresses in the top layer of the substrates. As the roughness increases the quenching effect and possibly the adhesion strength also increases resulting in a less negative *Iq*. Differences between *Iq* of 3 μm and 5 μm roughness are considered small and probably not important in terms of adhesion strength. Wang et al [29] reported that the adhesion strength for WC-Co HVOF coatings finds a threshold roughness of about 3 μm above which increases in bonding strength are not measurable. Evolution of the curvature during spraying is shown in Figure 5-15a.
- Second set of experiments is representative of the actual applicability of *Iq* as process control indicator. Highest *Iq* is reached in the roughest substrate (Ra 5 μm) owing to the improved adhesion and reduced peening due to the prior strain hardening of the blasting. Substrate of Ra 1 μm accepts more strain hardening and with lower adhesion ends in a slightly negative *Iq* value. Finally,

although the rusted sample presents similar roughness as the highest *Iq*, the poor adhesion of the particles makes them to act as like they were blasting without depositing. As a result, *Iq* ends highly negative. Figure 5-15b illustrates the remarkable differences that in-real time the operator can identify during the deposition of the first layer.

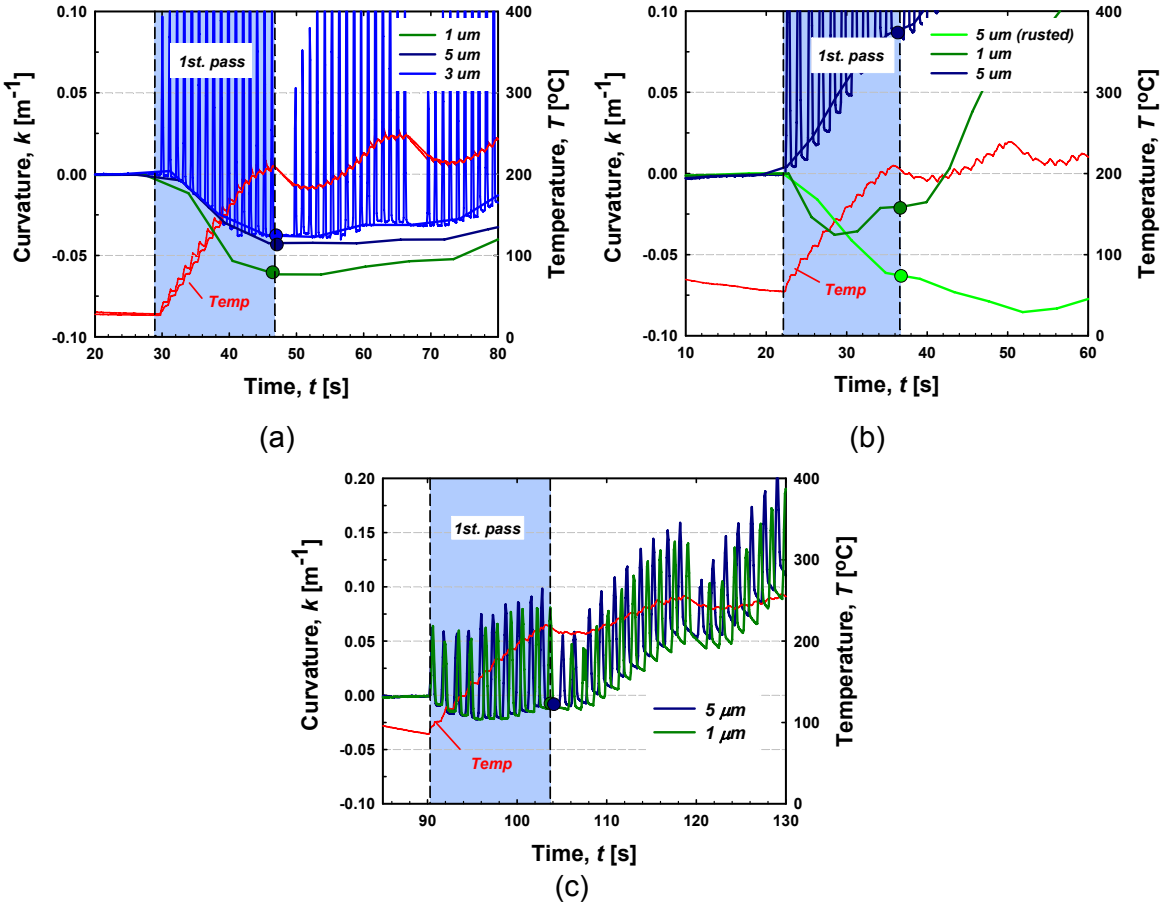

Figure 5-15. Curvature and temperature evolution during spraying on ICP sensor of WC-CoCr coatings by HVOF-DJ 2700 System: a) Steel substrates of different roughness and vacuum annealed, b) Steel substrates of different roughness as-grit blasted – no vacuum annealed, c) Aluminum substrates of different roughness and annealed in air. Raw data and smoothed curves are presented to avoid overlapping

- A third set of experiments was carried out over a low yield strength and ductile substrate. Aluminum was the material chosen. *Iq* values are close to zero which indicates that the peening effect on the substrate equates the quenching of the coating and the resultant bending is near zero. Observation of splats collected on Al substrates, as seen in Figure 5-16, showed that particles easily encrust in the soft material during impact. Therefore, thermal spraying in surfaces of different roughness does not show any difference inasmuch as the impact deforms any roughness profile.

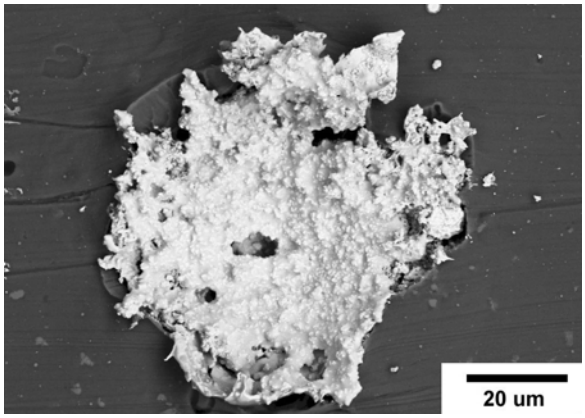

Figure 5-16. WC-CoCr collected splat over Aluminum substrate

Since the residual stresses from grit blasting were relieved by heat treatment and the differences in roughness are ruled out, the interaction in both cases is the same, as illustrated in Figure 5-15c.

5.14.2.2 WC-CoCr by HVOF- JP-5000 on various substrate materials

Figure 5-18 shows quenching intensity factors for WC-CoCr sprayed over different substrate materials. Process parameters were kept constant as well as the substrate roughness. Differences in *Iq* values arise from several factors, including: 1) strain, strain rate and strain hardening characteristic of the substrate material, 2) relief of stress from grit-blasting during the deposition (heat from the spray stream –particles and flame), and 3) quenching stresses – formation and relaxation mechanisms.

Ip in all four cases shows an important contribution of the quenching effect. Aluminum substrate owing to its lower strength (higher plastic deformation on impact of particles) holds higher peening effect and its *Iq* drops showing balance of both effects with almost no resultant bending. *Iq* in steel and Ti_6Al_4V showed similar behavior with dominance of quenching. The higher *Iq* for Ti_6Al_4V versus steel is explained by its higher strength that reduces the peening action. A substantial curvature change was observed when spraying on stainless steel (SS316). Experiments carried out rastering the gun on the plates without feeding powder revealed that only SS316 show an important curvature change due to stress relieve on the surface facing the flame. This phenomenon would account for the high initial bending.

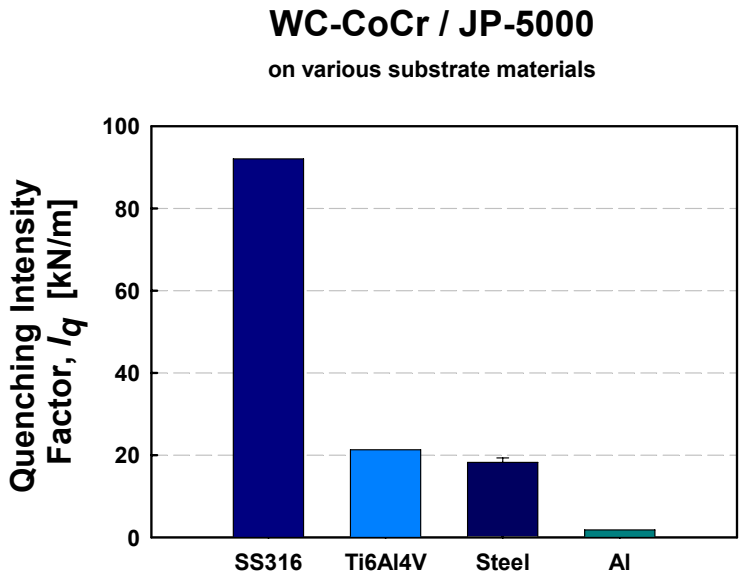

Figure 5-17. Quenching intensity factors for WC-CoCr coatings deposited by HVOF-JP-5000 on: grit blasted substrates (Ra 5 μm) of various materials. Steel *Iq* shows standard deviation bar calculated from three repeatability experiments.

5.14.3 HVOF Metal/Alloys: by DJ2700 and JP-5000

5.14.3.1 Ni-20Cr by HVOF-DJ2700

Similar trends as when thermal spraying WC-CoCr were observed with Ni-20Cr coatings. Figure 5-18 shows that rough substrates enhance quenching effect. This is more pronounced for the strain hardened steel and less for Al owing to its increased plastic deformation. In heat treated samples, differences in *Ip* are strictly due to enhanced quenching in rough substrates, whereas in the other two cases, steel and Al grit-blasted (GB), differences are due to lower peening and higher quenching for rough substrates and otherwise.

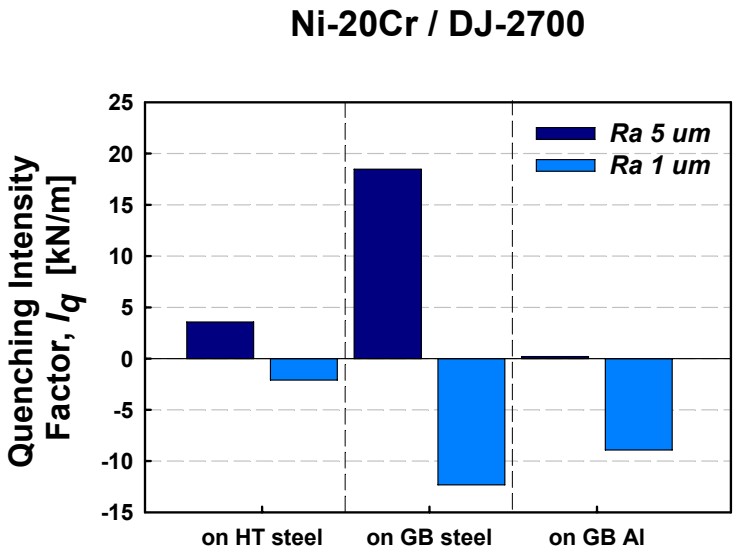

Figure 5-18. Quenching intensity factors of NiCr coatings deposited by HVOF-DJ 2700 on various substrates: steel grit blasted and heat treated (HT), steel grit blasted (GB) and non-heat treated, and Al grit blasted (GB) non heat treated.

5.14.3.2 NiCrAlY by HVOF-JP-5000

Seeking to expand the applicability of the principle, similar experiments were carried out by spraying NiCrAlY with a different HVOF system (JP-5000). Again, *Iq* is higher when better bonding is assured by using rough substrates, whereas in low roughness levels such as Ra 1 μm particles peen the substrate with poor deposition.

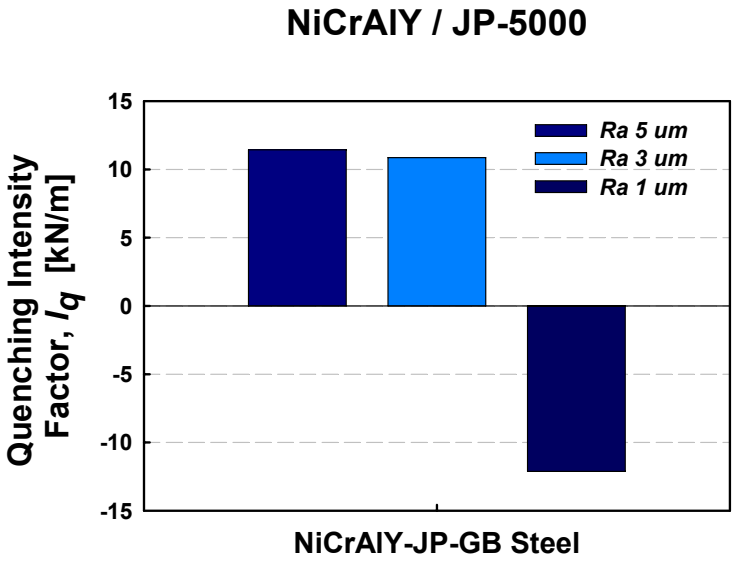

Figure 5-19. Quenching intensity factors of NiCrAlY coatings deposited by HVOF-JP-5000 on steel substrates of various roughness

5.15 Conclusions

The interaction between the first deposited layer and the substrate material was studied by analysis of the residual stress developed during deposition. The stress is sensitive to relief mechanisms such as micro-cracking, sliding, yielding or creep. The present study was aimed to use the stress developed in the system: coating-substrate as principle of measurement to evaluate the occurrence of stress buildup mechanism (quenching and peening) including relief mechanisms.

It is hypothesized that coatings deposited on substrates of different roughness underwent different levels of sliding due to the constraint of the asperities in the points of contact, resulting in different quenching stresses retained.

The applicability of this principle was demonstrated spraying Mo on steel substrates by APS. It was found that higher tensile stresses are retained when using rougher substrates. However, it is noted that some materials (e.g. Ni) may not be able to reflect a relation between adhesion improvement and residual stress because other mechanisms occur easily, even when adhesion is not perfect.

In HV spraying systems, the interaction of the first layer and substrate is highly affected by the large strain field determined by the impact of particles. The hardness and elastic-plastic properties of the substrate and coating play a role in the magnitude of peening effect induced on the underlying layer by an impinging particle. In this regard, different substrate roughness obtained by grit blasting results in substrates of different level of strain hardening. Thereupon, when depositing coatings on rough substrates, the induction of peening on a hardened surface is going to be lower and the quenching would be enhanced owing to the contact in the asperities, and otherwise. In this study, this principle was successfully demonstrated for several processes, materials and surface preparation conditions. Stress relief on the substrates was also observed as curvature change when heat is input to the substrates.

An adhesion-metrics factor was defined by evaluating the curvature change in the first pass using a simplified approach to evaluate stress in thin films , after Stoney [25], and named as *quenching intensity factor Ip*. It is envisioned that such factor can readily be implemented as a process control indicator in a production environment to monitor reproducibility and repeatability of the spraying sessions in real time.

5.16 PART II.
Stress Evolution in Thermal Spray Coatings

5.17 Introduction

As discussed in previous sections, stress development is an approach that can be used to monitor in real time the formation of thermal spray coatings. Determining and understanding the effect of each of the different stress factors of formation and/or relaxation and how they evolve into the final stress state is of key interest to process design. Coating designers require properties from sprayed coatings that range from hardness, toughness to porosity, and micro-cracking for strain tolerance. Distortion may also be a criterion since it results as a consequence of residual stress. These and many other criteria can be correlated to the stress evolution provided that the stress is an indicator of the strain and elastic-plastic state at which the coating is being subjected during deposition. Table 5-3 summarizes many of the property requirements for coatings sprayed by HV systems and their correlation to the mechanisms of stress: formation and relaxation.

Coating Design Requirements – HV systems	Mechanism of Stress formation and/or relaxation
Strain tolerance for coatings (including cracks and pores)	Enhance quenching until microcracking / macrocracking
Stiff, dense coatings	Enhance Peening,
Hard Coatings	Strain harden and strain rate harden from peening
Improved Splat-Splat Cohesion	Enhanced Quenching /avoid cracking
Low Distortion	Equate peening, quenching and thermal deflections

Table 5-3. Summary of coating design requirements and their correlation to the mechanism of stress buildup.

In the following sections, the evolution of the stress for many coating materials, substrates, processes and spraying parameters will be discussed. First, the behavior of various metal/alloys and cermets coatings deposited by different processes is investigated. Substrate temperature and particle states effects by means of changing feed rate or cooling, and/or torch parameters respectively are also discussed in terms of microstructure evolution and achieved properties.

5.18 Experimental Procedure

Table 5-1 summarizes the experiments carried out to study the stress evolution. Several materials, processes and process parameters were varied to address different effects.

Coating Material	Substrate Material	HV System	Effect under Study
NiCrAlY	Steel 1018	DJ-2700s	Metal/Alloys behavior
Ni	Steel 1018	DJ-2700	Metal/Alloys behavior
T-800	Steel 1018	DJ-2700	Metal/Alloys behavior
T-800	Steel 1018	JP-5000	Metal/Alloys behavior
WC-CoCr	Steel 1018	JP-5000	Cermets behavior
WC-12Co	Steel 1018	DJ-2700	Cermets behavior
WC-17Co	Steel 1018	DJ-2700	Cermets behavior
WC-10Co4Cr	SS316	JP-5000	Substrate Material
WC-10Co4Cr	Ti_6Al_4V	JP-5000	Substrate Material
WC-10Co4Cr	Al6061	JP-5000	Substrate Material
WC-10Co4Cr	Steel 1018	JP-5000	Substrate Material
WC-17Co	Steel 1018	JK-3000	Low substrate temperature
WC-17Co	Steel 1018	JK-3000	High substrate temperature
WC-17Co	Steel 1018	JK-3000	Increase in feed rate
WC-12Co	Steel 1018	WOKA Star	Flame Energy
WC-12Co	Steel 1018	WOKA Star	Flame Energy
WC-12Co	Steel 1018	WOKA Star	Flame Energy
CrC-NiCr	Steel 1018	JP-5000	Various process parameters: particle state, spray distance, rastering speed, feed rate
* Substrates were grit-blasted in both sides to obtain a zero initial curvature			

Table 5-4. Summary of experiments carried out to study the stress evolution for different materials, process and spraying parameters.

5.19 Results and Discussion

5.19.1 Evolution of stress in various materials/substrates

As stated in the introduction of this chapter, different materials behave differently during deposition owing to their particular thermo-mechanical behavior. In HV spraying, plastic deformation, strain and strain rate hardening play a significant role in the formation of the coating. Therefore, different materials: pure, alloys or composites are expected to behave differently depending upon the particle state and deposition

conditions. In the following sections, examples of the behavior of various materials thermal sprayed by various processes are shown. The presented evolution of the stresses is not meant to be material-specific but an example of the behavior of the chosen material-TS system.

5.19.1.1 Evolution of HVOF: Metal/Alloy Materials

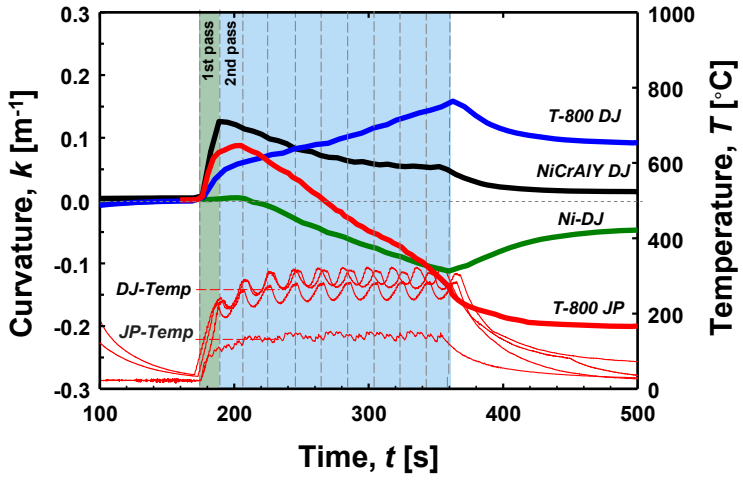

Figure 5-20. Curvature-Temperature evolution of various metal/alloy materials by DJ and JP-5000.

In Figure 5-20, the curvature -temperature evolution of various metal/alloys is presented. The analysis will be divided into three stages, being: 1) first layer and substrate interaction, 2) coating -layer by layer- evolution (steady state of stress development), and 3) Cooling and deflection due to thermal mismatch.

Concurrently with curvature evolution charts, stress evolution charts are also presented to compare the behavior of coatings involving effects of materials and thicknesses. The stress evolution is calculated by Stoney [25] approximation and taking only the steady state slope of $d\kappa/dt_h$ (κ-curvature change versus deposited thickness t_h) which represents the true development of stress in the coating.

- Considering the deflection caused by the deposition of the first layer in Figure 5-20, T-800 DJ and JP as well as NiCrAlY show dominance of quenching effect (positive deflection). This signifies that particles showed limited peening effect to the substrate and to the first deposited splats within the first raster of the gun. For Ni, the peening effect equated to the quenching with a resultant zero net stress. Being Ni of similar nature to NiCrAlY and not as tough as T-800, it is believed that its zero net stress is a result of higher contribution of peening over the Ni splats and not much to the substrate.
- After the first pass, the curvature change per time (or deposited thickness) reaches a steady condition, which represents that every pass develops similar amount of residual stress over the composite: substrate-coating, as seen in Figure 5-21. A positive slope represents dominance of quenching effect and tensile stress, which is the case of T-800 by DJ.

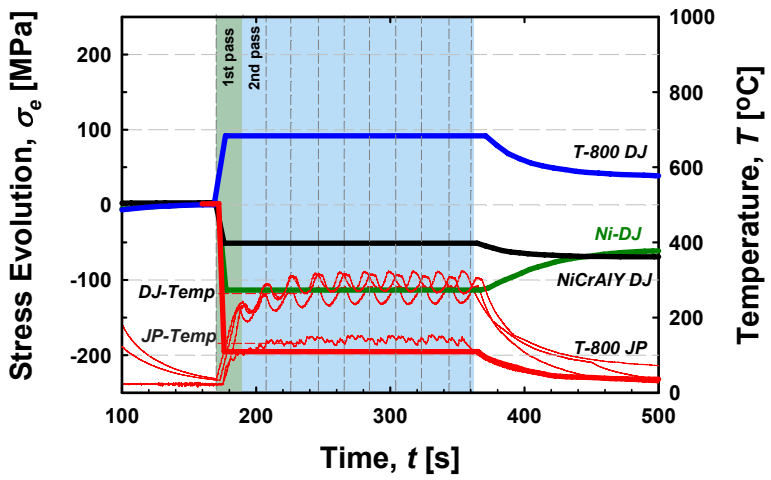

Figure 5-21. Stress-Temperature evolution of various metal/alloy materials by DJ and JP-5000.

T-800 (Tribaloy- Co alloy: Co, Cr, Mo, others) is a wear resistant coating with high toughness, which explains its limited capacity to be peened. Negative slopes, on the other hand, show dominance of peening effect, which includes Ni, NiCrAlY and T-800 by JP-5000.

Ni alloys are known to be prone to plastically deform and strain harden, whereas from the precedent result, T-800 was expected to develop tensile stress. However, JP-5000 system it is known to impart low heat input to the particles and high speeds. Therefore, the partially molten state could explain its higher peening intensity with lower quenching effect. The higher substrate temperature at which T-800 was sprayed with DJ system could have also contributed to decrease the peening effect.

- During cooling, the contraction of the steel substrate at higher rate than NiCrAlY and T-800 ($\alpha_{coat} < \alpha_{subs}$) induces compressive stresses in the coatings, whereas for Ni, since ($\alpha_{coat} > \alpha_{subs}$) the steel contraction induces tensile stresses in the coating.

It is worth noting that the absolute curvature of the sample does not necessarily represent the stress state in the coating. For instance, NiCrAlY in Figure 5-20 ends in positive final curvature. However, after the stress computation, the stress state of the coating is suggested to be in compression, as in Figure 5-21. More details about this estimation of stress state will be discussed in Chapter VI.

5.19.1.2 Evolution of HVOF: Cermet Materials

When spraying various cermet materials, significant differences were also observed. In Figure 5-22 and 23, curvature-temperature and stress evolution curves for various WC-cermet coatings (WC-17%Co, WC-12%Co, WC-10%Co-4%Cr) are presented, respectively.

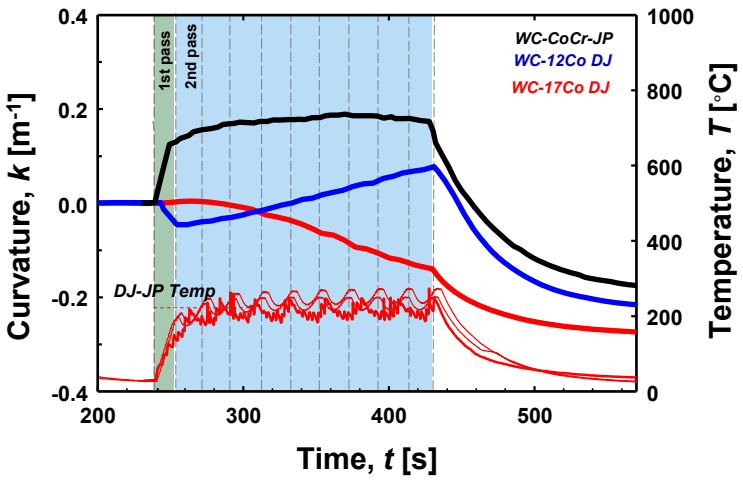

Figure 5-22. Curvature-temperature evolution of various cermet materials by DJ and JP-5000. JP-5000 used forced cooling with CO_2 jets

- The resultant deflection caused by the deposition of the first layer indicates that WC-12Co peens the substrate, WC-17Co shows neither dominance of peening, nor of quenching, whereas WC-CoCr favors quenching. WC-12Co can peen the substrate owing to its high carbide content, whilst in WC-17Co, its higher content of metal matrix reduces this. The positive inflection in WC-CoCr is believed to occur due to stress relief in the substrate from the flame and not much due to reduced peening capacity which is not the case of particles sprayed by JP-5000 system
- As the spraying progresses, all materials develop a steady buildup of stresses, tensile for WC-12Co, compressive for WC-17Co and slightly tensile for WC-CoCr. All differences are related to the Co-content, particle state, and substrate temperature. For this particular case, the overall substrate temperature reached the same value (~200 °C). However, the deposition temperature at which subsequent particles spread and form the coating may be different, specially for the case of JP-5000 run which used cooling jets of CO_2 to keep the overall temperature of the substrate low .

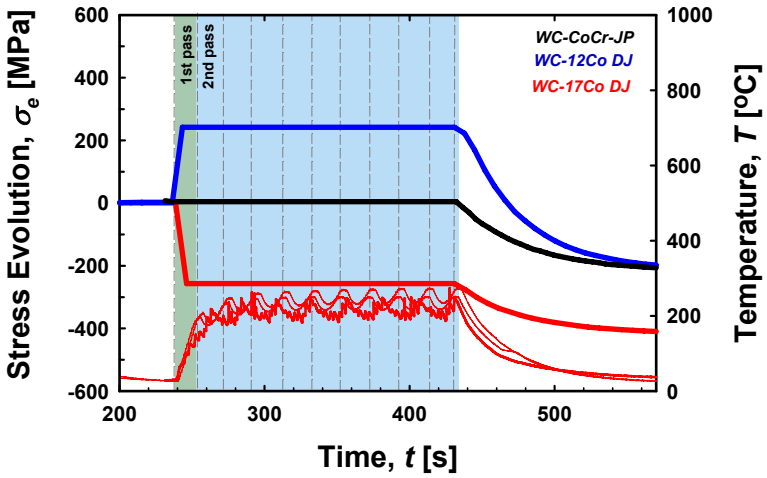

Figure 5-23. Stress evolution of various cermet materials by DJ and JP-5000. JP-5000 used forced cooling with CO_2 jets

- In the last portion of the runs, the lower α of WC-Co cermets (~$6x10^{-6}$ [1/°C]) compared to the steel (~$12x10^{-6}$ [1/°C]) induces compressive stresses in the coatings. Although, the evolution of the three coatings is different, all of them ended in compressive residual stress.

5.19.1.3 Evolution of HVOF: WC-CoCr on various substrate materials

WC-CoCr coatings with a JP-5000 system were sprayed over four different substrate materials: stainless steel 316, Ti_6V_4Al, steel 1018 and Al6061. Curvature-temperature evolution results are presented in Figure 5-24. Stress evolution curves are presented in Figure 5-25. Overall substrate temperature for all substrate materials was around (~200 °C).

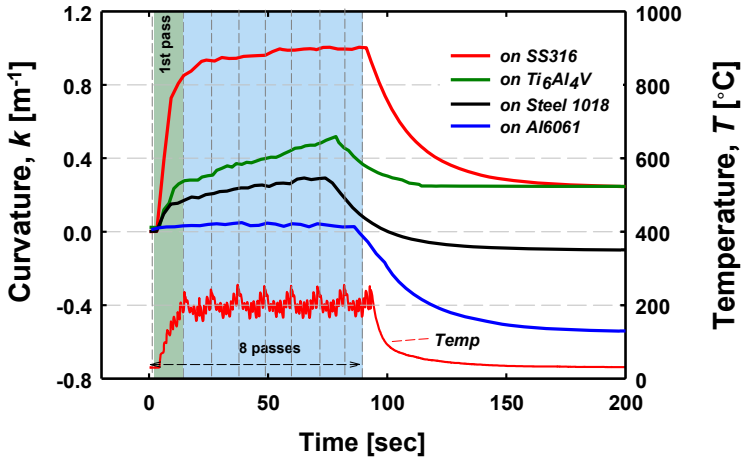

Figure 5-24. Temperature evolution of WC-CoCr coatings sprayed by JP-5000 system over different substrate materials. JP-5000 used forced cooling with CO_2 jets

- The interaction of the first deposited pass and the various substrate materials was discussed in Figure 5-17. In brief, the coatings developed zero to positive deflection with different peening intensities over the substrates. However, the peening over the deposited coating is assumed limited. Considerable stress relief of the substrate top layers is also expected due to flame heating and considered the main reason for the deflections, especially for SS316.
- The subsequent development of stress shows dominance of quenching effect with higher values for the higher yield strength substrate materials. It is possible that during the impact of the particles the strain field reaches the substrates. As a result, the peening effect may be enhanced in low yielding strength substrates like Al6061 and SS316, and reduced in high strength materials like Ti_6Al_4V.
- During cooling coatings are put into compression due to the negative α mismatch between coating and substrate. As the α of the substrate is larger[3], the thermal stress component is also larger.

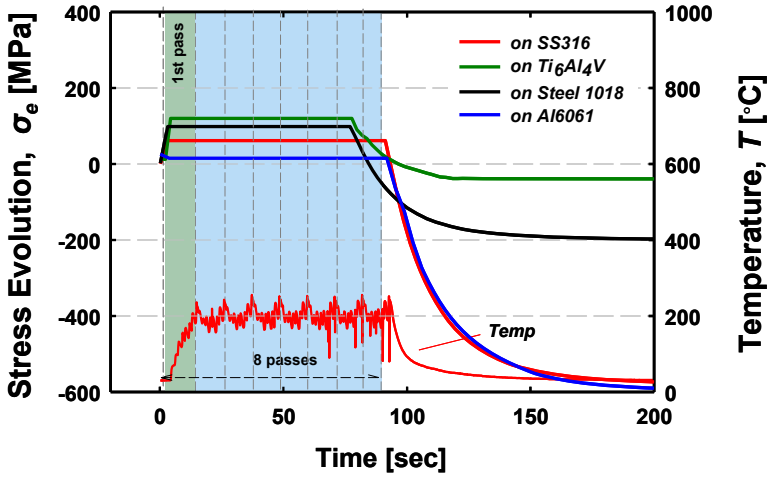

Figure 5-25. Stress evolution of WC-CoCr coatings sprayed by JP-5000 system over different substrate materials. Refer to Figure 5-24

It is highlighted that the stress evolution in comparison to the curvature evolution shows substantially different trends, i.e. in the case of SS316 substrate, curvature of the samples is positive, but very likely the stress in the coatings is compressive, as in Figure 5-25.

5.19.2 Effect of substrate temperature and feed rate in the evolution of stress

It has been discussed already that the coating formation and so, the stress evolution responds mainly to two factors: the particle state and the deposition temperature. In the

[3] Ti_6Al_4V, α= 8.6 x 10^{-6} [1/°C]; Steel 1018, α = 12 x 10^{-6} [1/°C]; SS316, α = 16 x 10^{-6} [1/°C]; Al6061, α = = 23 x 10^{-6} [1/°C]

this section, experiments directed to change the deposition temperature are discussed. The following section will discuss particle state changes.

To vary substrate temperature, one experiment was carried out by using cooling jets on the sides of the gun and the other by increasing the feed rate. The latter may have changed the particle state as well by effect of flame quenching. However, the change in stress evolution observed is explained basically by deposition temperature change.

In Figure 5-26, a typical commercial spray parameter was used to spray WC-17Co using a Jetkote gun with an overall substrate temperature of ~140°C achieved by setting air cooling jets (labeled as JK-WC-17Co). Dominance of quenching effect is observed during spraying. Upon cooling tensile stresses are diminished. It should be noted that WC-17Co can be sprayed with predominance of peening action (Figure 5-22, DJ-gun) or quenching (Figure 5-26, JK-gun) depending on the particle state and process conditions. A substrate at higher substrate temperature was sprayed under the same process conditions obviating the usage of cooling jets. Temperature arose to ~195°C, with a resultant increase in the quenching effect as a consequence of enhanced cohesion.

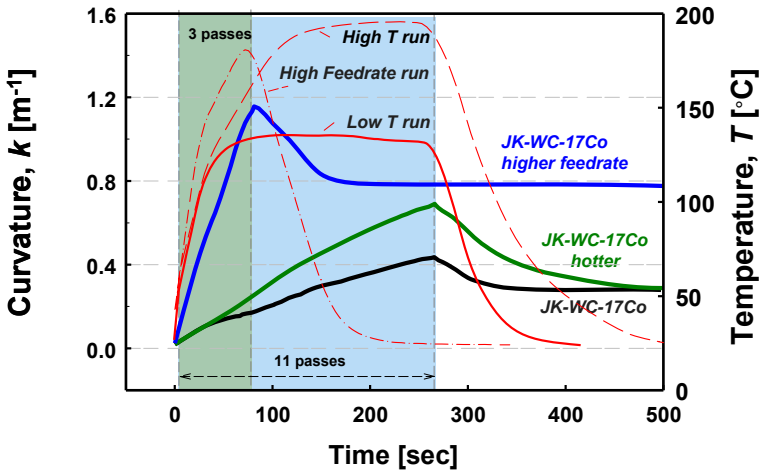

Figure 5-26. Temperature evolution of WC-17Co coatings sprayed by JK-3000 system at different substrate temperature and feed rate. 3 passes are needed to achieve similar thickness at higher feed rate vs 11 passes at lower feed rate.

The overall substrate temperature arose in 55°C, but locally at the particle to particle impact this temperature may have changed by a higher gradient. The availability of thermal energy at the splat formation improves the cohesion at the intersplat interfaces by improving wetting and metallurgical bonding.

It is worth noting that the final residual stress in Figure 5-26 for the two coatings sprayed at different substrate temperature is the same. Although, the quenching effect for the higher substrate temperature condition is higher, the thermal stress is also enhanced due to the higher thermal gradient.

A more significant effect of improved cohesion is observed when feed rate is increased. Under the same gun parameters but tripling the feed rate a severe increment of curvature and quenching stresses is observed. Here, the lapsed time between particles depositing is reduced in three times. Therefore, the temperature of the

underlying particle is substantially much higher at the time of impact, which results in improved cohesion and higher residual deposition stresses.[4]
The overall substrate temperature arose by 55°C, but locally at the particle to particle impact this temperature may have changed by a higher gradient .

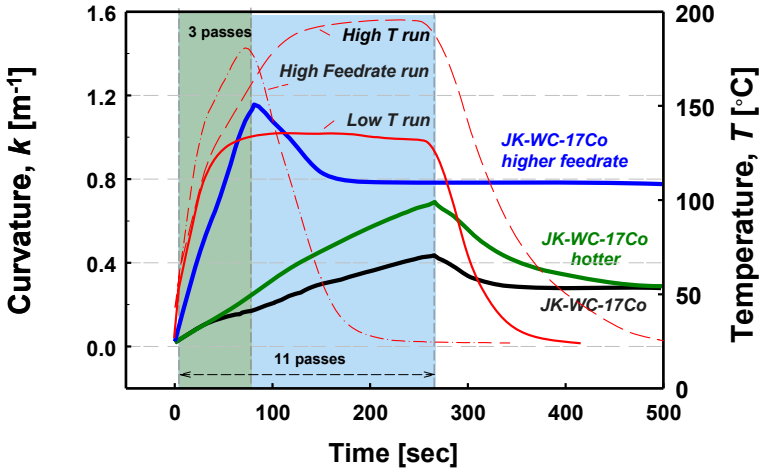

Figure 5-27. Temperature evolution of WC-17Co coatings sprayed by JK-3000 system at different substrate temperature and feed rate. 3 passes are needed to achieve similar thickness at higher feed rate

The latter result suggests that even though improved spraying systems can handle higher feed rates, there is a concomitant need to raster the gun at higher speeds to avoid the buildup of high quenching stresses that could result in undesired micro or macro-cracking of coatings during spraying.

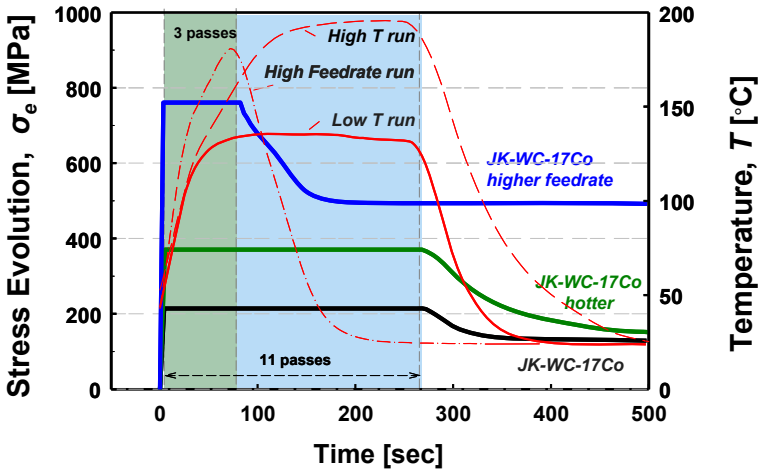

Figure 5-28. Stress evolution of WC-17Co coatings sprayed by JK-3000 system at different substrate temperature and feed rate. Rastering speed was kept constant at 1.25 m/s

[4] . It is noted that the stress calculation of the coating at high feed rate may have been affected by the increasing substrate temperature that defines a positive bending and thermal mismatch as the sample heats up.

5.19.3 Effect of particle state in the evolution of stress

Thick WC-12Co coatings (~0.5 mm thickness) were sprayed on steel substrates using three spraying parameters. First, typical commercial parameters were used as reference. Coating sprayed under this condition is named as "medium energy condition" (*med E*).

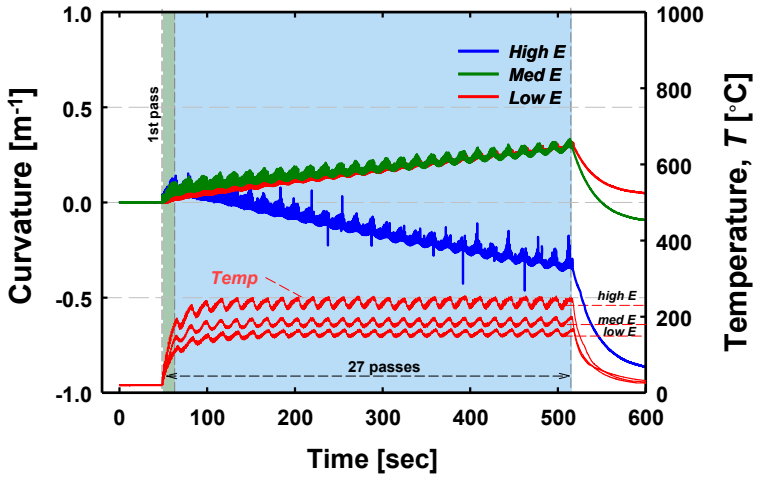

Figure 5-29. Curvature-temperature evolution of WC-12Co coatings sprayed by WOKA Star system at different spraying conditions: low, medium and high energy

The flow of oxygen gas and liquid fuel was reduced in 30% to define a "low energy condition" (*low E*) and increased in 30% to define a "high energy condition" (*high E*). Curvature evolution of these coatings was monitored by ICP sensor and results are presented in Figure 5-29.

All coatings developed a steady curvature change along the buildup of 27 passes, which evidences a consistent deposition of similar layers. When computing the stress evolution, as seen in Figure 5-30, the trend of higher peening intensity caused by particles sprayed at higher energy flames is observed.

The particle state of these three conditions can be predicted from the analysis of the evolution of the residual stress. The *low E* condition may have defined low speed and higher melting (longer dwell time) as to favor the development of quenching stress.

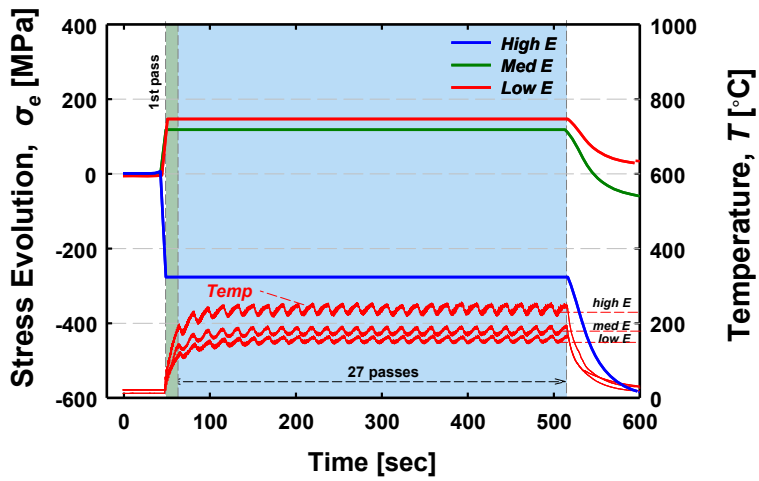

Figure 5-30. Stress evolution of WC-12Co coatings sprayed by WOKA Star system at different spraying conditions

As the flame energy was increased, the thermal and kinetic input was also increased in the particles. This resulted in favoring the peening effect, reducing the resultant tensile stress buildup for the *med E* condition until switching to compressive stress buildup for *high E* condition.

The tuning of flame energy also changed the heat input to the substrate by the flame and the particle stream. As the flame energy increased, substrate temperature also increased, and so, the thermal stress component. Adding the quota of residual stress from processing and thermal mismatch, the three conditions define three different residual stress states at the end of deposition: tensile for *low E*, compressive for *med E*, and highly compressive for *high E*.

Elastic modulus and hardness were evaluated by micro-indentation. Results are shown in Figure 5-31. The trend of stiffer and harder coatings correlated to the higher peening intensity is observed. Although the magnitude of the stress change versus the magnitude of the property change are substantially different, the evaluated peening effect can suggest a correlation of hardening of the metal matrix, compaction of the microstructure and enhanced intersplat contact, resulting in high elastic modulus and hardness. The heat contribution from the particles to improve the intesplat bonding strength is not clearly reflected in the stress developed, and there is probably where the differences in the trends lie.

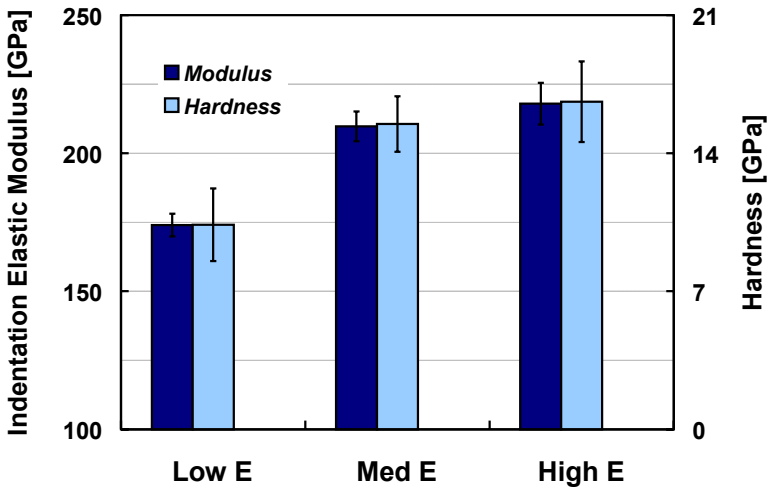

Figure 5-31. Indentation and hardness measured by micro-indentation on WC-12Co coatings sprayed by WOKA Star

5.19.4 Effect of process parameters in the evolution of stress

A 2^4 factorial set of experiments was carried out aiming to optimize the residual stress state of CrC-NiCr coatings sprayed by JP-5000. Coatings of 0.25-0.35 mm thickness were sprayed on ICP sensor. The variables considered in the optimization are:

1. Spraying parameters
2. Standoff distance

3. Feed rate, and,
4. Robot speed (rastering speed)

First three are aimed to tailor particle state and all the four of them change deposition temperature. The overall substrate temperature was significantly different between sets of experiments at two different rastering speeds due to the differences in residence time of the flame over the substrate. Consequently, the analysis was divided into two- 2^3 factorial sets of experiments, thus:

- Set #1: Robot Speed = 0.7 m/s, and a resultant average substrate temperature of 130 °C
- Set #2: Robot Speed = 0.42 m/s, and a resultant average substrate temperature of 200 °C

An illustration of the design of experiments (DoE) is presented in Figure 5-32. The key representing each case of DoE can be read as follows:

(+ = 14" Spray distance; + = 14 lb/hr Feedrate ;+ =1850/6.8 oxy/fuel)

(- = 13" Spray distance; - = 10 lb/hr Feedrate ; - = 1708/7.2 oxy/fuel)

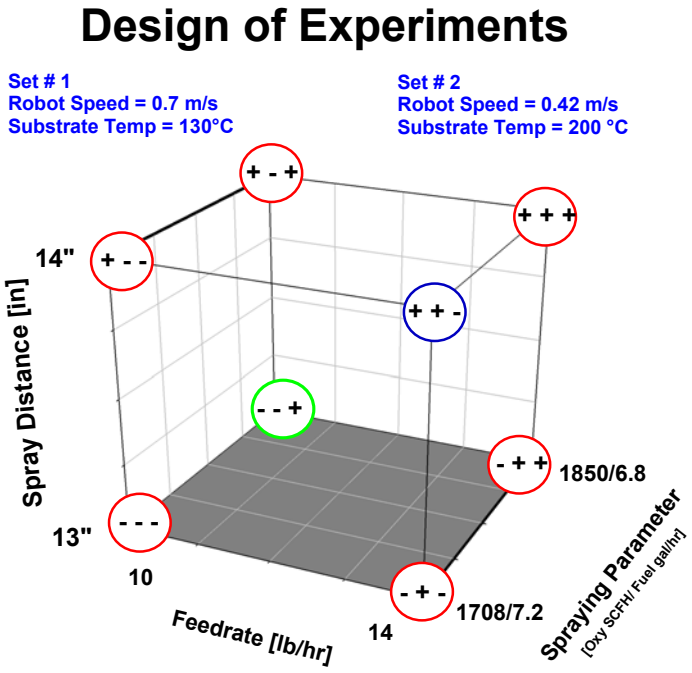

Figure 5-32. Illustration of the Design of Experiments (DoE) aimed to optimize residual stress state of CrC-NiCr coatings sprayed by a JP-5000 gun. Two sets of experiments are divided considering two different rastering speeds

The stress at the end of deposition and at the end of cooling was calculated via Brener-Senderoff's [30] approximation for thick film coatings using the curvature readings from ICP sensor. Results are presented in Figure 5-33.

Salient results are summarized as follows.

1. The overall stress state of coatings sprayed at lower rastering speed (0.42 m/s) is more compressive. This result is contrary to the trend of higher substrate

temperature showing higher tensile stress owing to enhanced cohesion. A key to explain this effect may be found in the analysis of Figure 5-5 that shows that when exceeding certain value of the deposition temperature, the quenching stress drops. The resultant overall stress with increasing substrate temperature can result in more compressive residual stress, during deposition and during cooling.

2. The thermal stress component adds to coatings compressive stress. Higher compressive component is applied to set #2 versus set #1 due to the larger thermal gradient.

3. The display of stress values in the DoE chart is analogous for both sets of experiments (#1 & #2), with the highest compressive stress at the corner (-, -, +), and highest tensile stress at the corner (+, +, -)

4. Particle state was monitored by DPV2000 in all spraying runs at a fixed spray distance and feed rate. Average results are presented in Table 5-5.

Spray Parameter Oxygen (SCFH)/ fuel (gal/h)	**Particle Temperature**	**Particle Velocity**
1850/6.8	1854 ± 23	745 ± 18
1708/7.2	1731 ± 29	775 ± 55

Table 5-5. Particle temperature and velocity for spraying parameters used to spray CrC-NiCr with a JP-5000 system

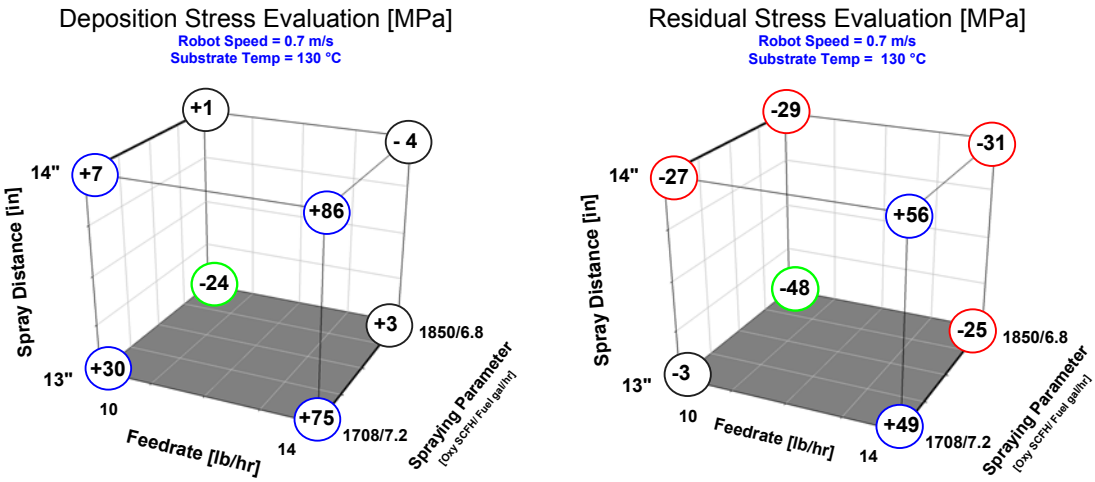

(a) **(b)**

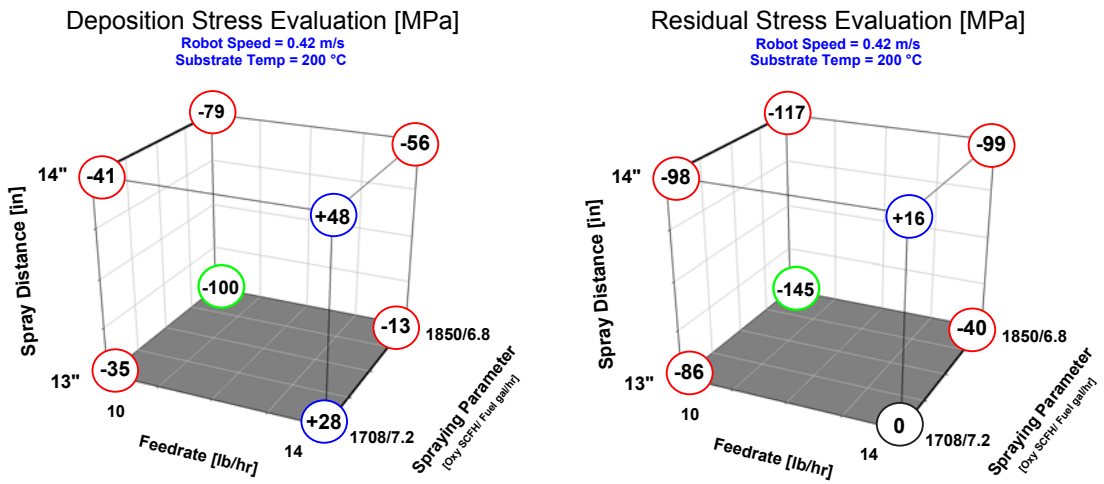

(c) **(d)**

Figure 5-33. Deposition and residual stress of two-2^3 factorial set of experiments spraying CrC-NiCr with a JP-5000 system. a) & b) show results of first set of experiments at a robot speed of 0.7 m/s. c) & d) shows results corresponding to robot speed of 0.42 m/s. Stress values are illustrated in color: green for the highest compressive value, red for compressive stress, blue for tensile stress, and black for near zero stress.

5. More compressive conditions were obtained by using 1850/6.8 process parameters. The overall particle velocity of both conditions is not significantly different and so, the peening intensity is not expected to be much different between the two parameters. However, the particle temperature shows significantly more difference. The higher particles temperature condition (1850/6.8) may be affected more strongly by yielding and/or creeping during deposition as to lower the quenching effect. This result is in agreement with the aforementioned analysis of substrate temperature in point 1 of this section.
6. Shorter spray distances as well as lower feed rate tend to favor the buildup of more compressive stresses. Only the overall effect is considered because there exists a wide range of possibilities to affect the particle state and deposition conditions under the control of these variables.

The in-plane elastic modulus of the samples produced after DoE was experimentally obtained via low temperature heat cycling tests. The curvature-temperature behavior during cooling was used to compute the elastic modulus of the coatings assuming a α value for CrC-NiCr of 9.8 x10^{-6} [1/°C]. The description of this experimental procedure is described elsewhere [6]. In Figure 5-34, the results of residual stress for the set of experiments #1 and #2 are plotted as a function of the elastic modulus. Additional results from experiments carried out with the same powder but different spraying system, this time Jet-Kote are also presented to illustrate the trend.

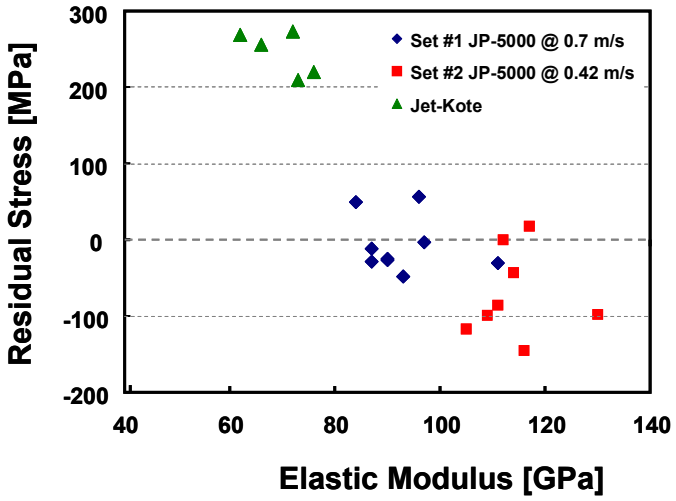

Figure 5-34. Correlation between residual stress state and coating elastic modulus as a result of deposition conditions

The contribution of peening effect during coating deposition to the compaction and stiffening of the coating results in higher compressive residual stress directly correlated to the elastic modulus. This trend does not intend to signify that there exists a fundamental and physical relation between residual stress and elastic modulus, but that there exists a process induced change in microstructure represented by its stress state and translate into mechanical property changes.

The present case of study highlights the influence of spraying parameters, other than the traditionally monitored particle temperature and velocity, in the coating formation and properties of the coatings. Virtually, only the monitoring of the stress evolution has enabled the observation of the effect of rastering speeds, feed rate and standoff distance during coating formation in real-time. All the variables used in this study have shown significant influence in the resultant stress state of the coating. The need of exploratory studies as to optimize the stress state is emphasized.

5.20 Conclusions

The formation of HV sprayed coatings was studied through recourse to monitoring the stress evolution during deposition. The buildup of coatings by impacting particles with high kinetic and thermal energies occurs with a significant quota of plastic strain, strain and strain rate hardening, named as peening. The action of peening effect results in reduced porosity, compaction, enhanced intersplat bonding and hardening of coatings. The intensity at which peening occurs during deposition is evaluated by the induction of compressive residual stresses.

During deposition, particles sprayed by HV systems develop tensile stress due to quenching, and compressive due to peening on the underlying layer. This generation of stresses can lead to dominance of either tensile or compressive stress depending upon the thermal-mechanical behavior of the particles at impact. Therefore, the stress

evolution takes place with particular characteristics for different materials according to their particle thermal/kinetic state and the deposition conditions of temperature, cleanliness (adsorbates/condensates), roughness, etc. Thus, metal/alloys feedstock materials generally show compressive stress buildup, whereas cermets favor tensile stresses as the ceramic phase content increases.

The stress evolution analysis has allowed the understanding of coating formation. Adhesion/cohesion, micro-cracking, and hardening, among others, are qualitatively evaluated accordingly to the stress developed within the microstructure. For instance, higher peening intensity was correlated to stiffer and harder coatings in cermet materials (WC-Co and CrC-NiCr coatings). The great potential of this finding is that optimization of coating properties can be achieved and addressed in real time. . This is particularly important in production of carbides coatings where meeting standard specifications is demanded. Process variables, such as, feed rate, robot speed, spray distance, etc that typically are not monitored by any sensor are observed *in situ* by principle of stress buildup examination.

Provided that the every feedstock material may behave particularly under certain spraying conditions, optimization methods applied to process parameters to achieve desired residual stress states are encouraged.

5.21 References

[1] S. Kuroda, T. W. Clyne, Thin Solid Films 200 (1991) 49-66.
[2] M. Kobayashi, T. Matsui, Y. Murakami, International Journal of Fatigue 20 (1998) 351-357.
[3] F. Hugot, J. Patru, P. Fauchais, L. Bianchi, Journal of Materials Processing Technology 190 (2007) 317-323.
[4] T. Nakamura, Y. Liu, International Journal of Solids and Structures 44 (2007) 1990-2009.
[5] S. Kuroda, Fukushima, T., Kitahara, S Vacuum 41 (1990) 1297-1299.
[6] J. Matejicek, S. Sampath, Acta Materialia 51 (2003) 863-872.
[7] A. Tricoire, Vardelle M., Fauchais P., High Temperature Material Processes (An International Quarterly of High-Technology Plasma Processes): An International Journal 9 (2005) 401-413.
[8] L. Bianchi, Lucchese, P., Denoirjean, A., Fauchais, P., Kuroda, S., Evolution of quenching stress during ceramic thermal spraying with respect to plasma parameters in: 1995 Advances in Thermal Spray Science and Technology. Proceedings of the 8th National Thermal Spray Conference, Houston, USA, 1995, pp. 267-271.
[9] S. Sampath, X. Jiang, Materials Science and Engineering A 304-306 (2001) 144-150.
[10] S. Sampath, X. Y. Jiang, J. Matejicek, A. C. Leger, A. Vardelle, Materials Science and Engineering A 272 (1999) 181-188.
[11] X. Jiang, J. Matejicek, S. Sampath, Materials Science and Engineering A 272 (1999) 189-198.
[12] M. Fukumoto, Y. Huang, Journal of Thermal Spray Technology 8 (1999) 427-432.
[13] X. Jiang, Y. Wan, H. Herman, S. Sampath, Thin Solid Films 385 (2001) 132-141.
[14] ASTM_G65-00e1, Standard Test Method for Measuring Abrasion Using the Dry Sand/Rubber Wheel Apparatus, in: vol ASTM International, ASTM International.
[15] Y. Itoh, M. Saitoh, M. Tamura, Journal of Engineering for Gas Turbines and Power 122 (2000) 43-49.
[16] S. Kuroda, Y. Tashiro, H. Yumoto, H. Fukanuma, Proceedings of International Thermal Spray Conference 1997 1 (1997) 805-811.
[17] S. Kuroda, Y. Tashiro, H. Yumoto, S. Taira, H. Fukanuma, 15th International Thermal Spray Conference 1 (1998) 569-574.
[18] P. Bansal, P. H. Shipway, S. B. Leen, Acta Materialia 55 (2007) 5089-5101.
[19] T. Schmidt, F. Gartner, H. Assadi, H. Kreye, Acta Materialia 54 (2006) 729-742.
[20] M. Watanabe, S. Kishimoto, Y. Xing, K. Shinoda, S. Kuroda, Journal of Thermal Spray Technology 16 (2007) 940-946.
[21] G. R. Johnson, W. H. Cook, Eng. Fract. Mech. 21 (1985) 31-48.
[22] L. Li, X. Y. Wang, G. Wei, A. Vaidya, H. Zhang, S. Sampath, Thin Solid Films 468 (2004) 113-119.
[23] P. Fauchais, A. Vardelle, M. Vardelle, M. Fukumoto, Journal of Thermal Spray Technology 13 (2004) 337-360.

[24] L. B. Freund, ebrary Inc., S. Suresh, Thin film materials stress, defect formation, and surface evolution, in: Cambridge University Press, Cambridge, UK ; New York, 2003, pp. xviii, 750 p.
[25] G. G. Stoney, Proceedings of the Royal Society, London A82 (1909) 172-175.
[26] J. Matejicek, S. Sampath, Acta Materialia 49 (2001) 1993-1999.
[27] L. Li, Stony Brook University, On the deposit formation dynamics and multiscale characterization of thermal sprayed splat structures, in: Stony Brook University, 2004., 2004, pp. xv, 153 leaves.
[28] A. Vaidya, T. Streibl, L. Li, S. Sampath, O. Kovarik, R. Greenlaw, Materials Science and Engineering: A 403 (2005) 191-204.
[29] Y. Y. Wang, C. J. Li, A. Ohmori, Thin Solid Films 485 (2005) 141-147.
[30] A. Brenner, S. Senderoff, J. Res. Natl. Bur. Stand. 42 (1949) 105-123.

Chapter 6

RESIDUAL STRESS MEASUREMENTS BY NEUTRON AND X-RAY DIFFRACTION, AND CURVATURE APPROACH BY *IN SITU* COATING PROPERTY (ICP) SENSOR

In HV spraying, in addition to the usual quenching and thermal mismatch stresses, one also observes peening stresses associated with particle impact at high velocities (600-800 m/s). The peening effect induces compressive stresses due to plastic deformation of the substrate and deposited layers. Competition among tensile stresses (due to quenching) and compressive stresses (due to peening) is present during spraying. Peening effect occurs between subsequent layers and among the layer itself. (Refer to section: peening stress, in Chapter V for more details). The model of Tsui and Clyne to predict residual stresses in thermal spray coatings can be applied to HV spraying coatings with certain limitations and considerations.

In the present chapter, the evaluation of residual stress by curvature analysis is compared to diffraction measurements. A detailed description of ICP-sensor and data analysis is presented as reference for other chapters in this dissertation in which ICP sensor data has been presented.

6.1 Residual Stress Profiles

The presence of residual stress profiles in relatively thin plates causes their bending. Consider a coating sprayed by APS in which tensile stresses due to quenching are developed, as illustrated in Figure 6-1. The tensile stress exerted by quenching is balanced in the substrate by compressive stresses. In order to balance the moment, curvature of the composite occurs. The final stress profile is the result of the summation of the quenching stress and the stress produced by the bending.

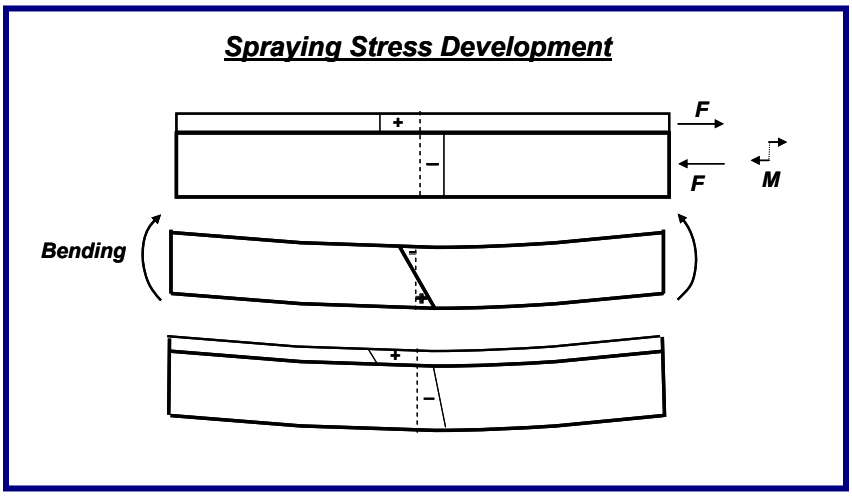

Figure 6-1. Residual stress profile and bending: example of quenching stress in an APS coating

Considering this time the peening effect due to grit blasting, the balance of forces and moments occurs as follows. Plastic deformation of the top layer induces compressive stress in the surrounding material. The balance of forces through the thickness generates tensile forces beneath the compressive region. To balance the moment, the plate bends and imparts tensile stress in the convex side and compressive stress in the concave. The resultant stress profile would likely show compressive stress in the blasted layer, tensile in the center layers and tensile or compressive at the bottom depending upon the intensity of the peening. Peening effect is illustrated in Figure 6-2.

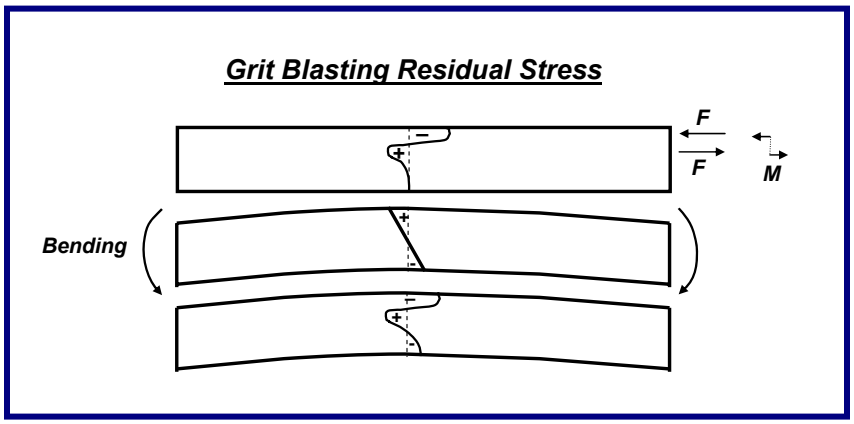

Figure 6-2. Residual stress profile and bending: example of peening stress due to grit blasting

In HV thermal sprayed coatings analysis of the stress will include the effect of quenching stress in addition to the peening effect for each layer, as illustrated in Figure 6-3. Here, depending upon the balance between the quenching stress and the peening stress, the curvature of the plate can be either compressive or tensile. Note that the

curvature of the plate does not necessarily indicate the stress in the coating, it responds to the stress profile and the balance of moments.

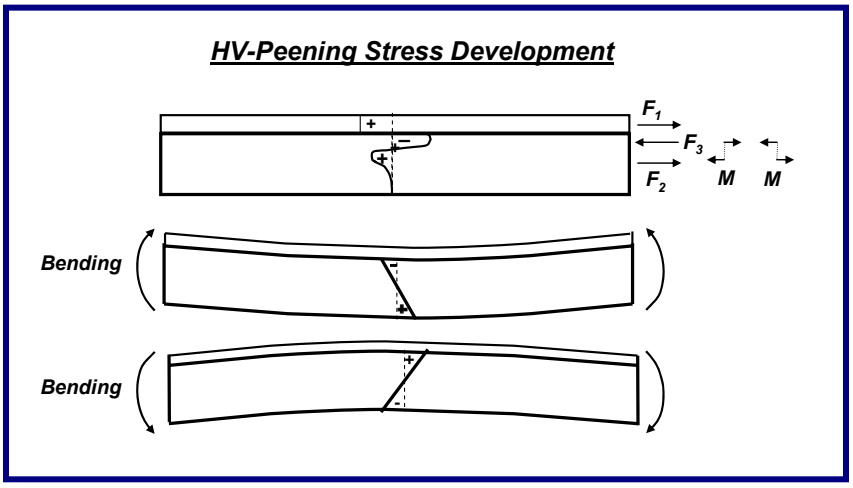

Figure 6-3. Residual stress profile and bending: example of HV thermal spraying: quenching +peening stresses

The magnitude of the force exerted to the peened layer and the thickness of it depend mainly on the plasticity of the substrate (or deposited layer), the strain hardening characteristics of the substrate, the deposition temperature and the momentum of the sprayed particles.

6.2 Methods to measure residual stresses

Several methods have been applied to measure residual stresses in TS coatings. At a microscopic level, residual stresses are present as a result of strained lattice planes (stretched *d*-spacing between atoms). Techniques such as X-ray, synchrotron or neutron diffraction are suitable methods to measure the residual stress state by evaluating the shift of a selected diffraction peak. In contrast, at the macroscopic level, the developed techniques are based in measuring a sample shape change. Destructive techniques, such as, hole-drill or layer removal can be used by means of machining layers of the sample while strain gages sense the change in strain [1]. A similar principle is used to investigate residual stress profiles combining layer removal and X-ray diffraction on the new exposed surface. A non-destructive technique based on measuring the adopted curvature of a sprayed plate has been used at Center for Thermal Spray Research by developing an *In situ* Coating Property Sensor (ICP) [2]. This method allows monitoring the evolution of the stress state during spraying and post-spraying.

6.3 Experimental Methods

6.3.1 ICP - Curvature Sensor

The curvature sensor is based on laser sensing of deflections in a strip during thermal spraying which is converted to plate curvature. A simultaneous measurement of temperature is achieved via multiple thermocouples in contact to the back side of the sample. Sensor and setup are illustrated in Figure 6-4.

By spraying on a thin substrate and monitoring its curvature while spraying, the interaction of substrate and deposited layers with the new layers can be observed. Variables such as feed rate, pass rates, as well as particle states can be correlated to residual stress in real-time.

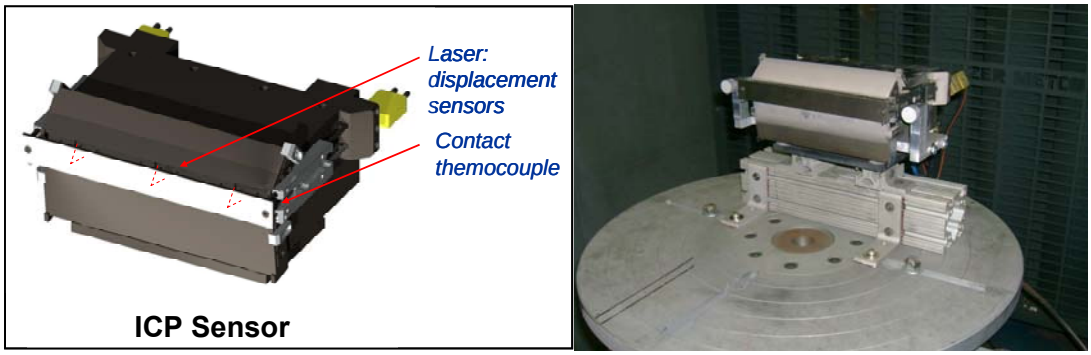

Figure 6-4: ICP sensor: (right) schematic showing laser sensor positions, (left) sensor and substrate mounted on the knife edge set-up. Bending occurs freely during spraying

6.3.2 Curvature Sign Convention

Curvature sign convention is described as follows. If the plate is bending with the coating in the concave side, the curvature is of positive sign, whereas if the plate is bending with the coating in the convex side, the curvature is of negative sign.

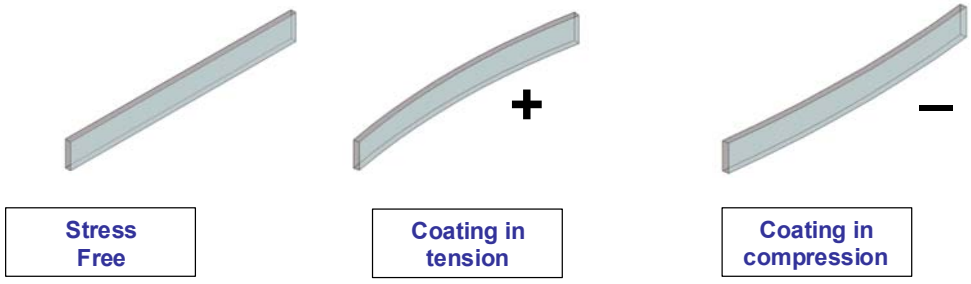

Figure 6-5. Curvature sign convention: coating is on the front face of the plates. Stress sign convention is only valid if the curvature is produced by the stress in the coating only (as illustrated in Figure 6-3).

6.3.3 Evolution of Residual Stress

Evolution of residual stresses is discussed by considering that during HV spraying, induction of quenching (tensile) and peening stresses (compressive) stresses happen simultaneously. Dominance of quenching stress is observed as positive curvature changes, whereas peening stresses appear as negative curvature changes. During cooling, the difference in thermal contraction will input further tensile stresses in the coatings, when the coefficient of thermal expansion (α) of the coating is higher than the substrate and vice versa.

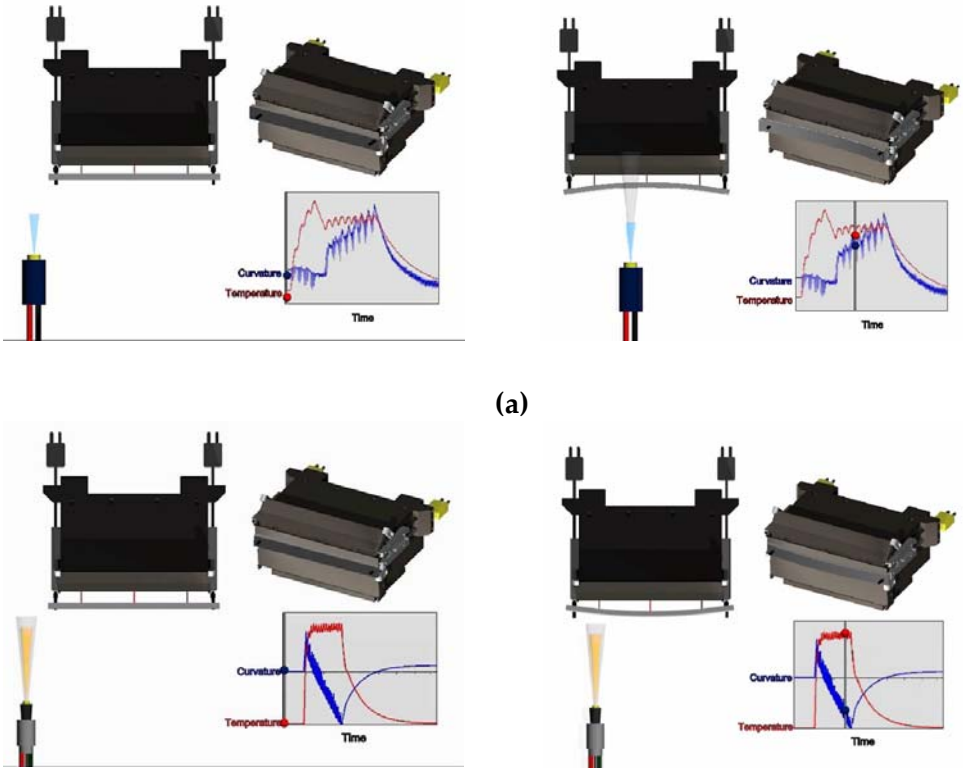

Figure 6-6. Analysis of Stress Evolution and Residual Stress by ICP. (a) dominance of quenching effect, (b) dominance of peening effect

6.3.4 Stress Evaluation

The stress analysis is developed as follows. Biaxial stress state is assumed in the coatings, where in-plane elastic moduli are calculated from:

$$E_c' = \frac{E_c}{1-\nu_c}, \text{ and } E_s' = \frac{E_s}{1-\nu_s} \qquad (1)$$

Subindex c represents coating values and s substrate values. E' is the in-plane elastic modulus, and υ is the Poisson's ratio.

From the slope of curvature vs. time (see Figure 6-7), the deposition stress is calculated by using Stoney [3] approach:

$$\sigma_d = \frac{E_s' t_s^2}{6} \frac{dk}{dt_c} \qquad (2)$$

where σ_d is the deposition stress in the layer of dt_c thickness causing a $d\kappa$ curvature during deposition, and t_s is the substrate thickness. $d\kappa/dt$ is usually taken after the first or second deposited pass because these layers usually are affected by interaction with the substrate.

The principal assumptions in this analysis are summarized, as follows:

- Contribution of the new deposited layers to the stiffness of the substrate (composite of substrate and new deposited layers) is negligible.
- The residual stress induced when a layer is deposited is assigned to that thickness layer; considerations of thickness of the underlying peened layer are not included.
- Linear deposition of coating thickness per unit time is assumed.

It is noted that κ is always analyzed as relative curvature change, since the interaction in the first layers would bias the calculation of the stress in the coating if absolute κ values were used.

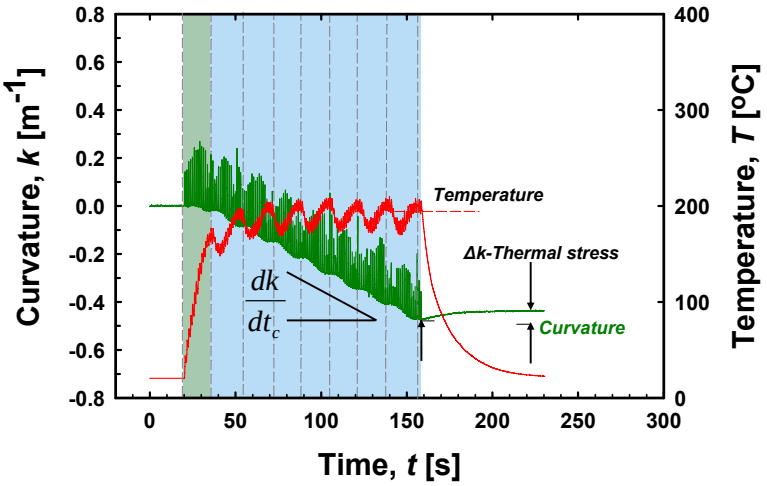

Figure 6-7. Example of curvature-temperature evolution of a NiCr-sprayed coating with HVOF.

Thermal stress of coatings is calculated with good approximation by using Brenner and Senderoff's formula [4]:

$$\sigma_t = \frac{\Delta\kappa E_s' t_s}{6t_c}\left(t_s + \left(\frac{E_c'}{E_s'}\right)^{5/4} t_c\right) \qquad (3)$$

where σ_t is the thermal stress in the coating, $\Delta\kappa$ corresponds to the curvature change during cooling. E_c modulus of the coating is either estimated from bulk values,

indentation modulus results, or analysis of the curvature-temperature curve during cooling. The latest can be obtained from the cooling curve of the spraying run. When plotting, κ vs. T (temperature), a linear behavior can be observed during the cooling after deposition. Using equation (4)

$$\frac{\Delta\kappa}{\Delta T} = \frac{6E_c' E_s' t_c t_s (t_s + t_c)\Delta\alpha}{E_c'^2 t_c^4 + 4E_c' E_s' t_c^3 t_s + 6E_c' E_s' t_c^2 t_s^2 + 4E_c' E_s' t_c t_s^3 + E_s'^2 t_s^4} \quad (4)$$

where $\Delta\kappa/\Delta T$ is an experimental result, and $\Delta\alpha$ is the difference in thermal expansion between deposit and substrate, E_c' can be readily computed, and fed into equation (3)

Final residual stress state σ_{rs} is computed by:

$$\sigma_{rs} = \sigma_d + \sigma_t \quad (5)$$

6.4 Description of Experiments

6.4.1 Thin coating: NiCr on Al - DJ torch

A thin coating (~0.060 mm) was sprayed onto an aluminum 6061 substrate and evaluated at ICP. Post through thickness residual stress measurement was carried out by neutron diffraction. The substrate was annealed in oven at 350°C during 1 hour to relieve any residual stress from the production process and grit blasting prior to spraying. Process conditions are described in Table 1 in Chapter III. A condition was used to deposit this coating. The dimensions of the substrate were 228.6 mm length, 25.4 mm width and 3.2 mm thickness.

6.4.2 Thin coatings: NiCr on steel - DJ torch

Two thin coatings (~0.3 mm) were sprayed onto steel 1018 substrates and evaluated at ICP. Process conditions are described in Table 1 in Chapter III. A and C conditions were used to deposit these coatings. The dimensions of the substrate were 228.6 mm length, 25.4 mm width and 1.6 mm thickness.

6.4.3 Thick coating: NiCr on steel - JP-5000 torch – Residual Stress Profiles

One thick coating (~0.9 mm) was sprayed onto steel 1018 substrate and evaluated at ICP. Process conditions are described in Table 4 in Chapter IV. The dimensions of the substrate were 228.6 mm length, 25.4 mm width and 2.4 mm thickness.

A ladder pattern as illustrated in Figure 6-8 was used to coat individual layers, namely a pass in all the experiments.

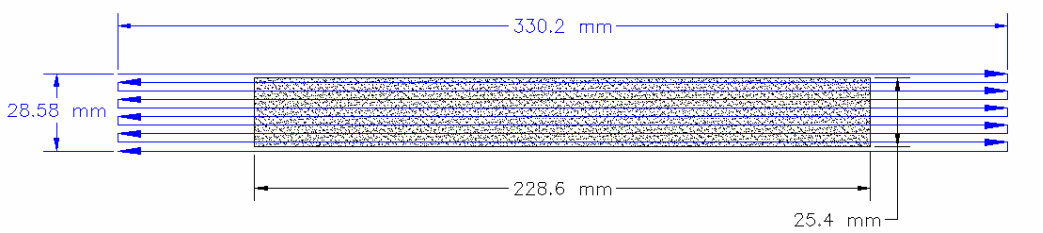

Figure 6-8. Schematic of spraying pattern used at ICP sensor

6.4.4 X-ray diffraction and neutron diffraction

The diffraction stress experiments were performed at the neutron stress diffractometer BT8 at the NIST Center for Neutron Research. Measurements were performed at the neutron wavelength of λ=1.67 Å produced by the Si (400) monochromator reflection at a take-off angle of 2θM=76°. This provided the desired near 90° scattering geometry (best spatial resolution and symmetrical condition for in-plane/transmission and normal/reflection measurements) for the most useful reflections, which were: 2θ = 102° for Ni (311) and 2θ = 90° for Fe (211). Diffraction peaks (022) and (002) planes of Al (E= 70 GPa, υ= 0.3) were used.

The neutron counting statistics uncertainty obtained in these experiments were of Δd = ~5×10-5 Å, which is a very acceptable approximation in the measured values. The resolution of neutron diffraction measurements was given by a volume gage of 0.3 x 0.3 x 15 mm^3. Thin and thick coatings were evaluated with neutrons. Only one average volume measurement was possible in thin coatings. Note that the center of gravity of the gage volume must lie approximately at the mid-plane of the coating in order to obtain diffraction peaks from inside the material avoiding possible partial illumination. Such coincidence is attempted by using "entering curves", a technique that finds the position of the sample surfaces very accurately by means of tracking sample translation via illumination.

X-ray diffraction was used to measure stresses on thin coating samples. The data was collected using a Siemens D500 diffractometer with chromium radiation in Ψ-mode of the standard $\sin^2\Psi$-method with Ψ-angle range of ± 90° and 30° step tilts, using reflection from Ni (420) peak (E = 207 GPa, υ = 0.31)

6.5 Results and Discussion

6.5.1 Thin coating: NiCr on Al-6061

In Figure 6-9 and Figure 6-10, curvature-temperature evolution and through thickness residual stress profiles, respectively, are presented for a thin NiCr coating sprayed over Al. Curvature graph indicates dominance of peening during spraying, and further induction of compressive stresses on the coating due to thermal mismatch.

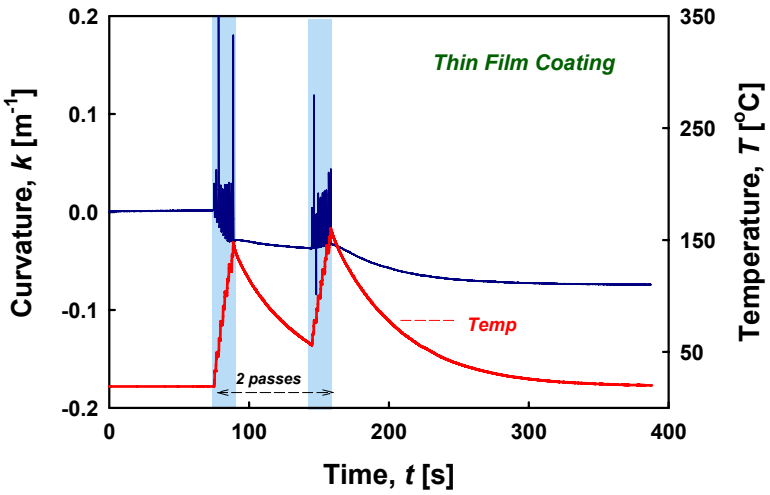

Figure 6-9. Curvature temperature history of a thin NiCr coating (0.06 mm), two passes were deposited on Al substrate.

The composite was subjected to through thickness residual stress measurement in the substrate by neutron diffraction and residual stress measurement in the coating by X-ray diffraction. A modified Tsui and Clyne [5] model was applied to the analysis of residual stress.

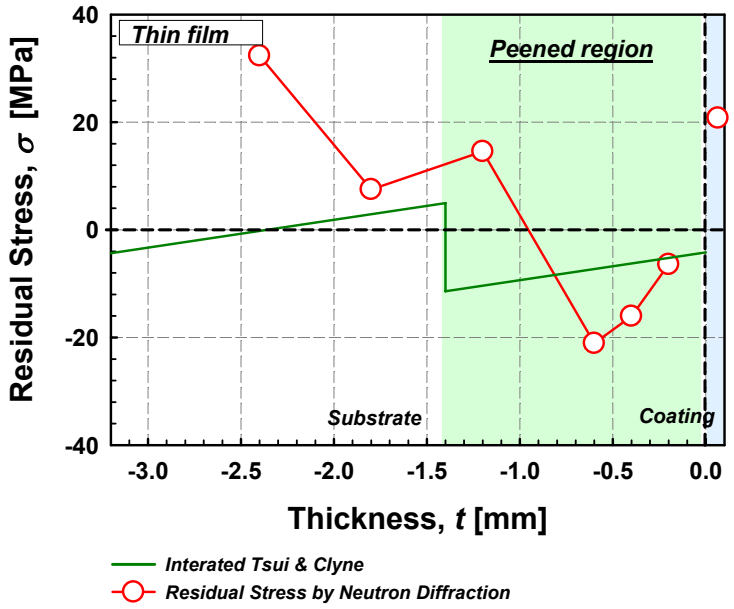

Figure 6-10. Through thickness profile of residual stresses in NiCr thin coating deposited on Al6061 substrate by neutron diffraction (on the substrate), X-ray diffraction (on the coating) and by an iterated-modified Tsui and Clyne model.

Note the following:

- Assumed: a 1.4 mm substrate later was assumed to be subjected to peening effect.

- The main restriction to this new approach is that the three forces (F_1, F_2 & F_3 in Figure 6-3 can not be computed with only two equations available, namely: $\Sigma F_i = 0$ and $\Sigma M(F_i) = 0$ (where F is the force, M is the moment)
- In the present results, an iterative analysis was used to obtain F_1 by approaching the residual stress value measured by X-ray diffraction on the coating. The results were presented in Figure 6-10.

The aluminum substrate showed a reversed residual stress profile along the thickness, with compressive stresses near the coating and tensile stresses at the bottom. In the coating, it was found that tensile stresses from quenching predominated over the compressive stresses that were originated by the peening within the coating and by the mismatch contraction. Although exact values of residual stresses were not verified by the iterated Tsui and Clyne model, the observed trends validate the used approach.

In the presented case, evaluation of the stress by curvature fails to predict the stress in the coating due to the fact that the bending responds to the balance of stress in the composite and not only the stress in the coating.

	Residual Stress in the Coating [MPa]				
	By curvature			**X-Ray**	**Neutron**
	σ_d	σ_t	σ_{rs}		
Coating	-102	-113	-215-	21 ± 14	-
σ- d: deposition, t: thermal, r.s. residual stress.					

Table 6-1. Summary of residual stress values evaluated by different methods for thin coating deposited on Al substrate.

6.5.2 Thin coatings: NiCr on steel - DJ torch

In Figure 6-11 and Figure 6-12, curvature-temperature evolution and through thickness residual stress profiles, respectively, are presented for thin NiCr coatings sprayed over steel with two different spraying parameters, named A and C.

Curvature graph indicates dominance of quenching in the first pass, subsequent dominance of peening during the following passes, and further induction of compressive stresses on the coating due to thermal mismatch.

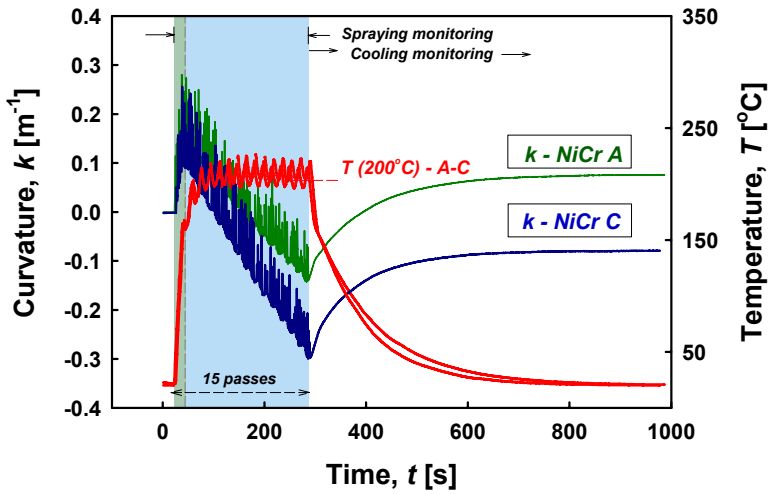

Figure 6-11. Curvature temperature history of thin NiCr coatings (0.3 mm), sprayed at two different conditions (A-C) deposited on steel substrates.

The composites were subjected to through thickness residual stress measurements in the substrate and coating by neutron diffraction. Tsui and Clyne model was not applied to this case. Through thickness profiles were calculated using curvature data from ICP.

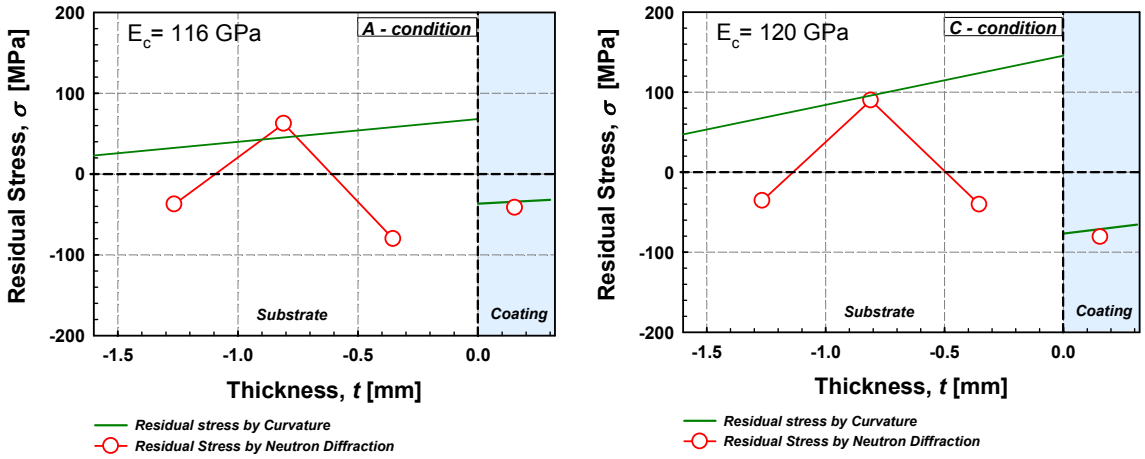

Figure 6-12. Through thickness profile of residual stresses in NiCr thin coatings by neutron diffraction (on the substrate) and one average measurement in the coating, and by curvature analysis.

The evaluation of residual stress in the coating coincides with the neutron diffraction measurements for both coatings (A, C). Profiles in the substrates are dissimilar probably due to the peening residual stress from grit-blasting and/or from the spraying run.

The adopted analysis for evaluation of stress from the curvature evolution successfully estimates the stress state in the coating. Note that if absolute values of curvature were used for stress evaluation, residual stress in the coating would be biased (e.g. in Figure 6-11, the final curvature of plate-A is positive, which would indicate

tensile stress in the coating. Considering the relative curvature change, the coating is calculated to be in compression)

In Table 6-2, a summary of residual stress values evaluated by different techniques is presented. Note that X-ray diffraction results fail to represent the overall stress in the coatings, provided that the last layer of splats experiences quenching and not peening.

Coating	Residual Stress in the Coating [MPa]				
	By curvature			X-Ray	Neutron
	σ_d	σ_t	σ_{rs}		
A	-135	96	-39	183 ± 4	-42 ± 13
C	-187	98	--89	158 ± 5	-81 ± 14
σ- d: deposition, t: thermal, r.s. residual stress.					

Table 6-2. Summary of residual stress values evaluated by different methods for two thin NiCr coatings.

6.5.3 Thick coating: NiCr- JP-5000 torch – Residual Stress Profiles

In Figure 6-13 and Figure 6-14, curvature-temperature evolution and through thickness residual stress profiles, respectively, are shown for a thick NiCr coating sprayed over steel.

Curvature graph indicates dominance of peening along the deposition run (two sessions of ten passes), and further induction of compressive stresses on the coating due to thermal mismatch.

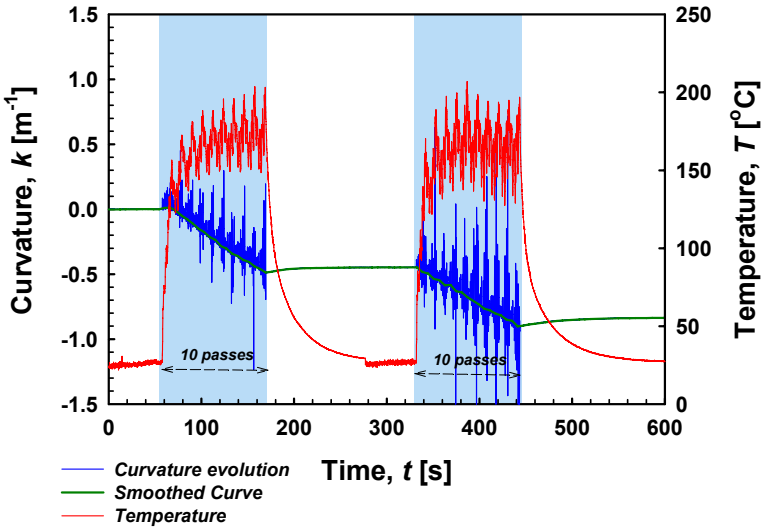

Figure 6-13. Curvature temperature history of thick NiCr coating (0.9 mm), sprayed deposited on steel substrate.

The composite was subjected to through thickness residual stress measurements in the substrate and coating by neutron diffraction. Tsui and Clyne model was applied to this case to estimate through thickness profiles using curvature data from ICP.

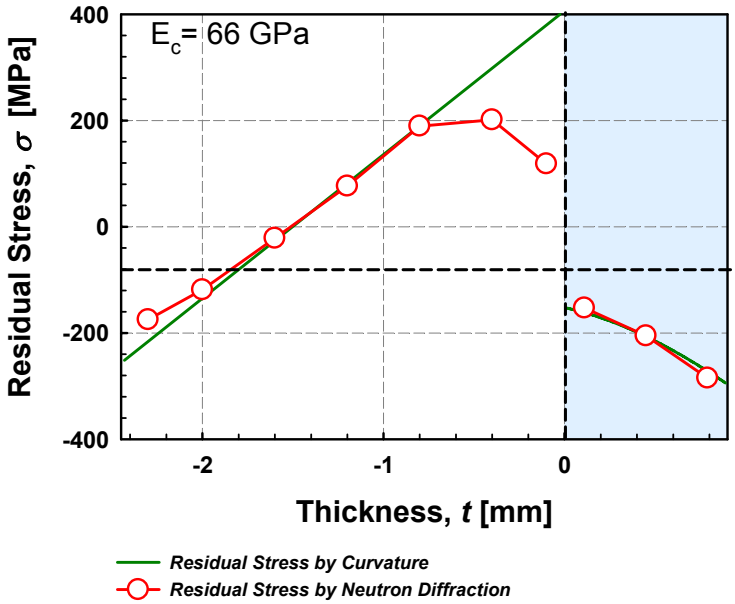

Figure 6-14. Through thickness profile of residual stresses in NiCr thick coatings by neutron diffraction, and by Tsui-Clyne model using curvature data from ICP sensor

The evaluation of residual stress in the coating with Tsui and Clyne model and ICP data coincides with the neutron diffraction measurements. Profiles in the substrates near the interface are dissimilar probably due to peening residual stress from grit-blasting and/or from the spraying run.

6.6 Conclusions

The residual stress evolution of NiCr coatings was studied by recourse to measuring the curvature change of HVOF sprayed plates, and comparing these results to the ones obtained by neutron and X-ray diffraction techniques.

An approach to predict through thickness residual stresses was proposed by modifying Tsui and Clyne model for very thin coatings. The approach proposes the exertion of a peened layer underneath the coated layer subjected to compressive force. Results were comparable to measurements done by neutron diffraction. Curvature approaches (Stoney [3], Brener-Senderoff [4]) fail to predict the stress in a very thin coating because the peening affects substantially the stress in the underlying layer.

Traditional curvature approaches can be used to evaluate the stress in thin coating (~0.3 mm thickness). It is highlighted that relative curvature changes would lead to a correct estimation of the stress.

In thick coatings, Tsui and Clyne model [5] was successfully applied to predict the stress profiles.

6.7 References

[1] T. W. Clyne, S. C. Gill, Journal of Thermal Spray Technology 5 (1996) 401-418.
[2] J. Matejicek, S. Sampath, Acta Materialia 51 (2003) 863-872.
[3] G. G. Stoney, Proceedings of the Royal Society, London A82 (1909) 172-175.
[4] A. Brenner, S. Senderoff, J. Res. Natl. Bur. Stand. 42 (1949) 105-123.
[5] Y. C. Tsui, T. W. Clyne, Thin Solid Films 306 (1997) 23-33.

Chapter 7
SYNTHESIS

This dissertation critically examined strategies and opportunities to design the deposition process of *reliable* HV thermal sprayed coatings. Integrated experimental methods under the methodology of Process Maps were used to investigate particle state, coating formation and properties. The work presented in preceding chapters connects several strategies to:

- Control process parameters as to achieve specific particle states
- Understand differences in coating formation in real time
- Tailor residual stress states
- Correlate resultant microstructures and properties

All were discussed within the framework of the particularities of HVTS coatings: layer by layer structure, rapid heating and solidification, oxidation, high impact formation, among others. This chapter attempts a unified discussion of the presented results.

7.1 1st Order Process Maps and Process Parameters Design

Careful manipulation of the spraying parameters allowed us to build first order process maps in which the flame energy and chemistry were related to the particle state and the extent of the oxidation reactions. Particle state was analyzed considering the "true" melting state depending on the particle history in the spray stream. The developed first order process maps can give the operator the opportunity to spray particles at desired T-V conditions (more appropriately, melting index and kinetic energy). Note that a similar design-of-experiments for process parameter control in other HV systems will not necessarily replicate the presented trends of particle state behavior. Differences may arise due to variations in the feedstock, combustion reactions of different fuel gases or nozzle designs, and upstream-downstream interactions (flame-particle and surroundings-particle interactions, respectively).

7.2 2nd Order Process Maps and Property Design

Second order process maps were developed for NiCr coatings for various properties in seek for generalized insights (rather than material-specific) relating process conditions to coating properties.

Properties were studied across two groups of coatings:

- Group I: coatings deposited at different spray parameters and with the same torch (Chapter III); and,
- Group II: coatings deposited at various spray parameters and various torches (Chapter IV).

Enlarged opportunities for property selection were found in group II. Salient results of property ranges and dependence of each one on key aspects of the architecture of the coating (potentially *tailorable*) are shown as follows:

- Elastic modulus by indentation in coatings did not exceed 60% of the bulk property. The range of this property was of 5% for group I and 25% for group II. This property was found to be dependent mainly on the contact between splat-splat, which depends on compaction (high particle velocity), mechanical interlocking and metallurgical bonding (high melting state).
- Hardness showed pronounced sensitivity evaluating the coatings. Hardness ranged between 70%-190% of the bulk property. The range was of 24% for group I and 110% for group II. This property was found to be dependent mainly on work hardening –inherent to the formation by impacting particles-, residual stress, and splat bond strength.
- Thermal conductivity (through the thickness) was lower than 70% of the bulk property. The range of this property was of 7% for group I and 24% for group II.
- Electrical conductivity (in plane) was in the range of 40-100% of the bulk property. The range of this property was of 8% for group I and 58% for group II. These last two properties were found to be dependent on the true contact between splat-splat, wherein the presence of defects and oxides in the interfaces affect the movement of electrons through free paths across the microstructures.

7.3 Key Factors in Process Design

Experimental evidence and fundamental principles suggest that the key parameters to be controlled to accomplish successful process design are: particle state and deposition temperature. Manipulation of these variables can lead to design intersplat interfaces, phase content, residual stress, oxidation, among others. Both variables define the architecture of the coating, thus:

1) Depending upon the particle state, before impact particles melt and change in chemistry, and during impact particles flow, deform, micro-crack, oxidize.
2) Depending upon the deposition temperature, particles during impact flow, wet, deform, solidify, adhere, micro-crack, oxidize, re-melt deposited splats.

However, the control of both of them is limited due to the large number of variables in the process. The stochastic occurrence of several phenomena during particle by particle coating formation limits the micro-scale control and only allows a macro-scale assemble evaluation of their effect.

7.4 Coating Formation via Advanced *in situ* Monitoring

The *in situ* monitoring of residual stress buildup in HV sprayed particles showed the induction of tensile stresses (due to quenching) and compressive stresses (due to peening). The magnitude of these stresses under different spraying conditions evidenced several mechanisms of formation of the coatings. Salient results are summarized here:

- Enhanced peening effect determines higher strain hardening, compaction and compressive residual stress in the coating, which results in coatings of high hardness and high elastic modulus.
- The magnitude of the residual stresses during deposition depends upon particle state and deposition temperature. A second order process map revealed that as particles show high momentum and reduced melting state they produce enhanced peening effect. As the deposition temperature increases the cohesion is enhanced (measured as an increment in quenching stress –exceptions are material-specific). The right assessment of process parameters to adjust these two, particle state and deposition temperature, can lead to design coatings of desired residual stress states.
- The stress developed during deposition of the first layer of coating on the substrate can reveal qualitatively the adhesion strength, peening on the substrate, and stress relief due to heating.

7.5 Residual Stress Measurements

In Chapter VI, residual stress measurements by neutron and X-ray diffraction were compared to results from the curvature method. Provided that peening effect changes the stress state of the underlying layer over which the particle is depositing and stress evaluation via curvature approach relates the radius of curvature to the stress in the coating and not to stress profiles (as resultant from peening effect), stress evaluation via curvature measurements can be biased. This deviation was found to be important in thin layers (due to peening over the substrate), but not in thick coatings were the involved error is lowered. It is highlighted that the analysis of curvature evolution can lead to the correct calculation of residual stress, whereas the usage of absolute sample curvatures misleads the computation.

Layer by layer analytical models based on elastic bi-material composites can be applied to predict the stress profiles in thick coatings. X-ray diffraction measurements failed to predict the stress of HV sprayed coatings due to the fact that the last layer of splats does not get peened, and therefore, does not represent the stress state of the whole coating.

Chapter 8
SUGGESTION FOR FUTURE WORK

Over the duration of this research and associated survey of the literature , many research opportunities and interests have been identified and not fully investigated within this dissertation. Some of those topics are presented here as suggestions for future research.

8.1 Development of Process Maps for Cermets Materials (e.g. WC-Co)

8.1.1 Preliminaries

Process maps were developed with DJ-2700 systems on WC-12Co and CoCr. Various process parameters and fuel types were examined [1]. 1st and 2nd order process maps were developed with no clear trends in process control and property assessment. Differentiation of process conditions from diagnostics data and property evaluation was limited by the resolution of the characterization techniques.

NiCr and WC-Co first order process map were investigated under similar condition to cross-compare their behavior. Control of particle state was not fully achieved due to lack of clear trends, as seen in Figure 8-1.

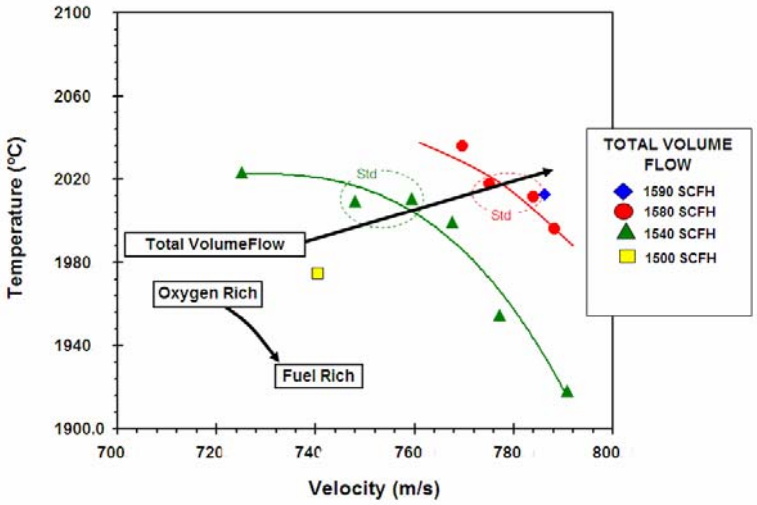

(a)

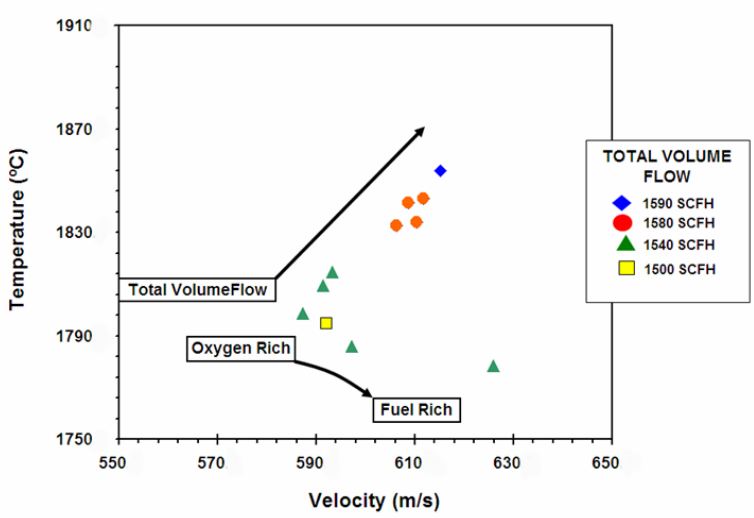

(b)

Figure 8-1. First order process maps for NiCr and WC-CoCr at identical process conditions

8.1.2 Considerations

- Process diagnostics measurements may be biased by the temperature measurement due to decomposition of particles during in-flight and associated changes in emissivity.
- Property measurements such as indentation or in-plane elastic modulus evaluation via curvature are affected by the scale size of the material sampled.

8.1.3 Suggestions

- Develop process maps in carbide materials with usage of multiple diagnostics systems and not only varying particle states but deposition conditions, such as rastering speeds, feed rate, spray distance, etc.
- Identify the main parameters that affect the microstructure and evaluate key properties that can be correlated to the microstructure-property-performance relationship.

8.2 *In situ* (ICP) and *Ex situ* (ECP) Coating Property: expansion of capabilities and implementation in the field

8.2.1 ICP: Design of strain tolerant coatings

8.2.1.1 Preliminaries

As discussed in Chapter V, quenching stress during deposition can be enhanced until nucleating vertical cracks in the structure of the coating. The presence of vertical cracks imparts strain tolerance to the structure of the coating by absorbing part of the load by elastic crack opening.

Preliminary results suggest the achievement of strain tolerant microstructures in Al_2O_3 dense coatings. The curvature versus temperature curve of three samples sprayed

at different rastering speeds with an HV-2000 system (inherent change in deposition temperature and enhanced quenching stress) is presented in Figure 8-2 . At 750 and 500 mm/s of speeds the behavior of the samples is linear, whereas when speed is lower 300 mm/s the behavior turns out to be non-linear.

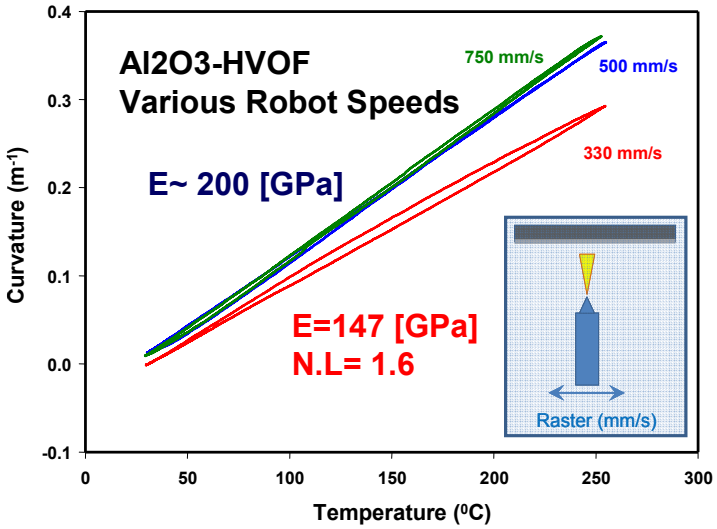

Figure 8-2. Curvature-temperature heat cycles from ICP for three Alumina dense coatings. In-plane elastic modulus and degree of non-linearity [2] are presented.

8.2.1.2 Considerations

- Density, size and distribution of vertical cracks are important for strain tolerance.
- However, diffusion of species that may affect the structures beneath the strain tolerant coating are compromised by allowing further oxidation, for instance.

8.2.1.3 Suggestions

- Develop experiments with YSZ coatings targeting for vertically cracked structures. Upon tailoring, deposition temperature (preheating, rastering speeds, feed rate, spray distance) the quenching stress would reach thresholds when vertical cracks would be nucleated. ICP monitoring would potentially reveal this stress levels.

8.2.2 ICP: Design of damage tolerant coating by gradation of microstructure

8.2.2.1 Preliminaries

Several authors [3, 4] have identified great potential in graded structures. Thermal spray in particular is a technology that readily can combine progressively powder feedstock as to deposit graded coatings. Some of the benefits include improved wear resistance, reduction of stress concentrations, tailoring residual stress, flaw tolerance, among others.

Graded coatings (100%SS316 to 100%WC-12Co) were sprayed on ICP sensor. Results of the stress buildup for each composition are shown in Figure 8-3. As the WC-Co percentage increases the quenching stress also increases.

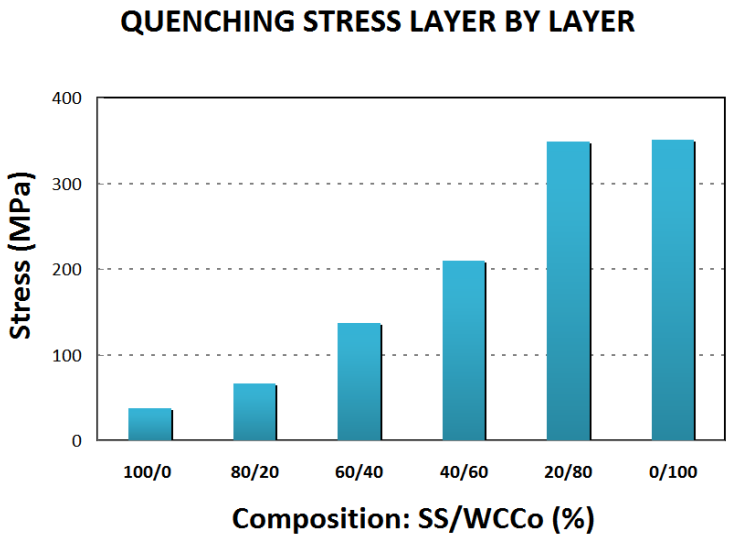

Figure 8-3. Stress development from ICP for functionally graded coating. Quenching stress buildup is shown for the various compositions.

8.2.2.2 Considerations

- Spraying graded materials will result in residual stress gradation through the thickness. Tailoring of stress (by tuning spraying parameters or material combinations) during deposition will allow us to enhance coating performance.
- The residual stress control would also allow us to deposit thicker coatings.

8.2.2.3 Suggestions

- Develop experiments two achieve the following structures:
  - Elastically graded surfaces (e.g. WC-17Co & WC-12Co)
  - Reduce tensile stress and/or promote compressive stresses near the substrate interface (e.g. NiCr & CrC-NiCr)
  - Minimize thermal residual stresses between the materials being combined.

8.2.3 ICP: Adhesion measurement in thick coatings

8.2.3.1 Preliminaries

Four point bending and three point bending tests have been used in bi-material samples to evaluate adhesion. Delamination at the interface is regularly caused by introducing a vertical crack which grows to the interface during loading. Analogously, delamination can also be produced during coating deposition (usually thick coatings) due to stress buildup. Failure usually initiates at the edges of the substrate. The effect of the residual stress build up and adhesion strength on the debonding of coatings has

been modeled and related to sudden curvature change at which the failure was produced [5, 6].

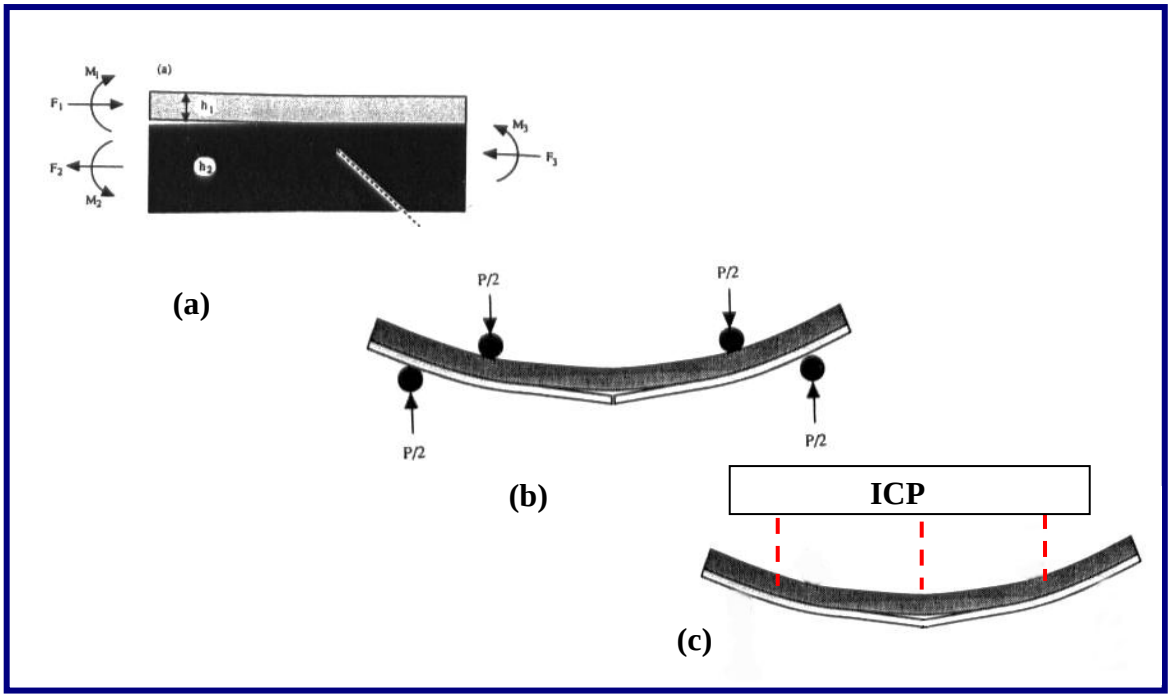

Figure 8-4. (a) Analytical model of debonding interface including effect of residual stress [5], (b) Four point bending tests (proposed experiment is analogous to this one) (c) Set up of ICP plate with crack introduce in the interface.

8.2.3.2 Considerations

- As coatings get sprayed thicker and thicker, the overall force acting on the cross-section of the coating moves away from the interface imposing moment. This moment eventually can trigger delamination.

8.2.3.3 Suggestions

- Introduce a crack at the interface by coating a section with graphite (before spraying), for example, and/or not grit blasting a region of the substrate, and proceed to thermal spray thick coatings.
- Monitor a sudden change in curvature, which would indicate the failure of the interface.

8.2.4 ICP: Layer by layer coating formation

8.2.4.1 Preliminaries

Previous work by Li [7], Chi [8], Matejicek [9] suggested that coating microstructures and properties may vary through the thickness as the coatings get deposited layer by

layer. Deposition of Mo coatings in ICP has demonstrated that the stress that each layer carries out is different as well; and differences may be accentuated depending upon the process conditions, as observed in Figure 8-5 for Mo coatings.

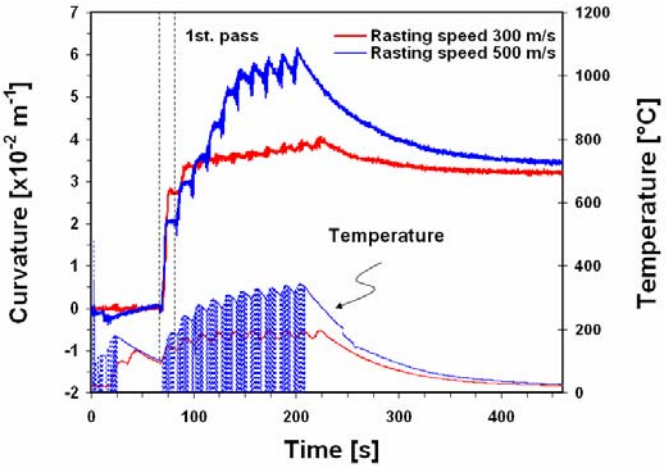

Figure 8-5. Stress evolution from ICP for Mo –APS coatings. Quenching stress buildup is not constant for each layer.

8.2.4.2 Considerations

- The differences in residual stress buildup are related to stress relief mechanisms of different magnitudes. They can be caused by difference in deposition temperature (heat transfer from the new layer to a thicker and thicker coating) and/or roughness effects.

8.2.4.3 Suggestions

- Select materials and process conditions that show significant differences in stress buildup layer by layer. Spray coatings of different number of passes and observe microstructural changes from top view and cross-section.

8.2.5 ECP: Incremental strain and inelastic behavior due to asperity friction in the cracks

8.2.5.1 Preliminaries

Heat cycling experiments of YSZ coatings have shown that at low thermal strain levels, coatings show inelastic effects probably due to friction in the asperities existent within the cracks. As the thermal strain is incremented, more inelasticity is observed.

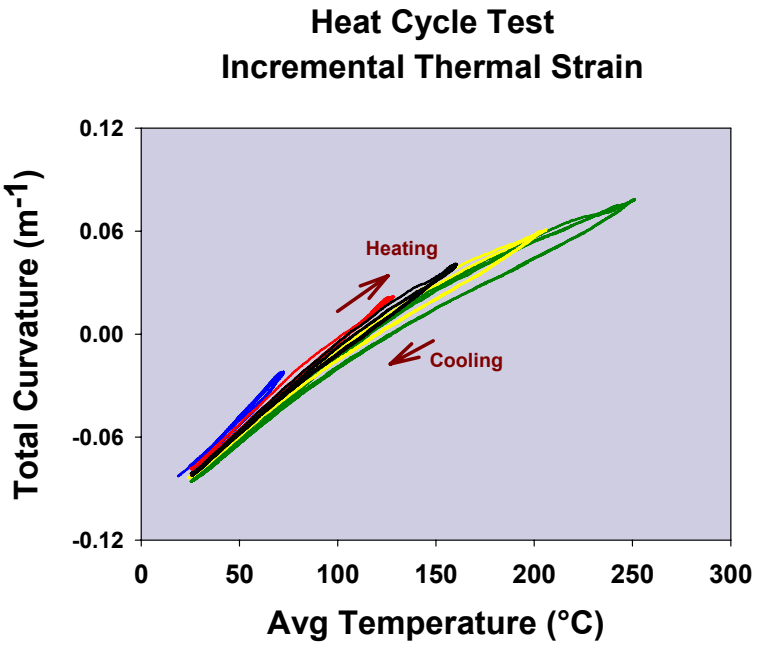

Figure 8-6. Thermal cycling test of YSZ coating under incremental thermal strain conditions.

8.2.5.2 Considerations

- At low temperature and low thermal strain conditions, only friction in the cracks could explain inelastic phenomena.
- The analysis of friction in the cracks may be important when considering the number of points in contact within the interlamellar porous. This information could potentially be related to sintering rates as this depends on the number of contact points.

8.2.5.3 Suggestions

- Investigate the elastic behavior of various coating materials by incremental thermal strain tests.
- The degree of inelasticity occurring in the coating may be related to the structure and hysteresis if present.

8.2.6 ECP: Thermal gradient effects on the elastic modulus and thermal conductivity measurements

8.2.6.1 Preliminaries

Heat cycling experiments of YSZ coatings have suggested that a thermal gradient through the thickness of a bi-material plate can generate curvature of the sample (independently of the isothermal gradient). As the temperature varies through the thickness, the non-uniform thermal expansion of the materials generates thermal mismatch strain. Once the thermal gradient stabilizes (reaches a steady temperature profile), the isothermal consideration to evaluate the elastic modulus [10] is valid.

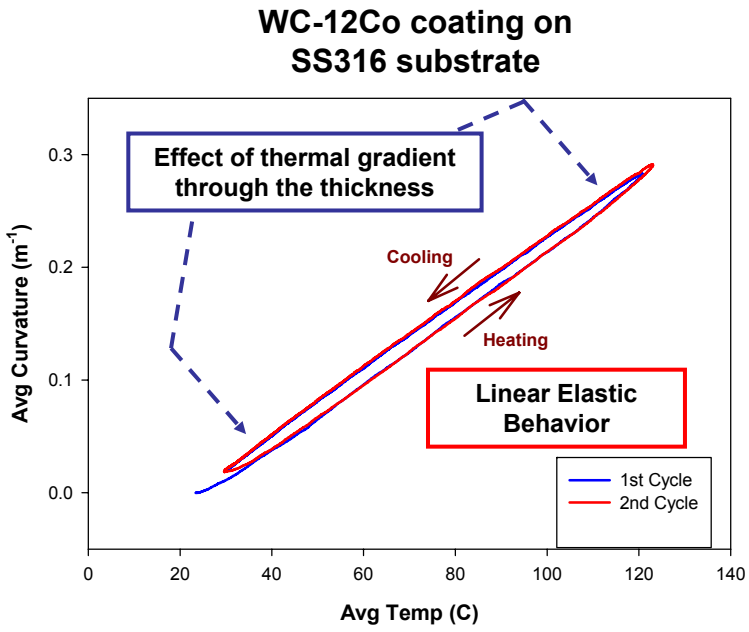

Figure 8-7. Thermal cycling tests of WC-Co coating on SS316. Coating behavior is linear elastical. Curves during heating and cooling do not overlap due to differences in the through thickness temperature profile (no-hysteresis)

8.2.6.2 Considerations

- In order to evaluate the in-plane elastic modulus of the coating with accuracy, any thermal gradient through the thickness needs to be ruled out and carefully monitored.
- If a thermal gradient through thickness in steady state is deliberately created in a bi-material system, the bending produced by the thermal gradient would be related to the temperature at the interface.

8.2.6.3 Suggestions

- Monitor thermal gradients through the thickness of coatings so as to rule out their effect on the evaluation of elasticity, and anelasticity properties of coatings.
- It is envisioned that:
    - If the elastic modulus of the coating is accurately evaluated in an isothermal thermal cycle test, and,
    - A sufficient thermal gradient through thickness in steady state can be generated in the sample, then, the resultant curvature can be related to the temperature at the interface and from here to the thermal conductivity of the coating.

8.3 Addressing Particle state in HV systems

8.3.1 Preliminaries

Snapshots of the spray stream were collected with a guillotine like set-up to analyze splat maps. Salient observations were found when comparing splat maps at low feed rate (9 g/min) versus high (23 g/min) of a same condition, Figure 8-8. Even though diagnostic measurements indicate particle temperatures far beyond the melting point (T_m = 1400 °C), collected splats at high feed rate seem to be only thermally softened, Figure 8-8a, and not molten, Figure 8-8b.

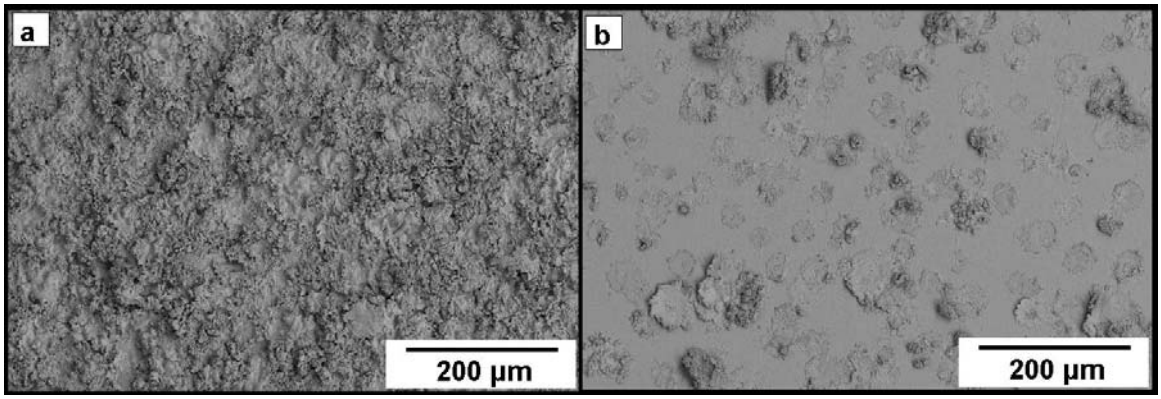

Figure 8-8. Splat maps of NiCr (a) at low feed rate (9 g/min) and (b) high feed rate (23 g/min). Views are of the center point of the snapshot of the spray stream.

8.3.2 Considerations

- Temperature reading from diagnostic systems is only of the surface of the particle.

8.3.3 Suggestions

- Monitor particle temperature at different feed rates, and collect splats (splat maps and scattered splats) as to analyze their melting state.
- Differences in grain sizes between splats and feedstock can help to investigate the melting state.

8.4 References

[1] A. Valarezo, Choi, W.B., Gouldstone, A., Sampath, S., Proceedings of International Thermal Spray Conference (2006).
[2] Y. Liu, T. Nakamura, V. Srinivasan, A. Vaidya, A. Gouldstone, S. Sampath, Acta Materialia 55 (2007) 4667-4678.
[3] S. Suresh, Science 292 (2001) 2447-2451.
[4] L. Prchlik, S. Sampath, J. Gutleber, G. Bancke, A. W. Ruff, Wear 249 (2001) 1103-1115.
[5] S. J. Howard, Y. C. Tsui, T. W. Clyne, Acta Metallurgica et Materialia 42 (1994) 2823-2836.
[6] Y. C. Tsui, S. J. Howard, T. W. Clyne, Acta Metallurgica et Materialia 42 (1994) 2837-2844.
[7] L. Li, Stony Brook University, On the deposit formation dynamics and multiscale characterization of thermal sprayed splat structures, in: Stony Brook University, 2004, pp. xv, 153 pages
[8] W. Chi, Stony Brook University, Thermal Transport Properties of Thermally Sprayed Coatings: An Integrated Study of Materials, Processing and Microstructural Effects, in: Stony Brook University, 2007, pp. xv, 153 pages.
[9] J. Matejicek, Stony Brook University, Processing effects on residual stress and related properties of thermally sprayed coatings, in: State University of New York at Stony Brook, 1999., 1999, pp. xv, 154 pages.
[10] J. Matejicek, S. Sampath, Acta Materialia 51 (2003) 863-872.

8.5 Appendix A.

J-C model is used to evaluate plastic stress, *that is to say the stress that is associated with plastic strain, or the stress that persists after unloading,* and limited to consider particles in solid state, thermally softened but not molten.

The J-C model is stated as follows:

$$\sigma = \left[A + B\left(\varepsilon^{pl}\right)^{n}\right]\left[1 + C\ln\left(\frac{\dot{\varepsilon}^{pl}}{\dot{\varepsilon}_{o}}\right)\right]\left(1 - \hat{\theta}^{m}\right)$$

$\hat{\theta}$ is a non-dimensional temperature, define as:

$$\hat{\theta} = \begin{cases} 0 & for \quad \theta < \theta_{transition} \\ \dfrac{(\theta - \theta_{transition})}{(\theta_{melt} - \theta_{transition})} & for \quad \theta_{transition} \le \theta \le \theta_{melt} \\ 1 & for \quad \theta > \theta_{melt} \end{cases}$$

where ε^{pl} is the equivalent plastic strain, $\dot{\varepsilon}^{pl}$ is the equivalent plastic strain rate, and A, B, C, m, n and $\dot{\varepsilon}_{o}$ are material parameters measured at or below the transition temperature, $\theta_{transition}$, above which thermal softening is assumed to occur. Parameters for J-C model are all positive in sign and material-specific.